Computational and Structural Biotechnology Journal 20 (2022) 1306–1344

COMPUTATIONAL AND STRUCTURAL BIOTECHNOLOGY JOURNAL

journal homepage: www.elsevier.com/locate/csbj

Review

Inhibition of the main protease of SARS-CoV-2 (M^{pro}) by repurposing/designing drug-like substances and utilizing nature's toolbox of bioactive compounds

Io Antonopoulou [1,*], Eleftheria Sapountzaki [1], Ulrika Rova, Paul Christakopoulos

Biochemical Process Engineering, Division of Chemical Engineering, Department of Civil, Environmental and Natural Resources Engineering, Luleå University of Technology, SE-97187 Luleå, Sweden

ARTICLE INFO

Article history:
Received 27 December 2021
Received in revised form 10 March 2022
Accepted 11 March 2022
Available online 14 March 2022

Keywords:
Enzyme inhibition
Main Protease
SARS-CoV-2
Coronavirus
Repurposed drugs
Natural compounds
Extracts

ABSTRACT

The emergence of the Severe Acute Respiratory Syndrome Coronavirus-2 (SARS-CoV-2) has resulted in a long pandemic, with numerous cases and victims worldwide and enormous consequences on social and economic life. Although vaccinations have proceeded and provide a valuable shield against the virus, the approved drugs are limited and it is crucial that further ways to combat infection are developed, that can also act against potential mutations. The main protease (M^{pro}) of the virus is an appealing target for the development of inhibitors, due to its importance in the viral life cycle and its high conservation among different coronaviruses. Several compounds have shown inhibitory potential against M^{pro}, both *in silico* and *in vitro*, with few of them also having entered clinical trials. These candidates include: known drugs that have been repurposed, molecules specifically designed based on the natural substrate of the protease or on structural moieties that have shown high binding affinity to the protease active site, as well as naturally derived compounds, either isolated or in plant extracts. The aim of this work is to collectively present the results of research regarding M^{pro} inhibitors to date, focusing on the function of the compounds founded by *in silico* simulations and further explored by *in vitro* and *in vivo* assays. Creating an extended portfolio of promising compounds that may block viral replication by inhibiting M^{pro} and by understanding involved structure–activity relationships, could provide a basis for the development of effective solutions against SARS-CoV-2 and future related outbreaks.

Contents

* Corresponding author.
E-mail address: io.antonopoulou@ltu.se (I. Antonopoulou).
[1] Equal contribution.

https://doi.org/10.1016/j.csbj.2022.03.009
2001-0370/

1. Introduction

As of the beginning of 2020, the world is going through a pandemic, which apart from a severe public health crisis counting>219 million cases and>4.5 million deaths, has had a tremendous impact on economic and social life. In December 2019, in the city of Wuhan, Hubei province, China, a series of pneumonia cases were reported, exhibiting symptoms such as fever, dry cough, chest discomfort or even dyspnea and bilateral lung infiltration. Further investigation led to the identification of a novel coronavirus, Severe Acute Respiratory Syndrome Coronavirus-2 (SARS-CoV-2), as the responsible pathogen. The disease caused by the virus, was named as COVID-19 (Coronavirus disease 2019) and was widely spread all over the world, resulting in the World Health Organization (WHO) declaring a pandemic on 11 March 2020 [1,2]. SARS-CoV-2 is the third coronavirus creating a public health concern in the past 20 years, after the severe acute respiratory syndrome-coronavirus (SARS-CoV) and Middle East respiratory syndrome (MERS-CoV), which created an outbreak in 2002 and 2012, respectively. SARS-CoV-2 shares common genomic sequence by a percentage of 79% with SARS-CoV and 50% with MERS [3].

Therapeutic targets to combat COVID-19 include structural and functional proteins of the virus, as well as virulence factors and host proteins that are useful for viral proliferation. So far, only remdesivir, an inhibitor of the RNA dependent RNA polymerase of the virus, has been FDA-approved for use in COVID-19 patients [4], while some monoclonal antibody treatments have received authorizations for emergency use [5].

The translation of the viral RNA of SARS-CoV-2, once it enters the host cells, leads to the synthesis of two polyproteins, pp1a and pp1ab. After auto-processing its own N- and C- terminals to release itself from the polyproteins, SARS-CoV-2 main protease (M^{pro} or 3CL) cleaves the peptide bonds of pp1a and pp1ab, catalyzing the formation of nonstructural proteins necessary for the construction of the replication transcription complex that the virus needs in order to synthesize new RNA [6–8]. The proteolysis takes place in>11 cleavage sites. The amino acid sequence that the enzyme recognizes as a cleavage site is (Leu-Gln)-(Ser/Ala/Gly), with the peptide bond being hydrolyzed after Gln. The vital role of M^{pro} in the reproduction of SARS-CoV-2 and the release of many of its proteins, combined with the fact that its structure and mechanism have been investigated, make it a very appealing target to block viral activity. Moreover, the fact that there is no human enzyme cleaving proteins after the Gln residue is another advantage of M^{pro} as target for the development of inhibitors to act as antiviral drugs or immune-boosting compounds, as it increases its specificity and limits unwanted side effects. Lastly, the high conservation of the protease among coronaviruses, depicted by the high amino acid sequence identity (96% sequence identity between SARS-CoV and SARS-CoV-2 main proteases), is another factor that implies that the development of M^{pro} inhibitors can be useful for different SARS-CoV-2 strains and mutants or future coronavirus outbreaks [9–15].

The present work is a collective presentation of the existing research results regarding potential inhibitors of the major functional protein of SARS-CoV-2, M^{pro}, including drug-like and natural compounds that have been investigated *in silico* and *in vitro*. Recent developments for compounds that have been selected for *in vivo* and clinical trials are also discussed, highlighting the importance of M^{pro} as target among the recurring virus mutants. In particular, the impressive number of published research during the past 2 years on proposing novel solutions for M^{pro} inhibition highlights the need for complementary measures to vaccination and medication strategies, such as developing functional aids that can help in boosting immunity and aid protection against infections by coronaviruses.

2. The main protease of SARS-CoV-2 (M^{pro})

SARS-CoV-2 M^{pro} is a cysteine protease (EC 3.4.22.69) and a member of the PA clan of proteases. Proteases are enzymes that hydrolyze peptide bonds and thus belong to the category of hydrolases. The first crystal structure of SARS-CoV-2 M^{pro} was determined by X-ray diffraction at a resolution of 2.16 Å and was deposited at the Protein Data Bank (PDB) by Jin *et al.* and released on February 5, 2020, under the PDB ID 6LU7 [7]. Since then, many structures of the protease have been deposited, including the enzyme co-crystallized with various inhibitors. The active form of the enzyme is a homodimer (Fig. 1). The structure of a single monomer consists of a 306-residue-long polypeptide chain, which can be divided into three domains: domain I (residues 8–101), domain II (residues 102–184) and domain III (residues 201–303). Domains I and II are composed of antiparallel β-barrels and host the active site in a cleft formed between them, whereas domain III consists of 5 α-helices and plays a role in the dimerization of the enzyme. Residues 185–200 form a loop that connects domains II and III [7,15,16]. The enzyme is active only as a dimer because

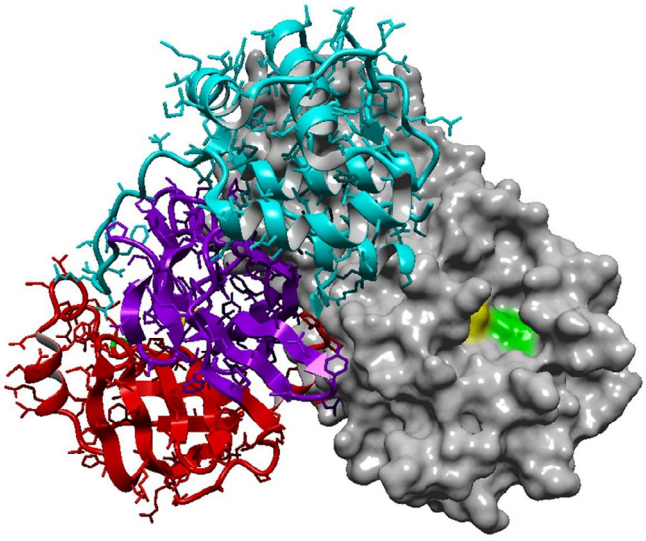

Fig. 1. SARS-CoV-2 M^{pro} in the active form of a homodimer (PDB ID:7JKV). The right monomer is shown as surface while the left monomer portrays the secondary structure and the three domains of the enzyme. Domain I is in red, domain II in purple and domain III in cyan. Catalytic residues His41 and Cys145 are highlighted in yellow and green, respectively. (For interpretation of the references to colour in this figure legend, the reader is referred to the web version of this article.)

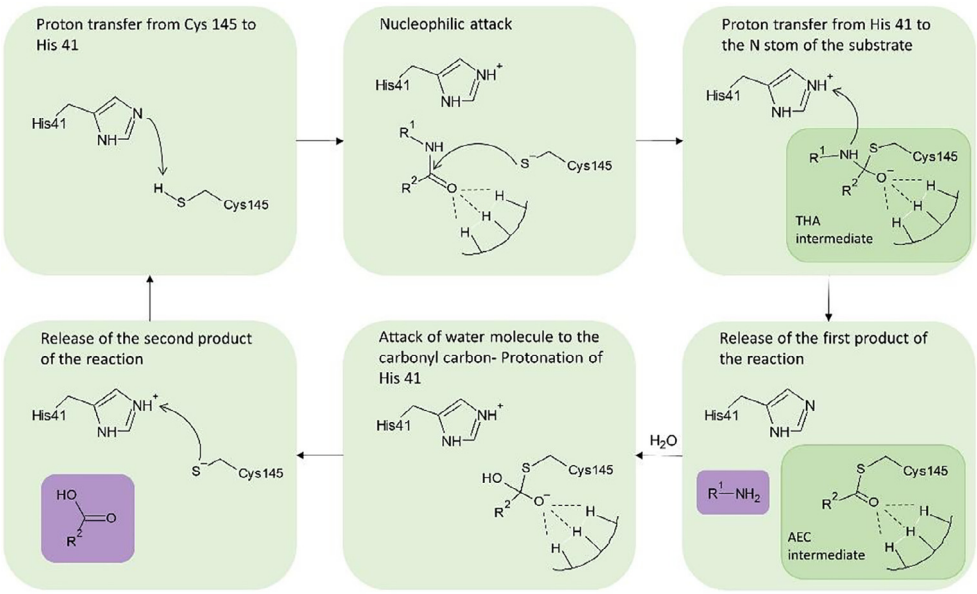

Fig. 2. Catalytic mechanism of SARS-CoV-2 M^{pro} as described by [13] (THA: thiohemiketal; AEC: acyl-enzyme complex). The two reaction products are highlighted in purple. (For interpretation of the references to colour in this figure legend, the reader is referred to the web version of this article.)

the NH_2-terminal of each protomer interacts with residue Glu166 of the other protomer and contributes to the formation of the S1 subsite of active site [17]. Due to this interaction, the NH_2-terminal of a monomer is positioned between domains II and III of this monomer and domain II of the other monomer. The dimeric structure of the enzyme is regulated through a salt-bridge between residues Glu 290 of one protomer and Arg4 of the other [15]. At its active site, the enzyme has a cysteine-histidine catalytic dyad (Cys145-His41). The existence of the stabilizing oxyanion hole, consisting of residues Gly143, Ser144 and Cys145, is also noteworthy. During catalysis, the negative charge of the carbonyl oxygen in the scissile bond of the natural substrate of the protease is being balanced by the oxyanion hole. It is also reported that the oxyanion hole similarly stabilizes inhibitors, as many of them form a hemithioacetal intermediate with a negatively charged oxygen atom and bind to the Cys145 residue of the protease with a similar geometry as the tetrahedral intermediate formed by the natural substrate [10,13,15]. Except for the catalytic dyad (Cys145, His41), the active site of M^{pro} is demarcated by residues Ser46, Gln189, Thr190, Ala191, Pro168, Glu166, Leu141 and Asn142 [16]. It consists of four main subsites, S1, S1′ S2 and S4, similar to the active sites of the main proteases of other coronaviruses [9,18]. More specifically, out of the 306 residues of the protease sequence, only 12 are different between the main proteases of SARS-CoV-2 and SARS-CoV, which corresponds to 96% identity [19].

The proposed catalytic mechanism of the enzyme is based on a reaction of nucleophilic addition (Fig. 2). The cleavage of the peptide bond is suggested to be initiated by a proton transfer from the thiol group of Cys145 to the imidazole of His41. Then, a highly reactive nucleophilic ion pair is formed. The Cys residue attacks the carbonyl portion of the scissile peptide bond, forming a thiohemiketal intermediate, while the protonated His attacks the N-atom of the peptide bond, creating the acyl-enzyme complex intermediate. A polypeptide chain is released as the first product of the reaction. Then, an active water molecule attacks the carbonyl carbon atom of the Gln residue, whereas His is being reprotonated, no longer maintaining the acyl-enzyme complex. Lastly, Cys145 is released, as the covalent bond with the peptide is broken. The water molecule taking part in the above series of reactions is also part of interactions between residues His41, His164 and Asp187, balancing the polar contacts between them. Kneller *et al.* have pointed out its role, characterizing it a part of a potential non-canonical catalytic triad [10].

3. Desired characteristics of SARS-CoV-2 M^{pro} inhibitors

In search of additional therapeutic routes, various compounds have been investigated for their ability to inhibit M^{pro}, including repurposed drugs or other coronavirus' main protease inhibitors, designed and optimized drug molecules, as well as natural compounds. Inhibition can occur through covalent binding of the inhibitor to the catalytic cysteine, through a mechanism of nucleophilic addition. In this case, the inhibitor often mimics the natural peptide substrate of the enzyme. Although such molecules have higher specificity towards the protease, their pharmacokinetic properties might pose a hindrance to their use as pharmaceuticals. There is also the possibility of non-covalent, reversible inhibitors, which usually have better pharmacokinetic properties and can be more efficiently used as drugs. However, it is more challenging to develop a non-covalent inhibitor, since the structure–activity relationship and the interactions with the protease, which lead to effective inhibition, are not based on the already available information provided by the natural substrate binding and the mechanism of the protease, as it happens in the case of peptide-like, covalent inhibitors. In the case of irreversible inhibitors, the design might be easier but the risk of toxicity due to low selectivity is concerning [20]. In order to establish the interactions that are required with the active site residues to consider a compound as inhibitor, a molecular dynamics study involved different inhibitors in complex with M^{pro} was performed and revealed that Glu166, His41, Gly143, Ser144 and Cys145 are major interacting residues [14].

In the case of covalent peptidomimetic inhibitors, a common way of approaching their structural analysis is through the system of nomenclature for the peptide substrates of proteases. According to this, substrate residues are numbered, beginning from the scissile bond, as P1′, P2′ etc., to the direction of the C-terminus and as P1, P2 etc. to the direction of the N-terminus (Fig. 3). The catalytic residues are located the between S1 and S1′subsites, so that they are accessible by the scissile bond [21]. Several inhibitors have been designed having a glutamine analog at the P1 position, but

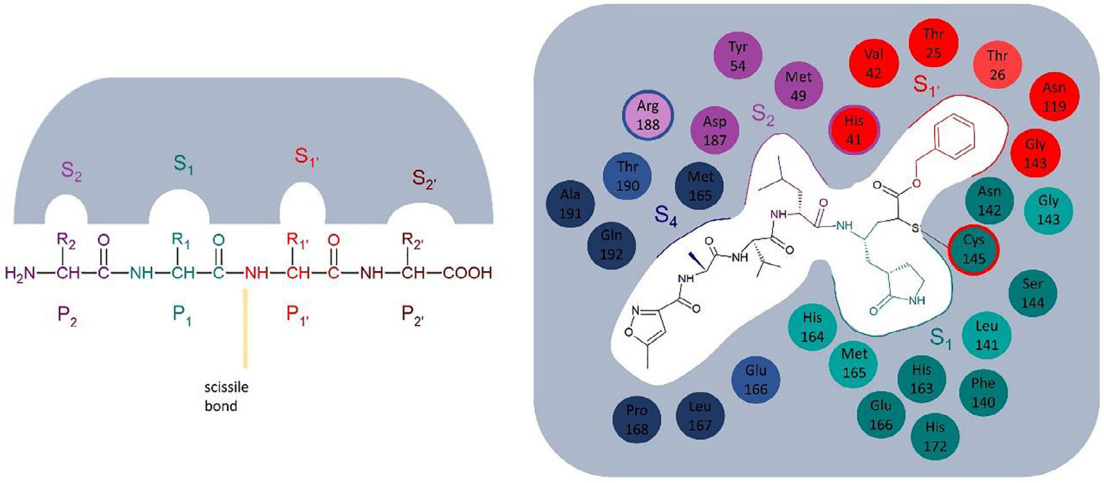

Fig. 3. Proteolytic enzyme substrate nomenclature. S2, P2 is marked in purple, S1-P1 in green, Sí-Pí in red and Sź-Pź in brown (left). Example of the binding of inhibitor N3 in the active site of M^{pro} (right). The residues that form each subsite, as described by [3], are shown in the respective colors. The light colors correspond to residues that contribute with their backbone to the formation of the subsite, while the darker colors to the ones that contribute with their side chain. The residues depicted in two colors are common between the two respective subsites. (For interpretation of the references to colour in this figure legend, the reader is referred to the web version of this article.)

research has provided indications that different, hydrophobic moieties can be used in this position [17]. This review includes various studies that have explored the effect of different functional groups in different positions, as well as the potency of different warheads in forming a covalent bond with the catalytic cysteine. An overview of the reported drug-like compounds to date demonstrated as inhibitors of M^{pro} is presented in Table 1. The inhibitors are categorized as covalent, non-covalent, allosteric, and inhibitors with non speficied binding mode.

4. Repurposed drugs and designed drug-like compounds as inhibitors of M^{pro}

4.1. Covalent M^{pro} inhibitors

Research has led to the identification of multiple compounds as M^{pro} inhibitors, which include both already known drugs, as well as compounds designed for the specific target. The co-crystallization structure of the inhibitors in complex with the enzyme proves that the majority of identified inhibitors bind covalently to the active site. The most dominant strategy in the design of such compounds is mimicking the native peptide substrate of the enzyme, and screening different functional groups to achieve the most favorable interactions. However, several smaller compounds have also been investigated. As mentioned above, due to the high conservation of the active site of the main proteases of various coronaviruses, many already tested inhibitors for SARS-CoV or other coronaviruses are also investigated against SARS-CoV-2.

4.1.1. Peptidomimetic inhibitors with a γ-lactam moiety in the P1 position

A common characteristic among numerous covalent inhibitors is the presence of a γ-lactam group in the P1 position. The carbonyl and the –NH groups of the lactam ring allow the formation of hydrogen bonds in the S1 subsite of the protease, therefore contributing to the reinforcement of the binding of the inhibitor. Most of these inhibitors also possess a carbonyl warhead, either as an aldehyde group or as part of a larger moiety, while they often have a *tert*-butyl group or another hydrophobic group in the P2 position.

N3 is such compound that successfully inhibits the protease, as it binds to its active site very similarly to the natural substrate. It is the most widely accepted inhibitor in literature, and the one most often used as a reference to evaluate the inhibitory effect of other compounds. It is a Michael acceptor, and acts as a time-dependent, irreversible inhibitor. Its 50% cytotoxicity concentration (CC_{50}) is reported to be>133 μM, whereas the half-maximal effective concentration (EC_{50}) is 16.77 μM. In the original publication that provided the crystal structure, the interactions between the enzyme and N3 are described in detail. More specifically, the inhibitor forms a 1.8 Å covalent bond with the sulfur atom of residue Cys145 of the protein. Moreover, N3 forms one hydrogen bond with each one of residues Gly143, His 163, His164, Gln189 and Thr190 and two hydrogen bonds with Glu166 [7].

GC376 is a broad-spectrum antiviralcompound, which is also often used as a reference for the evaluation of other potential inhibitors, due to its inhibitory potency and successful prevention of coronavirus infections in animals which sets a direction for clinical trials in humans [22]. It has a half-maximal effective concentration (EC_{50}) of 0.70 μM against SARS-CoV-2, which is very close to the approved anti-SARS-CoV-2 drug remdesivir (EC_{50} = 0.58 μM). In order for GC376 to form a covalent bond, its bisulfite group is removed. The compound forms one hydrogen bond with residues Phe140, Gly143, Cys145, His163, His164 and two with Glu166. It also interacts with the hydrophobic pocket residues Arg40, His41, Met49, Tyr54 and Asp187 [23]. Effective against SARS-CoV-2 is the parent compound of GC376, **GC373**. It shows no toxicity in cell culture and inhibits M^{pro} with a half-maximal inhibitory concentration (IC_{50}) value of 0.40 μM. The inhibition occurs through a reversible reaction of the thiol of Cys145 with the carbonyl of GC373 resulting in a hemithioacetal. The conformation of the inhibitor in the active site is stabilized with hydrogen bonds with the oxyanion hole residues Gly143, Ser144, Cys145. There is also one hydrogen bond formed with His163 and two with Glu166. There are also hydrophobic interactions present, both with S2 subsite residues His41, Met49 and S1 subsite residues Met165 and His172. [24].

Various derivatives exploring the potential of different substitutions in the P2 and P3 positions have been investigated in a study by Vuong *et al.* [24], where the compounds with the bisulfite moiety (similar to GC376) showed better inhibitory potency compared to the respective aldehydes (such as GC373). The derivatives that stand out are **inhibitors 2c and 2d**, where a cyclopropyl group has been introduced in the P2 position of both inhibitors, as it was proven to be the most favorable substitution and a 3-fluorobenzyl or a 3-chlorophenylethyl moiety, respectively, took

Table 1
Drug-like compounds with inhibitory effect against SARS-CoV-2 M^{pro} and their inhibitory properties.

Name	PDB ID	H-bonds	IC_{50} (μM)	Calculation method	EC_{50} (μM)	Calculation method	CC_{50} (μM)	Calculation method	Reference
Covalent inhibitors									
N3	6LU7	Gly143, His163, His164, Glu166, Gln189, Thr190	–	–	16.77	Plaque reduction assay	133	MTS cell proliferation assay in Vero E6 cells	[7]
GC376	7D1M	Phe140, Gly143, Cys145, His163, His164, Glu166	0.19	FRET–based assay	0.92	Plaque reduction assay	>200	CellTiter-Glo assay in Vero E6 cells	[24]
GC373	6WTK	Gly143, Ser144, Cys145, His163, Glu166	0.4		1.5		>200	CellTiter-Glo assay in Vero E6 cells	
Compound 2c	–	Not described	0.07		0.57		>200	CellTiter-Glo assay in Vero E6 cells	
Compound 2d	–	Not described	0.08		0.7		>200	CellTiter-Glo assay in Vero E6 cells	
Compound 2	7K0E	Phe140, His163, His164, Glu166, Gln189	0.18	FRET–based assay	0.086 / 0.069	Antiviral activity assay in Vero E6/ $A549^{+ACE2}$ cells	>100	Cytotoxicity assay in Vero E6 and CRFK cells	[25]
MPI1	7JPZ	Not described	0.100	Fluorescent peptide	>10	Virus-based microneutralization assay	–	–	[26]
MPI3	7JQ0	Asn142, Cys145, His163, Met165, Glu166, Gln189	0.0085	assay	>10	in Vero E6 cells	–	–	
MPI5	7JQ2	Not described	0.033		5/0.16–0.31	Virus-based microneutralization assay	–	–	
MPI8	7JQ5	Not described	0.105		2.5/0.16–0.31	in Vero E6/ $A549^{+ACE2}$ cells	–	–	
11a	6LZE	Cys145, His163, His164, Glu166	0.053	FRET–based assay	0.53	Plaque reduction assay	–	–	[9]
11b	6M0K	Cys145, His163, His164, Glu166	0.04		0.72		–	–	
UAWJ9-36–1	7LYH	Phe140, Asn142, Gly143, His163, Glu166	0.051	FRET–based assay	–	–	–	–	[27]
UAWJ9-36–3	7LYI	Phe140, Asn142, Gly143, His163, Glu166	0.054		–	–	–	–	
MI-23	7D3I	Phe140, Gly143, Cys145, His163, His164, Glu166	0.0076	FRET-based assay	–	–	>500	CCK8 assay	[18]
PF-00835231	–	His163, His164, Glu166	–	–	0.221/0.184	Antiviral assay in $A549^{+ACE2}$ cells	>10	CellTiter-Glo assay in $A549^{+ACE2}$ cells	[29,53]
PF-07321332	–	His163, Glu166, Gln189	–	–	0.0745/0.0779	CPE assay in Vero E6 cells/ Nanoluciferase reporter virus assay in $A549^{+ACE2}$ cells	>100 / > 3	Cytotoxicity assay in Vero E6 / $A549^{+ACE2}$ cells	[30]
5 h (YH-53)	7JKV/ 7E18	Gly143, Cys145, His164, Glu166, Gln189	0.0347[1]	Fluorogenic substrate enzyme inhibition assay	4.2	RNA-qPCR quantitative assay in VeroE6 cells	>100	RNA-qPCR quantitative assay in VeroE6 cells	[32,33]
SH-5	7E19	His41, Gly143, His163, Met165, Glu166, Gln189	0.0145[1]	Fluorogenic substrate enzyme inhibition	Blocked viral proliferation at	CPE assay in Vero cells	–	–	[32]
YH-71	–	Not described	0.0321[1]	assay	25 μM		–	–	
compound 4	7JT7/ 7JW8	Gly143, His163, Glu166, Gln189	0.151	Fluorescent peptide assay	2.88	CPE reduction assay in VeroE6 cells	>100	Cytotoxicity assays in Vero E6 cells	[34]
13b	6Y2G	His41, Phe140, Gly143, Ser144, Cys145, His163, Glu166	0.67	FRET-based assay	4–5	Antiviral activity assay in human Calu-3 lung cells		–	[15]
Boceprevir	7C6S	His41, Gly143, Cys145, His164, Glu166	5.4/ 1.59[2]	FRET–based assay	15.57	Plaque reduction assay		–	[23,35,36]
Narlaprevir	7JYC	His41, Asn142, Gly143, His164	16.11	FRET–based assay	7.23	Plaque reduction assay	>200	Cytotoxicity assay on Vero E6 cells.	[37]
Telaprevir	7K6D/ 6XQS	His41, Gly143, Ser144, His164, His166, Gln189	18	FRET–based assay	–	–	–	–	[10,18]
ABT-957	7AEH	Asn142, Gly143, Ser144, Cys145, His164	3	Fluorescent peptide assay	10	CPE assay on HIH7_mCherry cells	>10	Cytotoxicity assay in HUH7 cells	[39]

Table 1 (*continued*)

Name	PDB ID	H-bonds	IC_{50} (μM)	Calculation method	EC_{50} (μM)	Calculation method	CC_{50} (μM)	Calculation method	Reference
Calpain inhibitor II	–	Not described	0.97	FRET-based assay	2.07/3.70	CPE assay/ secondary viral yield reduction assay in Vero 76 cells	>100	Cytotoxicity CPE assay on A549, MDCK, HCT-8 and Caco-2 cells	[38]
Calpain inhibitor XII	–	His163, Glu166	0.45	FRET-based assay	0.49/0.78	CPE assay/ secondary viral yield reduction assay in Vero 76 cells	>100	Cytotoxicity CPE assay on A549, MDCK, HCT-8 and Caco-2 cells	[38,56]
Mg-132	7BE7	Not described	0.36	CPE assay in Vero E6 cells	–	–	2.9	Vero E6 imaging assay	[40]
Calpeptin	7AKU	His164, Glu166	–	–	0.072	Antiviral activity assay in vero E6 cells	>100	CCK8 assay in Vero E6 cells	[41]
SDZ-224015	–	Nor described	30	Fluorescent peptide assay	100	CPE assay on HIH7_mCherry cells	>100	Cytotoxicity assay in HUH7 cells	[39]
Rupintrivir	7L8I	Not described	68	FRET–based assay	34.08/ 25.38	Viral titer reduction assay on Vero E6/ Huh7 cells	>100	CCK8 assay in Vero E6 and Huh7 cells	[42,43]
Z-VAD(OMe)-FMK	7CUT	Not described	0.59	FRET–based assay	1.88	Antiviral assay on Vero E6 cells	>300	Cytotoxicity assay in Vero E6 cells (CCK8)	[45]
Z-DEVD-FMK	–	Not described	2.8		0.87		>300		
Z-IETD-FMK	–	Not described	1.61		0.64		>300		
Tolperisone	7ADW	His163	–	–	19.17	Antiviral activity assay in vero E6 cells	>100	CCK8 assay in Vero E6 cells	[41]
2-[β-(4-hydroxyphenyl)-ethylaminomethyl]-tetralone (HEAT)	6YNQ	His163	–	–	24.05		55.42		
Isofloxythepin	7AY7	His163	–	–	4.8		17		
Triglycidyl isocyanurate	7AQJ	Gly143, Gln166, His163	–	–	30.02		>100		
Quipazine maleate	7AHA	Asn142, Gly143, Cys145	–	–	31.64		>100		
MAC-5576	7JT0	–	0.081	Fluorescent peptide assay	–	–	>100	Cytotoxicity assays in Vero E6 cells	[34]
Ebselen	7BFB/ 7BAK	His41, Cys145	0.67	FRET-based cleavage assay	4.67	Plaque reduction assay	–	–	[142]
MR6-7–2	–	Not described	0.363	FRET–based assay	4.5	Antiviral activity assay on Vero E6 cells	–	–	[47]
MR6-18–4	–	Not described	0.345		3.74		–	–	
MR6-31–2	7BAL	His41, Cys145	0.824		1.78		–	–	
Carmofur	7BUY	Gly143, Cys145	1.82	FRET-based cleavage assay	24.3	qRT-PCR assay in Vero E6 cells	133.4	Cytotoxicity assays in Vero E6 cells	[48]
Compound 7d	–	Not described	0.073	FRET–based assay	15	CPE assay on Vero E6 cells	–	–	[49]
Compound 1	–	Not described	0.25		2.8		>100	not specified	
x2754 (PG-COV-34)	5RHF	Not described	–	–	–	–	–	–	[50]
x2705	5RH7	Not described	–	–	–	–	–	–	
Nelfinavir	–	Not described	234	FRET–based assay	–	–	–	–	[42]
Bedaquiline	–	Thr26, Gly143, Glu166	18.7	FRET–based assay	–	–	–	–	[35]
Manidipine	–	Cys145	4.81	FRET–based assay	–	–	–	–	
Lercanidipine	–	Not described	16.2		–	–	–	–	
Non-covalent inhibitors									
Perampanel	–	Not described	100–250	FRET-based assay	–	–	–	–	[35]
Compound 2	–	His163, Glu166,	10	FRET–based assay	–	–	–	–	[53]
Compound 3	–	Thr26, His163, Glu166	6.4		–	–	–	–	
Compound 4	7L10	Cys145, His163, Glu166	4		–	–	–	–	
Compound 21	7L13	Not described	0.018		11.3	Viral plaque assay in Vero E6 cells	1.7	MTT dye assay in Vero E6 cells	
Compound 5	7L11	Gly143, His163, Met165	0.14	FRET-based assay	1.5	Plaque reduction assay	22	MTT dye assay in Vero E6 cells	[52]
Compound 26	7L14	Not described	0.17		0.98		>100		
ML 188	7L0D	Gly143, His163, Glu166	2.5	FRET–based assay	–	–	–	–	[54,56]
ML300	7LME	Ser46, Cys145, His163, Glu166	4.99	FRET–based assay	19.9	CPE inhibition assay in Vero E6 cells	–	–	[55]
Compound 41 (CCF0058981)	–	Not described	0.068		0.497		>50	CPE inhibition assay in Vero E6 cells	

(*continued on next page*)

Table 1 (*continued*)

Name	PDB ID	H-bonds	IC_{50} (μM)	Calculation method	EC_{50} (μM)	Calculation method	CC_{50} (μM)	Calculation method	Reference
23R (Jun8-76-3A)	7KX5	Gly143, His163	0.2	FRET–based assay	1.27	Antiviral activity assay in vero E6 cells	>100	Cytotoxicity assays in Vero E6 cells	[56]
MUT056399	7AP6	Phe140, His163	–	–	38.24	Antiviral activity assay in vero E6 cells	>100	CCK8 in Vero E6 cells	[41]
F01	7P51	Cys145, His163, Glu166	54	FRET–based assay	150	Antiviral activity assay in vero-81 cells	>400	Cytotoxicity assays in Vero-81 cells	[57]
Zinc acetate	–	–	325.1	Enzyme inhibition assay	3.28	Antiviral activity assay in vero E6 cells	–	–	[58]
Zinc glycinate	7DK1	–	279.4		No activity		–	–	
Zinc gluconate	–	–	405.3		No activity		–	–	
Mcule-5948770040	7LTJ	–	–	–	–	–	–	–	To be published
x77	6 W63	–	–	–	–	–	–	–	To be published
x0104	5R7Z	Not described	–	–	–	–	–	–	[50]
x0161	5R80	Not described	–	–	–	–	–	–	
x0397	5RGI	Not described	–	–	–	–	–	–	
Allosteric inhibitors									
Pelitinib	7AXM	–	–	–	1.25	Antiviral activity assay in vero E6 cells	13.96	CCK8 in Vero E6 cells	[41]
AT7519	7AGA	Gln110, Asp153	–	–	25.16		–		
Ifenprodil	7AQI	–	–	–	46.86		>100		
RS-102895	7ABU	Asn142	–	–	19.8		54.98		
PD-168568	7AMJ	–	–	–	–	–	–	–	
Tofogliflozin	7APH	–	–	–	–	–	–	–	
Inhibitors with unspecified binding mode									
Ciprofloxacin	–	Met49, Cys145, Met165, Glu166	5.13	3CLpro antiviral assay	50.07 nM	qPCR viral load reduction assay on Vero cells	>16	MTT assay in Vero cells	[143]
7-(4-(N-substituted carbamoyl methyl) piperazin-1 yl)-chalcone	–	Gly143, Cys145	0.6		3.93 nM		>16		
Pimozide	–	Not described	42	FRET–based assay	–	–	–	–	[42]
Ebastine	–	Not described	57		–	–	–	–	
Bepridil	–	Not described	72		0.86/0.46	Live virus-based microneutralization assay in Vero E6 and human A549/ACE2 cells	–	–	
Seraconazole	–	Not described	76		–	–	–	–	
Rimonabant	–	Not described	85		–	–	–	–	
Oxiconazole	–	Not described	99		–	–	–	–	
Itraconazole	–	Not described	111		–	–	–	–	
Tipranavir	–	Not described	180		–	–	–	–	
Zopiclone	–	Not described	349		–	–	–	–	
Trihexyphenidyl	–	Not described	370		–	–	–	–	
Saquinavir	–	Not described	411		–	–	–	–	
Isavuconazole	–	Not described	438		–	–	–	–	
Lopinavir	–	Not described	486	FRET–based assay	12.01/ 7.79	Viral titer reduction assay on Vero E6/ Huh7 cells	80.82/ 64.43	CCK8 assay in Vero E6/ Huh7 cells	[42,43]
Clemastine	–	Not described	497	FRET–based assay	–	–	–	–	[42]
Metixene	–	Not described	635		–	–	–	–	
Duloxetine	–	Not described	3047		–	–	–	–	
Efonidipine	–	Not described	38.5	FRET–based assay	–	–	–	–	[35]
ALG-097111	–	Not described	0.007	Biochemical enzyme assay	0.2	Antiviral activity assay in $A549^{+ACE2}$	>100	Cytotoxicity assay in A549 cells	[59]
Ritonavir	–	Not described	–	–	19.88/ 11.68	Viral titer reduction assay in Vero E6/ Huh7 cells	94.71/ 83.73	CCK8 assay in Vero E6/ Huh7 cells	[43]
Ag7404	–	Not described	–	–	195.8/ 92.55	Viral titer reduction assay in Vero E6/ Huh7 cells	>400/ >400	CCK8 assay in Vero E6/ Huh7 cells	[43]

[1] : Inhibition constant K_i [2]: Different sources provide different IC_{50} values.

the place of the benzyl ring in the P3 position. The IC_{50} values for the designed molecules were >2-fold lower than the parent compound GC376 (0.07 and 0.08 μM respectively, as opposed to 0.19 μM for GC376 in the same assay). Deuterated derivatives of GC376 have been tested *in vitro* and *in vivo* in mice and showed improved inhibitory activity compared to GC376.

Sodium (2S)-1-hydroxy-2-((S)-4-methyl-2-(((phenylmethoxyd2)carbonyl)amino)pentanamido)-3-((S)-2-oxopyrrolidin-3-yl)propane-1-sulfonate, mentioned as compound 2 in the respective study, displayed a slightly enhanced IC_{50} value, as low as 0.18 μM. Significantly higher inhibition of viral replication in Vero E6 and A549-ACE2 cells was observed, since the EC_{50} values occurring from the respective antiviral assays were equal to 0.086 and 0.069 μM, respectively. Moreover, the cytotoxicity of the compound was low, as the CC_{50} value occurring from cytotoxicity assays in Vero E6 and CRFK cells was >100 μM [25].

Yang *et al.* [26] designed a series of β-(S-2-oxopyrrolidin-3-yl)-alaninal (Opal)-based reversible covalent inhibitors, which include dipeptidyl and tripeptidyl compounds. Their design resembles inhibitor GC376. Both dipeptidyl compounds named **MPI1** and **MPI2** showed an IC_{50} value approximately 100 nM, as opposed to 31 ± 4 nM for GC376, while the tripeptidyl structures yielded more encouraging results, with the most prominent compounds being **MPI3**, **MPI4** and **MPI5** with IC_{50} values as low as 8.5 ± 1.5, 15 ± 5 and 33 ± 2 nM respectively. The highest IC_{50}, calculated via a fluorescent peptide assay, was 105 ± 22 nM for compound **MPI8**, which, however, showed good inhibition of M^{pro} in further *in vitro* investigation in Vero E6 cells. More specifically, compounds MPI5, MPI7 and MPI8 inhibited the protease more efficiently than GC376, completely blocking SARS-CoV-2 induced cytopathogenic effect (CPE) at concentrations of 5–2.5 μM, compared to 10 μM for GC376. When further tested in A549/ACE2 cells, which are considered more suitable to test the SARS-CoV-2 inhibitors than Vero E6 cells, as they can be used to more accurately resemble human respiratory tract infection, MPI5 and MPI8 completely hindered CPE at concentrations of 160–310 nM, considerably lower than inhibitor 11a, which has the same effect at concentration of 5 μM. Overall, observation of the interactions of the various designed inhibitors with the active site concludes that the leucine residues in the P2 position results in more favorable binding [26].

Two other covalent inhibitors are **11a** and **11b**, that both are covalently bound to the S-atom of Cys 145, with a 1.8 Å bond. The enzyme-inhibitor complex is further stabilized with a hydrogen bond between the oxygen of the aldehyde group of 11a and 11b and Cys145. Additionally, they both form one hydrogen bond with Phe140, His163 and His164 and three with Glu166. Inhibitor 11b contains an F-atom that forms an additional hydrogen bond with Gln189. The cyclohexyl group of 11a inserts the hydrophobic pocket that makes up the S2 subsite, showing hydrophobic interactions with residues His41, Met49, Tyr54, Asp187 and Arg188. The indole moiety of the inhibitor also interacts hydrophobically with Pro168 and Gln189. As for 11b, the 3-fluorophenyl group interacts with the active site similarly to the cyclohexyl group of 11a, forming hydrophobic interactions with residues His41, Met49, Met165, Val186, Asp187 and Arg188. An important role in the stabilization of the inhibitors is played by some water molecules, which form hydrogen bonds with both 11a/11b and the residues of the binding cleft. At a concentration of 1 μM, 11a and 11b exhibited 100% and 96% inhibitory activity, respectively. Moreover, the IC_{50} values are promising, equaling 0.053 ± 0.005 μM for 11a and 0.040 ± 0.002 μM for 11b. Between the two inhibitors, results showed that 11a has a greater potential to act as an antiviral compound [9].

Xia *et al.* [27] have used superposition of the crystal structures of inhibitors GC376, telaprevir and boceprevir to design two novel hybrid inhibitors, which combine the chemical groups of their parent compounds that result in the most interactions and most favorable binding. The designed inhibitors are **UAWJ9-36–1**, as a hybrid of GC376 and telaprevir, and **UAWJ9-36–3**, as a hybrid of GC376 and boceprevir. Their inhibitory effect was evaluated via a fluorescence resonance energy transfer (FRET)-based enzyme inhibition assay, which resulted in IC_{50} values of 0.051 and 0.054 μM, slightly higher that the respective value calculated for GC376 in the same assay (0.041 μM). To confirm the inhibitory activity of the compounds in a cellular environment, a Flip-GFP assay was used. The calculated IC_{50} value for UAWJ9-36–1 was 11.10 μM, while for UAWJ9-36–3 was 3.40 μM. The latter exhibited greater inhibitory effect than GC376, for which IC_{50} was calculated 4.83 μM in this assay. The synthesized compounds displayed inhibitory effect against the main proteases of other coronaviruses as well, including SARS-CoV, MERS-CoV, HCoV-OC43, HCoV-229E, HCoV-NL63 and HCoV-HKU1. Therefore, they reveal a path towards the development of broad-spectrum antivirals.

Another potent compound is **MI-23**, which has been designed based on telaprevir and exhibits IC_{50} = 7.6 nM. It forms the characteristic 1.8 Å covalent bond with Cys145 and additionally hydrogen bonds with Phe140, Gly143, Cys145, His163, His164 and Glu166. The bicycloproline moiety is located in the hydrophobic S2 subsite, having hydrophobic interactions with residues His41, Met49, Met165, Leu167, Pro168, Asp187, Arg188 and Gln189 [18].

PF-00835231 and its phosphate prodrug **PF-07304814**, is the first anti-M^{pro} compound to proceed to clinical trials. PF-00835231 has been investigated *in vitro* and *in vivo*, providing indications of anti-SARS-CoV-2 activity, as well as synergistic effect with the FDA-approved drug remdesivir. A thermal-shift assay showed high affinity and specificity in the binding of PF-00835231 to M^{pro}, while a FRET protease activity assay revealed inhibitory effect of the compound against various types of coronaviruses. Evaluation of the antiviral effect of the compounds in cells via the CPE assay yielded encouraging results, with EC_{50} values equal to 0.23 μM in VeroE6–enACE2 cells and 0.76 μM in VeroE6-EGFP cells. This study was performed in the presence of the efflux transporter P-glycoprotein inhibitor, as the glycoprotein is expressed in Vero cells and PF-00835231 inhibits its action. Therefore, without the glycoprotein inhibitor, the concentration of the compound available to bind to M^{pro} would be lower than the desired one [28]. A different study, however, points out that the effect of the glycoprotein is minimal in airway epithelial cells, which are mostly infected by SARS-CoV-2 [29]. The same study included a comparative assay performed on $A549^{+ACE2}$ cells infected with two clades of SARS-CoV-2, where PF-00835231 showed better antiviral properties compared to RdRp inhibitor remdesivir. For clade A, the EC_{50} value calculated at 24 h post infection was equal to 0.221 μM for PF-00835231, as opposed to 0.442 μM for remdesivir, while the respective values for clade B were 0.184 and 0.283 μM. In a different cell assay, comparing the viral inhibition of PF-00835231 with that of GC376, the former exhibited again more promising properties, with EC_{50} values equal to 0.422 and 0.326 μM for clades A and B at 24 h post infection, compared to 0.632 and 0.529 μM for GC376 [29]. Lastly, it is worth mentioning that pharmacokinetic studies performed in rats and monkeys indicate short elimination-half life and limited oral bioavailability of the compound, suggesting that intravenous administration would be more efficient.

PF-07321332 is another highly potent M^{pro} inhibitor, which has been designed for optimized oral bioavailability and has also been subjected to clinical trials. It covalently and reversibly binds to the catalytic cysteine through its nitrile warhead, also forming hydrogen bonds with residues His163, Glu166 and Gln189. Its inhibitory effect has been quantified through the CPE assay in Vero E6 cells, the nanoluciferase reporter virus assay in A549-ACE2 cells and the viral titer reduction assay in differentiated normal human bronchial epithelial (dNHBE) cells. The assays resulted in EC_{50} val-

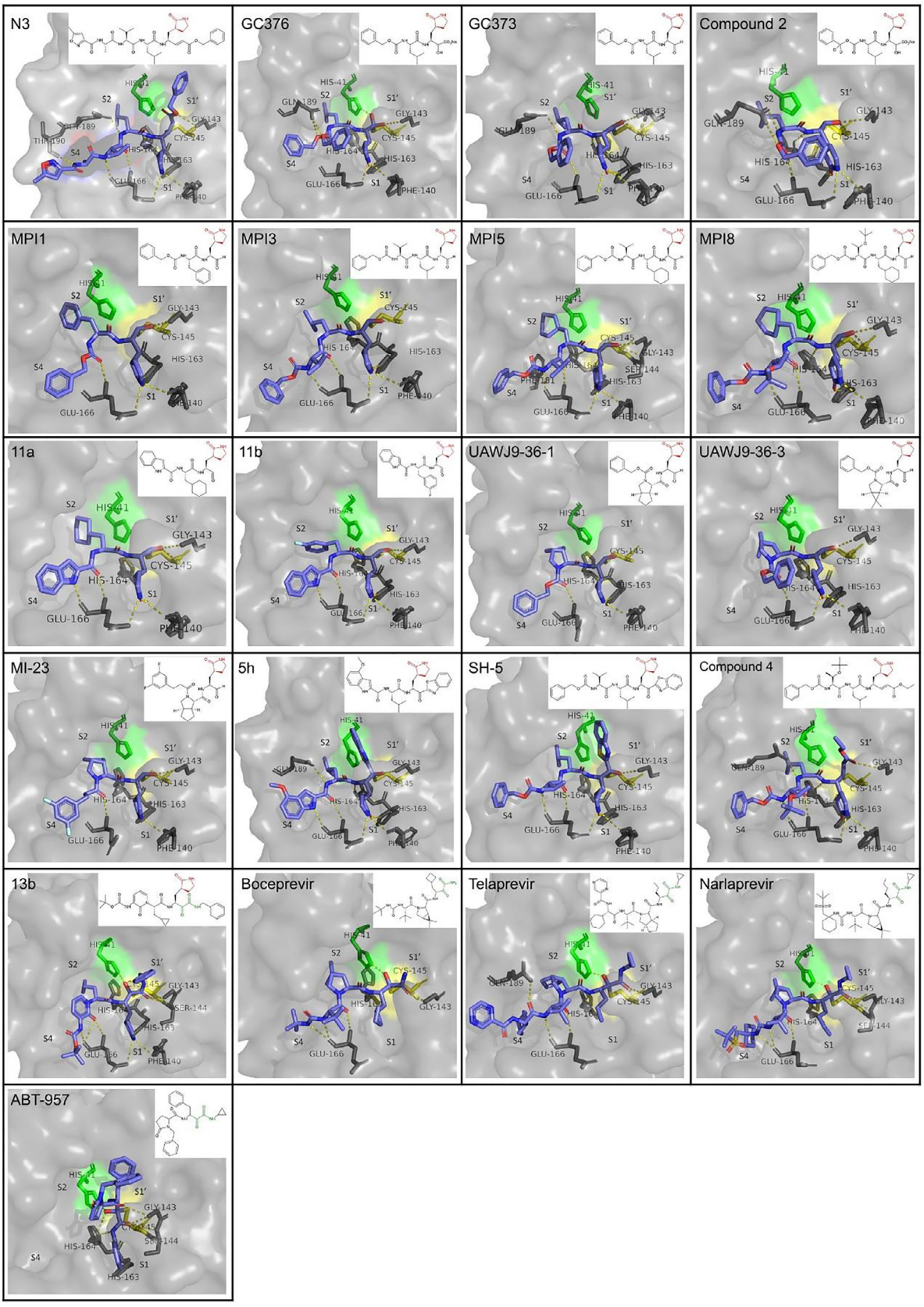

Fig. 4. Binding mode and structure of covalent peptidomimetic inhibitors with a γ-lactam (colored red) or α-ketoamide (colored dark green) moiety, based on available co-crystallization PDB structures in the active site of SARS-CoV-2 M^{pro}. Catalytic residues are colored (His41: green, Cys145: yellow). Important residues for binding are shown in sticks and hydrogen bonds are depicted as yellow dashes. The PDB ID for each inhibitor is indicated in Table 1. (For interpretation of the references to colour in this figure legend, the reader is referred to the web version of this article.)

ues of 74.5, 77.9 and 61.8 nM respectively, while the compound cytotoxicity was considerably lower in Vero E6 compared to A549-ACE2 cells (CC_{50} > 100 μM and CC_{50} > 3 μM, respectively). A FRET-based assay allowed measurement of its inhibition constant against M^{pro} (K_i = 2.5 nM), while also providing indications of its inhibitory effect against the main proteases of other known alpha and beta-coronaviruses, including SARS-CoV-1, HKU1, OC43, MERS, 229E and NL63 [30,31].

A tetrapeptide inhibitor of SARS-CoV-1 has been the basis for the design of peptide-like derivatives with an aryl (and more specifically benzothiazolyl) ketone warhead through which they covalently bind to the sulfur atom of Cys145 of SARS-CoV-2 M^{pro}. Three such compounds with very similar structures (having a benzothiazole in the P1′ position, a pyrrolidine-2-one in the P1 position and an isobutyl group in the P2 position) have been investigated, namely **SH-5**, **YH-53** and **YH-71**. The compounds inhibit both SARS-CoV-1 and SARS-CoV-2. The P1 group of the inhibitors interacts with residues His163 and Glu166 of SARS-CoV-2 M^{pro} through its carbonyl and amide groups, while the benzothiazole facilitates the formation of a hydrogen bond with His41. Particularly in the case of YH-53, its P2 amide forms a hydrogen bond with Gln189, resulting in a tighter binding. A fluorogenic substrate enzyme inhibition assay allowed the calculation of the K_i values for the three compounds which were 14.5, 34.7 and 32.1 nM, respectively. In addition, the compounds hindered viral replication in Vero E6 cells at concentrations of 25, 10 and 25 μM while showing low cytotoxicity. The activity of YH-53 was reinforced in the presence of CP-100356, an MDR-1 efflux transporter inhibitor. Its favorable safety and toxicity profile also encourages its development as a candidate drug. However, it should be noted that its bioavailability in rats was estimated to be as low as 3.6%. Apart from that, in all the inhibitors of this category, the concentrations at which significant antiviral activity in cells was observed deviated from the respective concentrations for enzyme inhibition, indicating a difficulty in cell entry or maintenance of a high intracellular concentration of the molecules [32].

YH-53 emerged as the most potent among other known protease inhibitors in the study Hattori *et al.* [33] as well, under the name "**compound 5 h**". The compound showed an EC_{50} equal to 4.2 ± 0.7 μM, while exhibiting low cytotoxicity with a CC_{50} value>100 μM. It is reported to form a reversible covalent bond with Cys145, via the same nucleophilic addition mechanism that other covalent inhibitors exhibit. More specifically, the sulfur atom of Cys145 attacks the carbonyl carbon next to the benzothiazole of 5 h. 5 h forms two hydrogen bonds with Glu166, and one with each one of Gly143, Cys145, His164 and Gln189. Also in this case, there are several water molecules that form hydrogen bonds with the inhibitor and the active site residues acting as intermediates and stabilizing the interactions between them. In addition, van der Waals interactions between the hydrophobic residues Leu27, Met49, Phe140, Met165, Ala191 and the inhibitor improve its binding affinity.

Another molecule that displayed successful inhibition of M^{pro} is **4-[2-(2-Benzyloxycarbonylamino-3-*tert*-butoxy-butyrylamino)-4-methyl-pentanoylamino]-5-(2-oxo-pyrrolidin-3-yl)-pent-2-enoic acid ethyl ester (designated compound 4)**. It is a peptidomimetic molecule, which binds to Cys145 through Michael addition and blocks subsites S1 and S2. An IC_{50} of 151 ± 15 nM was calculated in a fluorogenic peptide substrate enzymatic activity assay. The compound also hindered viral replication in Vero-E6 cells, as resulted from a cytopathic effect reduction assay from which an EC_{50} value of 2.88 ± 0.23 μM was derived [34].

4.1.2. Peptidomimetic inhibitors with an a-ketoamide moiety

Another structural characteristic observed in several inhibitors is the α-ketoamide warhead, whose one of the carbonyls forms a covalent bond with the catalytic cysteine. Alpha-ketoamide **13b** is such a compound that also possesses a butyrolactam group in its P1 position. It has been found to covalently inhibit SARS-CoV-2 with IC_{50} = 0.67 ± 0.18 μM and EC_{50} = 4–5 μM. Its conformation in the binding site is further stabilized by six hydrogen bonds with residues His41, Phe140, Gly143, Ser144, Cys145, His163 and three hydrogen bonds with Glu166 [15].

Boceprevir was originally identified as a hepatitis C virus protease inhibitor and has been FDA-approved, therefore it has known toxicity and pharmacokinetic properties. It can effectively inhibit M^{pro}, as quantified by the IC_{50} value of 5.4 μM [35], while also limiting viral replication with an EC_{50} value of 15.57 μM. A different study on boceprevir reports a lower IC_{50} value of 1.59 μM, also calculated via a FRET-based assay [36]. The keto carbon of boceprevir is the atom that takes part in the covalent bond formation. There are also hydrogen bonds formed with residues His41, Gly143, Cys145, His164 and Glu166. In particular, Glu166 forms three hydrogen bonds with boceprevir. Hydrophobic interactions between the inhibitor and the enzyme are mostly found in subsites S2 and S4, and more specifically with residues Met149, Met165, Asp187, Gln189, Thr190 and Gln192 [23].

Narlaprevir is also a potent antiviral compound, with an IC_{50} value of 16.11 μM and EC_{50} value of 7.23 μM. According to literature, except for the covalent bond, it creates four hydrogen bonds with residues His41, Asn142, Gly143 and His164 and three hydrogen bonds with Glu166. It also interacts with residues Leu141, Ser144, Met165, Pro168 and Gln192 [37]. Binding to the active site of SARS-CoV-2 M^{pro} in a very similar way to narlaprevir and boceprevir, peptidomimetic compound **telaprevir** acts as an effective inhibitor, with an IC_{50} of 18 μM [10]. More specifically, apart from the covalent bond with Cys145, telaprevir forms direct hydrogen bonds with His41, Gly143, Ser144, His164, His166 (with which there are two interactions) and Gln189. There is also shown to be a water-mediated hydrogen bond with Gln192, as well as pi-pi interactions with residues Thr190 and Ala 191 [18].

Calpain inhibitor XII is a cysteine protease inhibitor that exhibited an IC_{50} of 0.45 μM and an EC_{50} of 0.49 μM in a FRET-based and a CPE assay, respectively. A secondary viral yield reduction assay resulted in the calculation of an additional EC_{50} value, equal to 0.78 μM, while the compound also showed low cytotoxicity [38]. Another compound with an α-ketoamide group is a derivative of calpain 1 & 2, inhibitor **ABT-957** [39]. It stands out due to its better pharmacokinetic properties and lower cytotoxicity compared to the other tested compounds, but it has a higher IC_{50} value of 3 μM, while other hits of the same study that will be mentioned below achieve inhibition at nanomolar levels.

A summary of the binding mode and structure of the peptidomimetic inhibitors that include γ-lactam and/or a a-aketoamide moiety described above is presented in Fig. 4.

4.1.3. Other peptide-like inhibitors

Apart from the previously mentioned calpain inhibitor XII, **calpain inhibitor II** also showed great potential in the inhibition of SARS-CoV-2 M^{pro}, inhibiting the protease with an IC_{50} value of 0.97 using a FRET-based assay. The evaluation of its antiviral activity yielded EC_{50} values of 2.07 and 3.70 in a CPE and a secondary viral yield reduction assay respectively, both in Vero 76 cells. Moreover, it demonstrated low cytotoxicity (CC_{50} > 100 μM) [38]. Compound **MG-132** is a reversible M^{pro} inhibitor (IC_{50} = 0.36 μM, CC_{50} = 2.9 μM), that also inhibits other cysteine proteases. Its relatively large size allows effective blocking of the subsites of the protein. Although it shows very effective inhibition of the protease, its high cytotoxicity poses a concern to its use a pharmaceutical compounds [40]. Another peptidomimetic compound that has a comparable structure and binds in a similar manner to the binding site of M^{pro} is **calpeptin.** When in contact with the protease,

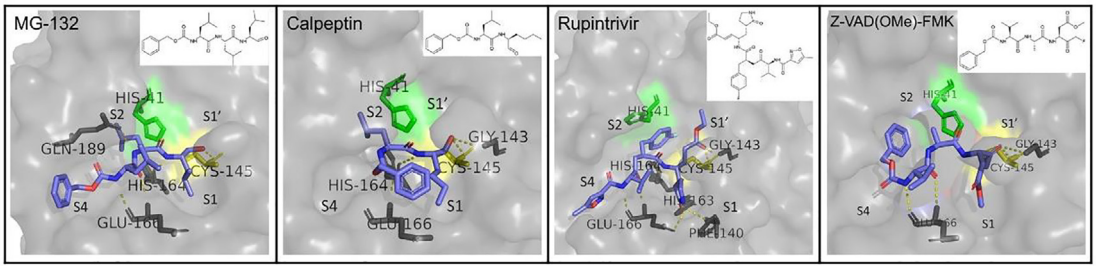

Fig. 5. Binding mode and structure of other covalent peptidomimetic inhibitors with available co-crystallization PDB structures in the active site of SARS-CoV-2 M^{pro}. Catalytic residues are colored (His41: green, Cys145: yellow). Important residues for binding are shown in sticks and hydrogen bonds are depicted as yellow dashes. The PDB ID for each inhibitor is indicated in Table 1. (For interpretation of the references to colour in this figure legend, the reader is referred to the web version of this article.)

Cys145 attacks its aldehyde group to form a thiohemiacetal intermediate. The compound forms two hydrogen bonds, with residues His164 and Glu166. In addition, Van der Waals forces are developed between calpeptin and residues Phe140, Leu141 and Asn142. Due to these interactions, the inhibitor successfully blocks part of the active site, showing an EC_{50} value of 72 nM and CC_{50} value>100 μM [41].

Emerging from the high throughput screening (HTS) of a library of compounds approved for investigation in humans, **inhibitor SDZ-224015** is an irreversible covalent inhibitor that reacts with the catalytic cysteine. It includes three ester groups, one of which is cleaved *in vivo* by esterases, leading to the formation of a metabolite which, however, has lower potency against M^{pro} inhibiting viral replication in HUH7_mCherry cells by 50% at 100 μM, as opposed to 10 μM by its prodrug. The HTS assay resulted in an IC_{50} of 30 nM for SDZ-224015 [39].

Rupintrivir is a compound designed to inhibit 3C-proteases, having a lactone moiety in the P1 position that plays an important role in binding to the active site. Specifically against SARS-CoV-2 M^{pro}, rupintrivir demonstrated low inhibition, with an IC_{50} value of 68 μM [42]. A different study reports IC_{50} values of 34.08 and 25.38 μM in viral titer reduction assays using Vero E6 and Huh7 cells, respectively, as well as a CC_{50} value>100 μM, as determined by the CCK8 assay in both cell types [43]. Lockbaum *et al.* [44] point out an interesting binding conformation of rupintrivir, which reveals an alternative mechanism of inhibition. Its fluorophenylalanine group, which normally occupies the S2 subsite in complexes of the molecule with other proteases, turns to the S1′ subsite, acting as an obstacle between the two catalytic residues. However, other works characterize rupintrivir as a non-potent antiviral, due to its relatively high IC_{50} and reported side effects in clinical trials [38]. An analogue of rupintrivir with enhanced oral bioavailability is AG7404. It inhibits viral replication in Vero E6 and Huh7 cells with IC_{50} values of 195.8 and 92.55 μM respectively, while also showing low cytotoxicity in both cell types (CC_{50} > 400 μM) [43].

Caspase inhibitors also form another category of repurposed molecules that have been investigated and successfully inhibit M^{pro}. The ones standing out possess a fluoromethylketone (FMK) moiety, which serves as a warhead for their covalent binding to the catalytic cysteine, as well as a non-bulky group in the P2 position. Three potent inhibitors identified include compounds **Z-VAD (OMe)-FMK**, **Z-DEVD-FMK** and **Z-IETD-FMK**, whose activity against SARS-CoV-2 and cytotoxicity were evaluated through a FRET-based enzyme inhibition assay and antiviral assay on Vero cells. Z-VAD(OMe)-FMK showed an IC_{50} value of 0.59 μM and an EC_{50} of 1.88 μM, Z-DEVD-FMK demonstrated an IC_{50} value of 2.80 μM and an EC_{50} of 0.87 μM, while Z-IETD-FMK IC_{50} showed the IC_{50} value of 1.61 μM and an EC_{50} equal to 0.64 μM. All three compounds displayed low cytotoxicity (CC_{50} > 300 μM) [45]. A summary of the binding mode and structure of the peptidomimetic inhibitors described in this paragraph is presented in Fig. 5.

4.1.4. Small non-peptidic covalent inhibitors

The same study that reports calpeptin as an M^{pro} inhibitor reported five other potent small compounds, which covalently bind to the active site of the protease [41]. These include **tolperisone**, **2-[β-(4-hydroxyphenyl)-ethylaminomethyl]-tetralone (HEAT)**, **isofloxythepin**, **triglycidyl isocyanurate** and **quipazine maleate**, for which EC_{50} values were 19.17, 24.05, 4.8, 30.02 and 31.64 μM. The CC_{50} was estimated to be higher than 100 μM for all the compounds, with the exception of HEAT and isofloxythepin, for which it was 55.42 and 17.00 μM, respectively. It is also noteworthy that triglycidyl isocyanurate shows indications of both covalent and non-covalent binding modes, inhibiting similar subsites of the active site (S1′, S1 and S2).

Another non-peptidomimetic, small molecule with anti-SARS-CoV-2 M^{pro} activity is **MAC-5576**, which covalently binds to the catalytic cysteine of the protease in a non time-dependent manner. It demonstrated a lower IC_{50} value and equal to 81 ± 12 nM when compared to GC376 and compound 4, but did not show significant reduction of viral replication in Vero-E6 cells. The compounds showed no cytotoxicity in the tested concentrations (up to 100 μM). Overlay of the binding modes of the above mentioned inhibitors, as well as other previously mentioned inhibitors, such as GC376, 11a, 11b and N3, provides indications that the design of an effective inhibitor could initially focus in strong interactions with S1, S2 and/or S1′ subsites, and then be optimized to establish contacts with other parts of the active site [34].

Ebselen is an auspicious organoselenium drug molecule worth mentioning, as it inhibits the protease with an IC_{50} of 0.67 μM and hinders viral replication with an EC_{50} of 4.67 μM, while also exhibiting very low cytotoxicity. In the case of ebselen, covalent inhibition, which occurs by the creation of a bond between the selenium atom of the molecule and the thiol group of Cys145, is reinforced by its non-covalent interaction with the active site residues, which are however not described in detail [7,46]. Moreover, derivatives of ebselen have been investigated and displayed improved antiviral properties, both in terms of M^{pro} inhibition, as well as in terms of limiting viral replication in cells [47]. More specifically, derivatives **MR6-7–2** and **MR6-18–4** inhibited the protease with IC_{50} values of 0.363 and 0.345 μM, which are almost twice as low as ebselen, whereas derivative **MR6-31–2** showed a remarkably higher antiviral effect in Vero cells, with an EC_{50} of 1.78 μM.

Carmofur is an antineoplastic drug that has also been proved to inhibit M^{pro}. Inhibitory effect and cytotoxicity have been tested on Vero E6 cells and resulted in an EC_{50} value of 24.30 μM and a CC_{50} value of 133.4 μM [48]. Unlike previous inhibitors that occupy multiple subsites of the protease, carmofur only binds to S2

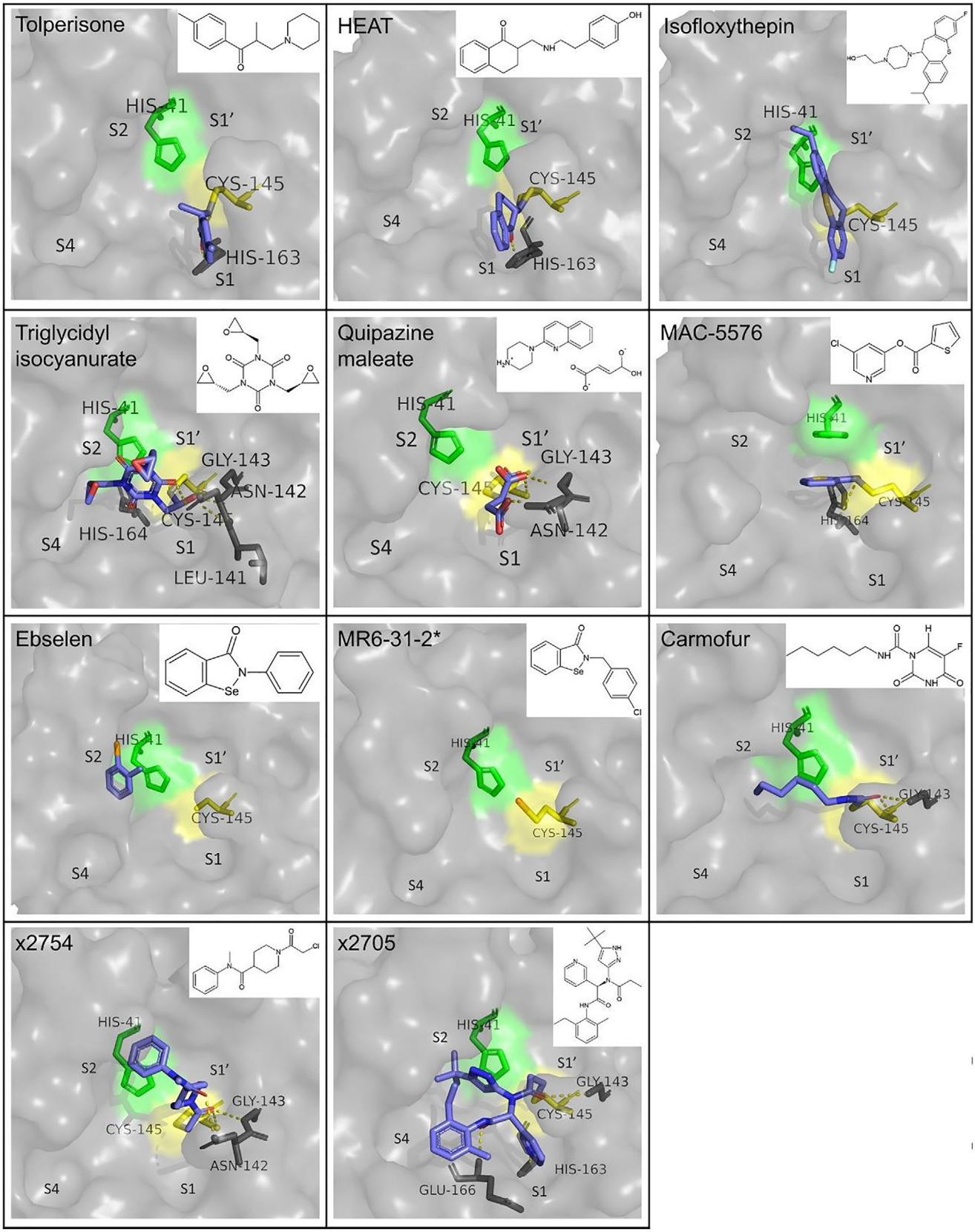

Fig. 6. Binding mode and structure of small covalent inhibitors with available co-crystallization PDB structures in the active site of SARS-CoV-2 M^{pro}. Catalytic residues are colored (His41: green, Cys145: yellow). Important residues for binding are shown in sticks and hydrogen bonds are depicted as yellow dashes. The PDB ID for each inhibitor is indicated in Table 1. *In the crystal structure of MR6-31–2 with the protease, only the selenium atom appears covalently bound to the active site. (For interpretation of the references to colour in this figure legend, the reader is referred to the web version of this article.)

subsite. The fact that this small compound is able to inhibit SARS-CoV-2 provides a good starting point from which more elaborate structures could be designed to inhibit the enzyme even more effectively. The mechanism through which the covalent bond is created is slightly different than the previously described cases, as the sulfur atom of Cys145 binds to the carbonyl group of the fatty acid tail of carmofur creating a 1.8 Å covalent bond. This reaction results in the release of the 5-fluorouracil moiety. The tail of carmofur inserts the S2 subsite and forms a hydrogen bond with each of Gly143 and Cys145. The conformation of the inhibitor in the active site is also affected by hydrophobic interactions with residues His41, Met49, Met165 and Asp187 [48].

Ghosh *et al.* [49] have evaluated 5-chloropyridin-3-yl ester derivatives with indole carboxylic acids for their inhibitory activity against M^{pro}. As deduced from the crystal structure of some representative derivatives in complex with the protease, the synthesized compounds covalently bind to the catalytic cysteine, forming a thioester bond through their indole carbonyl group. Among the derivatives investigated, the greatest potency in inhibiting M^{pro} was shown by **5-chloropyridin-3-yl 1-allyl-1H-indole-4-carboxylate (designated compound 7d)**, which includes an N-allyl substitution, with an IC_{50} of 0.073 μM as determined from a FRET-based enzyme inhibition assay. In a CPE assay on Vero E6 cells, the same compound exhibited an EC_{50} of 15 μM. In terms of the value of EC_{50}, the most potent compound was **5-chloropyridin-3-yl 1H-indole-4-carboxylate (designated compound 1)**, for which EC_{50} was equal to 2.8 μM, more than five times lower than compound 7d, while it also displayed a low IC_{50} of 0.25 μM. Lastly, crystal structures that have been deposited to the PDB provide evidence of covalent inhibition of M^{pro} by various fragments. Two of them are **PG-COV-34**, or **x2754**, a small amide [50], and **x2705**, a more complex compound, for which the supporting paper has not been published yet. In both cases, there is no documented description of their interactions with the residues of the active site, but the crystal structure itself is an important indication. A summary of the binding mode and structure of the small non-peptidomimetic covalent inhibitors described in this paragraph is presented in Fig. 6.

4.2. Non-covalent inhibitors of M^{pro}

Known drugs that show inhibitory effect on M^{pro} include antituberculosis drug **bedaquiline** (IC_{50} = 18.7 μM), HIV protease inhibitor **nelfinavir** (IC_{50} = 234 μM), calcium channel blockers **manidipine** (IC_{50} = 4.81 μM), **lercanidipine** (IC_{50} = 16.2 μM) and **efonidipine** (IC_{50} = 38.5 μM) and glutamate receptor antagonist **perampanel** (IC_{50} = 100–250 μM) [51]. With the exception of perampanel, the lack of co-crystallization structure of the drugs in complex with the protease cannot confirm whether their binding is covalent or non-covalent. However, based on their structure, non-covalent inhibition would be expected. Perampanel, in particular, has been further investigated and served as a parent compound for the synthesis of optimized derivatives. Zhang *et al.* [52] used free-energy perturbation calculations and Vero E6 cell assays to investigate the inhibitory potential and antiviral properties of the different derivatives. Perampanel binds to the active site of M^{pro} with its pyridinyl group occupying the S2 subsite, its phenyl group the S1 and its cyanophenyl group the S1′. Interactions were improved with reposition of the carbonyl group of perampanel from C2 to C6, as well as with an addition of a Cl atom in the benzene ring in the S2 subsite. This improvement was evident in **compound 2 (2-(3-(3-Chlorophenyl)-2-oxo-2H-[1,3′-bipyridin]-5-yl)benzonitrile)**, **compound 3 (5-(3-(3-Chlorophenyl)-2-oxo-2H-[1,3′-bipyridin]-5-yl)pyrimidine-2,4(1H,3H)-dione)** and **compound 4 (2-(3-(3,5-Dichlorophenyl)-2-oxo-2H-[1,3′-bipyridin]-5-yl)benzonitrile)**, which demonstrated IC_{50} values of 10.0, 6.4 and 4.0 μM, respectively. Further optimization of the interactions towards the S4 subsites yielded numerous effective inhibitors. Of them, the most effective inhibited the protease at nanomolar level concentrations. The lowest IC_{50} in this study was calculated for **compound 21** (5-(3-(3-Chloro-5-((2-chlorobenzyl)oxy)phenyl)-2-oxo-2H-[1,3′-bipyridin]-5-yl)pyrimidine2,4(1H,3H)-dione) and was equal to 0.018 μM. The compound also showed antiviral activity through a lower-throughput viral plaque assay in Vero E6 cells, with an EC_{50} of 11.3 μM. Unfortunately, no activity was detected in a respective methylthiazolyl-diphenyl-tetrazolium bromide (MTT) assay and considerable cytotoxicity was observed (CC_{50} = 1.7 μM in Vero E6 cells). The two most promising compounds were **compound 5** (2-(3-(3-Chloro-5-propoxyphenyl)-2-oxo-2H-[1,3′-bipyridin]-5-yl)benzonitrile) and **compound 26** (2-(3-(3-Chloro-5-(cyclopropylmethoxy)phenyl)-2-oxo-2H-[1,3′-bipyridin]-5-yl)benzonitrile). The difference in the structure of the two compounds is that the propyl group of compound 5 is replaced by a cyclopropyl group in compound 26. The calculated IC_{50} values for the two compounds were 0.140 μM and 0.170 μM respectively, indicating that the replacement of the propyl group by a cyclopropyl one leads to an increase of the IC_{50}. The anti-SARS-CoV-2 activity of the two compounds is demonstrated by EC_{50} values of 1.5 and 0.98 μM, as measured with the plaque assay and 2.5 and 2.0 μM as calculated by the MTT assay. The cytotoxicity of compound 5 was significantly higher than compound 26, as indicated by the CC_{50} values measured in Vero E6 and normal human bronchial epithelial (NHBE) cells, which were as low 22 and 20 μM, respectively, for compound 5 and higher than 100 μM in both cases for compound 26. Moreover, compound 5 provided evidence of synergy with remdesivir. In terms of interactions with the active site, compound 5 was shown to form three hydrogen bonds with active site residues Gly143, His163 and Met165, whereas the detailed interactions of compound 26 are not described [15,53].

A compound reported to inhibit SARS-CoV M^{pro}, **ML 188,** binds to the active site of SARS-CoV-2 M^{pro} as well, and inhibits its activity with an IC_{50} = 2.5 ± 0.3 μM. However, apart from pointing out the importance of the interaction with His41 for the inhibition, the interactions of the ligand with the active site are not described in detail [54]. Another molecule that inhibits both SARS-CoV and SARS-CoV-2 M^{pro} is **ML300** and its derivatives have also demonstrated non-covalent inhibition. ML300 displayed an IC_{50} value of 4.99 μM, while the most eminent of its derivatives had a respective value of 0.106 μM. Moreover, its antiviral activity, as calculated by a CPE inhibition assay in Vero E6 cells, was quantified by an EC_{50} value of 19.9 μM. An eminent derivative is **CCF0058981 (compound 41),** which achieves inhibition at nanomolar concentration, with an IC_{50} of 68 nM, an EC_{50} of 497 nM and a CC_{50}>50 μM [55]. Various non-covalent inhibitors of M^{pro} structurally related to ML 188 have been designed, synthesized and tested *in vitro* by Kitamura *et al.* [56]. The IC_{50} values calculated for the originally designed compounds ranged from 0.28 to>20 μM. The ones that showed greater inhibition potency, while combining low cytotoxicity, were further evaluated in an antiviral immunofluorescence assay in Vero E6 cells and resulted in EC_{50} values ranging from 0.82 to 13.06 μM. Among these compounds, **23R (Jun8-76-3A)**, with an IC_{50} of 0.20 μM, an EC_{50} of 1.27 μM and low cytotoxicity, was selected for further investigation. A second antiviral assay in human lung epithelial Calu-3 cells displayed an EC_{50} of 3.03 μM. Moreover, insights into the binding mode of the inhibitor in the active site revealed its orientation in S1, S1′ and S2 subsites, as well as the formation of another subsite between S2 and S4 caused by the binding of the ligand that sheds light on an additional parameter that can be taken into consideration in drug design. It is also noteworthy that 23R exhibited selectivity towards coronavirus M^{pro}s, when also tested among other viral proteases, as opposed to other inhibitors, such as GC376.

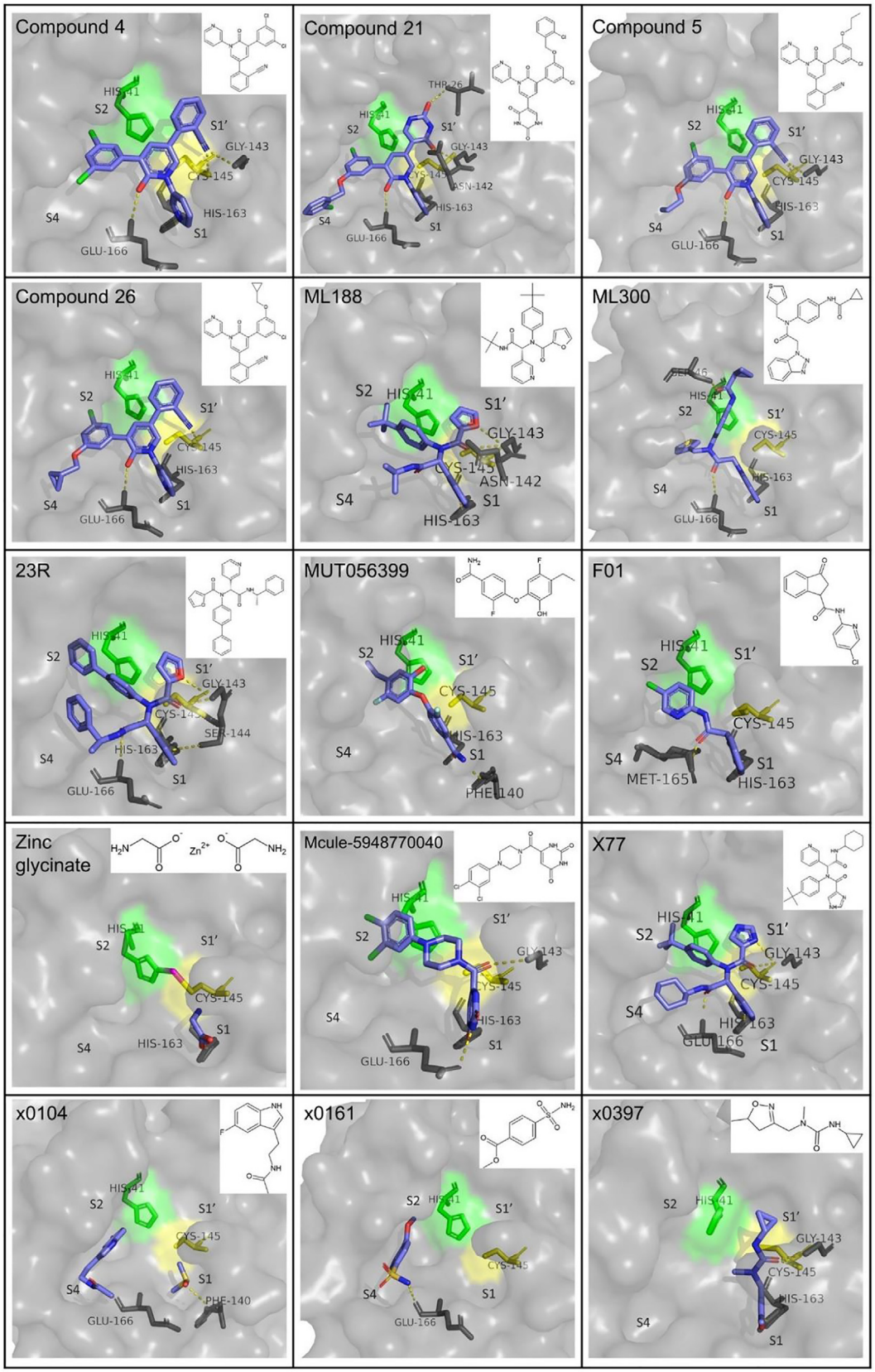

Fig. 7. Binding mode and structure of non-covalent inhibitors with available co-crystallization PDB structures in the active site of SARS-CoV-2 M^{pro}. Catalytic residues are colored (His41: green, Cys145: yellow). Important residues for binding are shown in sticks and hydrogen bonds are depicted as yellow dashes. The PDB ID for each inhibitor is indicated in Table 1. (For interpretation of the references to colour in this figure legend, the reader is referred to the web version of this article.)

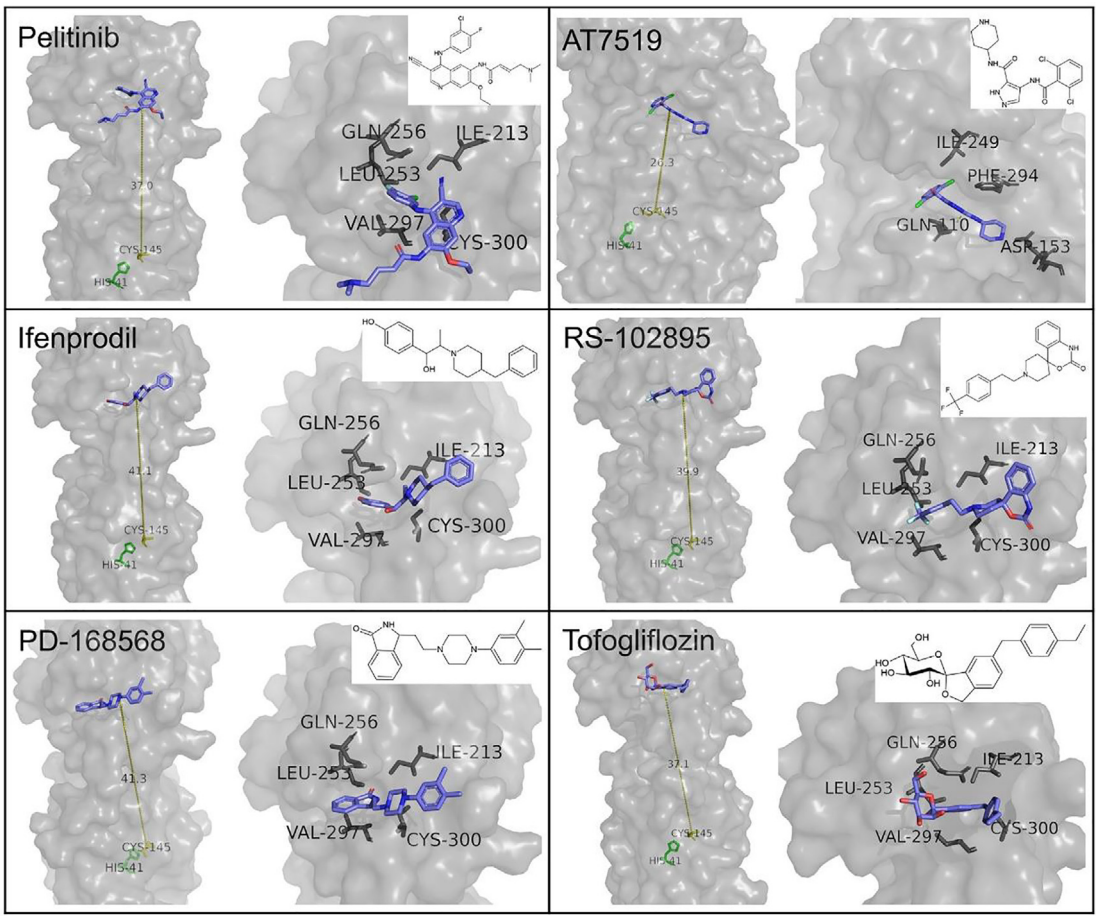

Fig. 8. Binding mode and structure of allosteric inhibitors of M^{pro}. Relative position of their binding site to the active site (His41: green, Cys145: yellow) (left); Close-up view with important residues involved in binding shown as sticks (right). The PDB ID for each inhibitor is indicated in Table 1. (For interpretation of the references to colour in this figure legend, the reader is referred to the web version of this article.)

MUT056399 is another compound that binds non-covalently to the active site, inhibiting it with an EC_{50} of 38.24 μM. It also shows low cytotoxicity, as described by a CC_{50} value>100 μM. Its carboxamide group binds to the S1 subsite, forming hydrogen bonds with residues His163 and Phe140. The other end of the molecule, consisting of an ethyl-phenyl moiety, occupies S2 pocket [41].

Cantrelle *et al.* [57] have performed a fragment screening through which three binding hotspots of M^{pro} and one particularly promising fragment have emerged. More specifically, two of the binding domains are located in the active site and the third one is found on the dimerization interface of the enzyme. The most eminent compound, named **F01**, was characterized as a reversible, non-covalent inhibitor, which inhibits the protease with an IC_{50} of 54 μM as determined from an *in vitro* enzymatic assay. Moreover, the presence of F01 in SARS-CoV-2-infected Vero-81 cells resulted in the reduction of the concentration of the viral N-protein, described by an EC_{50} value equal to 150 μM. The compound also exhibited low cytotoxicity (CC_{50} > 400 μM). Therefore, F01 is an auspicious lead molecule, on which the design of optimized antiviral compounds can be based on.

Another interesting discovery is that of the inhibition of M^{pro} by **zinc ion (Zn^{+2})**. Data indicated that ionic zinc reversibly forms a complex with the protease, aided by the presence of two crucial water molecules. An enzymatic activity assay testing zinc acetate allowed the determination of an IC_{50} of 325.1 μM. Zinc glycinate and zinc gluconate also inhibited the protease, with IC_{50} values of 279.4 and 405.3 μM, respectively. However, when the antiviral activity of the three zinc salts was tested in Vero E6 cells at their maximum non-toxic concentrations, only zinc acetate achieved 50% reduction of the viral titer, at a concentration of 3.227 μM. Additionally, the antiviral effect of Zn^{+2} proved to be enhanced by the presence of quercetin. More specifically, quercetin at double the molar concentration of zinc acetate resulted in more than twice as high antiviral activity [58].

Also, among other inhibitors, available crystal structures for two compounds, **Mcule-5948770040** and **X77**, prove their ability to non-covalently bind to the active site of the protease. The works framing the crystal structures though have not been published, therefore no additional information is available about them. However, the evident structural affinity between compounds X77 and ML188, which is also portrayed in their similar binding conformation in the active site of M^{pro}, could be an indication of comparable antiviral properties. Regarding Mcule-5948770040, the respective co-crystallization structure shows that its pyrimidine group is stabilized in the S1 subsite, while the dichlorophenyl moiety is inserted into the S2 subsite. A useful insight on how the M^{pro} active site can be inhibited, has been provided by the fragment screening performed by Douangamath *et al.* [50]. Compound **x0104** (Z1220452176) occupies the S2 subsite of the protease with its fluoroindole moiety and extends towards S4 subsite, whereas compound **x0161** (Z18197050) has its phenyl ring stabilized between S2 and S4 subsites and its sulfamoyl moiety blocking the S4 subsite. An interesting observation is related to the binding of compound **x0397** (Z369936976), which interacts with the two catalytic residues changing their conformation. This alteration changes the shape of S1′ subsite and consecutively the one of S1,

Table 2
M^{pro} inhibitors which have procedeed to evaluation in *in vivo* or clinical studies.

Drug	Type of inhibition	Delivery	Measure of efficacy				Source(s)
			In vitro	*In vivo*	Clinical Trials		
PF-07321332 (Nirmatrelvir)	Covalent, reversible	Oral	K_i = 3.11 nM (FRET assay); EC_{50} = 77.9 nM (CPE assay in A549-ACE2 cells)	Prevention of weight loss in BALB/c mice and reduction of viral lung titer (by 1.4 and 1.9 $CCID_{50}$ log_{10}/ml for doses of 300 mg/kg and 1000 mg/kg respectively)	89% reduction of risk of hospitalization or death	Phase 3/ EUA by FDA[1]	[30,60,61,]–[62]
PF-07304814 (Lufotrelvir)	Covalent	Intravenous	IC_{50} = 0.27 nM (FRET assay); EC_{50} = 39.8 μM, (CPE assay in VeroE6-enACE2)[2]	Dose-dependent reduction in lung viral titers of $\geq$ 3 log_{10} in BALB/c infected mice	Not available	Phase1	[65,66]
PBI-0451	Covalent, reversible	Oral	Not available	Not available	Not available	Phase 1	[68,69]
EDP-235	Not described	Oral	IC_{50} = 5.8 nM; EC_{90} = 33 nM in human airway epithelial cells	Not available	Not available	Phase 1	[70,71]
S-217622	Non-covalent	Oral	IC_{50} = 0.013 μM; EC_{50} = 0.37 μM (CPE assay in VeroE6/ TMPRSS2 cells)	Dose dependent inhibition of viral replication in lungs of infected mice	Antiviral effects confirmed in phase 2a	Phase 2b/3	[72,73]
Atazanavir	Non-covalent	Oral	K_i = 703 nM (FRET-based assay); EC_{50} = 0.49 (Antiviral assay in Calu-3 cells)	30% increase of survival of K18-hACE2-transgenic mice	Not available	Phase 2	[74,75]
Ebselen (SPI-1005)	Covalent	Oral	IC_{50} = 0.67 μM (FRET-based assay)	Not available	Not available	Phase 2	[76,142]
Lopinavir/ Ritonavir	Not described	Oral	IC_{50} = 10.9 μM (Enzyme inhibition assay)	Not available	No significant activity	Phase 2	[77]–[79]
Danoprevir	Non-covalent	Oral	EC_{50} = 87 μM (Antiviral assay in Vero E6 cells)	Not available	Positive results	Phase 4	[81,82 83]
13b	Covalent	Inhaled	IC_{50} = 0.67 μM (FRET-based assay)	Not available		Preclinical	[15]
GC376	Covalent	Not determined	IC_{50} = 0.19 μM (FRET-based assay)	20% increase of survival, limitation of viral loads, inflammation andtissue lesions in K18-hACE2 transgenic mice	Not available	Preclinical	[84]

[1] : Emergency use authorization by the US Food and Drug Administration [2]: These values refer to PF-00835231, which is the active drug to which PF-07304814 is metabolized.

too. Therefore, this fragment blocks both sites, with its N-methyl group also providing the potential to block S2 and S3 subsites. Although there is a crystal structure that proves the binding of these inhibitors to the active site of M^{pro}, there have not been *in vitro* experiments conducted yet to measure antiviral activity or cytotoxicity. A summary of the binding mode and structure of non-covalent inhibitors described in this paragraph is presented in Fig. 7.

4.3. Allosteric inhibitors

Günther *et al.* [41] discovered two regions outside the binding site of M^{pro} that act as allosteric binding sites, as well as inhibitors that bind to these allosteric sites exhibiting remarkable antiviral activity. Residues Ile213, Leu253, Gln256, Val297 and Cys300 form a hydrophobic pocket that serves as the first allosteric binding site. This pocket accommodates the aromatic groups of inhibitors **pelitinib, ifenprodil**, **RS-102895**, PD-168568, and tofogliflozin. Among these compounds, pelitinib shows good efficacy potential (EC_{50} = 1.25 μM) but not very high cytotoxicity of infected cells (CC_{50} = 13.96 μM). Although pelitinib does not occupy the canonical active site of M^{pro}, its ethyl ether group interacts with residues Tyr118 and Asn142, affecting the S1 pocket. The second allosteric binding pocket is located in the cavity between domains I and II, and domain III. Inhibition through binding to this site is connected to interactions of the inhibitor with residue Arg298, which plays a critical role in dimerization. Change in the conformation of Arg298 causes the alteration of the relative position of domains I/II and III and therefore destabilizes the oxyanion hole and the S1 subsite. Inhibitor AT7519 binds to this site forming Van der Waals contacts with residues Ile249 and Phe294 through its pyrazole ring. The carbonyl group interacts with Gln110 with a hydrogen bond and the piperidine group forms a hydrogen bond with Asp153. The reorientation of Asp153 is concomitant with a slight disposition of Tyr154 and its hydrogen-bonding to the inhibitor, as well as the interaction with Arg298, which is achieved through a salt bridge. The allosteric sites and the binding modes of the respective inhibitors are presented in Fig. 8.

4.4. Drug-like inhibitors with unspecified binding mode

Several drugs and drug-like molecules have been positively evaluated as promising SARS-CoV-2 inhibitors *in vitro*, but have not been co-crystallized with the protease or studied enough in order to provide a detailed description of the binding mode. Therefore, it is not confirmed whether the mode is covalent, non-covalent or allosteric. Such selective M^{pro} inhibitor, whose activity has also been evaluated *in vivo*, is **ALG-097111.** The compound inhibits the protease with an IC_{50} of 7 nM, while also exhibiting an EC_{50} of 0.2 μM in A549-ACE2 cells and low cytotoxicity (CC_{50} > 100 μM). When administrated to female SG hamsters, a day at a 200 mg/kg of dose in combination with ritonavir (50 mg/kg/dose) caused a 3.5log10 reduction of viral titer compared to the control group, measured 2 days post infection. Thus, ALG-097111 may be another compound standing out as an interesting lead in drug development [59].

Vatansever *et al.* [42] conducted a screening of FDA-approved drugs for their potential to inhibit M^{pro}, from which several mole-

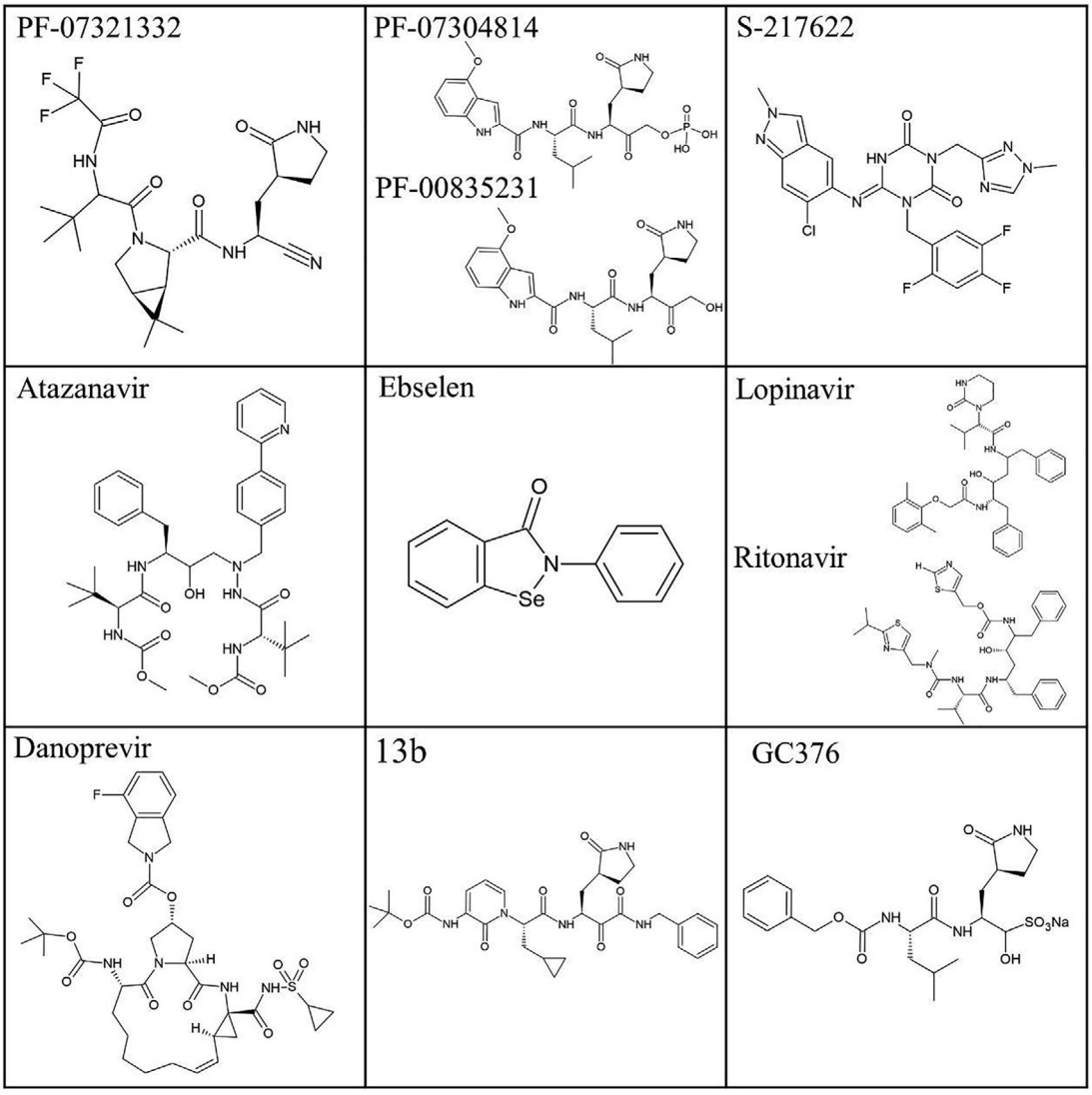

Fig. 9. Available structures for SARS-CoV-2 M^{pro} inhibitors evaluated *in vivo* and in clinical trials.

cules emerged. The lowest IC_{50} value among the tested drugs in a FRET-based assay was calculated for **pimozide**, equal to 42 μM. **Ebastine** (IC_{50} = 57 μM) was also a promising compound, structurally related to pimozide, as they both possess a diphenylmethyl moiety and the two aromatic rings which are inserted in S2 and S4 subsites. A similar geometry is observed in **bepridil**, due to the presence of a N-phenyl-N-benzylamine group, which also inhibits the protease with an IC_{50} of 72 μM. The three drugs were also tested in Vero E6 and human A549/ACE2 cells via a live virus-based microneutralization assay. Only bepridil hindered CPE, with an EC_{50} of 0.86 and 0.46 in the two cell lines, respectively. Other small drug molecules with inhibitory effect against M^{pro} are **sertaconazole** (IC_{50} = 76 μM), **rimonabant** (IC_{50} = 85 μM), **oxiconazole** (IC_{50} = 99 μM), **itraconazole** (IC_{50} = 111 μM), protease inhibitor **tipranavir** (IC_{50} = 180 μM), **zopiclone** (IC_{50} = 349 μM), **trihexyphenidyl** (IC_{50} = 370 μM), **saquinavir** (IC_{50} = 411 μM), **isavuconazole** (IC_{50} = 438 μM), **lopinavir** (IC_{50} = 486 μM), **clemastine** (IC_{50} = 497 μM), **metixene** (IC_{50} = 635 μM) and **duloxetine** (IC_{50} = 3047 μM). In another study, much lower IC_{50} values were calculated for lopinavir in Vero E6 and Huh7 cells (12.01 and 7.79 μM, respectively). Ritonavir was also tested and resulted in respective IC_{50} values of 19.88 and 11.68 μM, while also showing slightly lower cytotoxicity. A time-of-drug-addition assay for the two compounds located their activity at the post-entry stage of infection. However, a low free plasma concentration compared to the IC_{50} values, as designated from an In Vitro to In Vivo Extrapolation analysis, is discouraging for the further investigation of the compounds as antiviral agents [43].

Additional compounds with an inhibitory effect, which could not however be reliably quantified due to incomplete inhibition at the maximum concentration tested in the assay, include dopamine D1 receptor antagonist **periciazine**, histamine H1-receptors antagonist **azelastine**, prostaglandin synthesis inhibitor **cinnoxicam**, topoisomerase II inhibitor **idarubicin** and anti-bacterial drugs **clofamizine** and **talampicillin** [35,42].

5. Drugs with M^{pro} inhibitory effect that have proceeded to *in vivo* or clinical trials

Several repurposed drugs or newly designed compounds have been selected to be further evaluated *in vivo* or clinically. Among them, covalent M^{pro} inhibitor PF-07321332 (Nirmatrelvir) has exhibited high bioavailability and antiviral activity when tested in mice and humans. In the form of the oral antiviral drug Paxlovid™ (Nirmatrelvir/ritonavir tablets) developed by Pfizer, it received Emergency Use Authorization by FDA [62]. Moreover,

Table 3
Natural sources with inhibitory activity against SARS-CoV-2 M^{pro} demonstrated *in silico* and *in vitro* studies.

Compounds	Plant source[1]	IC_{50}	Calculation method	Binding energy (kcal/mol)	Software	PDB ID[2]	H-bonds	Reference (s)
Myricetin	*Polygoni avicularis, Moringa oleifera, Syzygium aromaticum*	3.68 μM	FRET-based assay	−8.47	Glide XP protocol	6LZE	Phe140, Glu166, Asp187	[106]
		0.22 μM	FRET-based assay	–	–	–	Not described	[40]
		2.86 μM	Colorimetric substrate enzyme inhibition assay	–	–	–	Not described	[105]
		0.63 μM	FRET-based assay	–	–	–	Not described	[104]
		–	–	−7.7	AutoDock Vina	6LU7	Not described	[107]
Dihydromyricetin	*Amelopsis japonica*	1.14 μM	FRET-based assay				Not described	[104]
		1.20 μM	Colorimetric substrate enzyme inhibition assay	–	–	–	Not described	[105]
Kaempferol		34.5 μM	CPE inhibition assay	−6.4	AutoDock Vina	Not mentioned	Phe140, Leu141, Asn142, His163, Glu166, Arg188	[109]
				−8.3	AutoDock Vina	6LU7	Thr24, Thr25, Thr26, Cys145, Gly143	[110]
Quercetin	*Azadirachta indica, Mangifera indica, Moringa oleifera, Citrus limon, Alium cepa, Alium sativum, Trigonella foenum-graecum, Mentha piperita*	7.40[3]	FRET-based assay	−7.2/-7.5	AutoDock Vina	6Y2E/6Y2F	Asn142, Ser144, Met165	[111]
		–	–	−7.5	AutoDock Vina	6LU7	Leu141, Ser144, His163, Gln189	[107]
		–	–	−7.16		5R84	Arg298	[144]
		–	–	−8.5/-7.5	Autodock 4.2 / Autodock Vina	6LU7	Glu166,Thr190	[112]
		–	–	−8.12	Glide XP protocol	6LU7	Not described	[113]
Rutin	*Pimenta dioica, Manilkara hexandra, Calendula officinalis*	31.0 μg/mL	CPE inhibition assay in Vero E6 cells	−9.19	MOE[4] 2019.012	6LU7	His41, Phe140, Cys145, His163, Glu166	[116]
		–	–	−11.33	AutoDock 4.2.6.	6LU7	Tyr54, Phe140, Cys145, His163, His164, Glu166, Gln192	[118]
		–	–	−8.21	MOE 2019	6LU7	Not described	[108]
		–	–	−8.8	Autodock Vina	6LU7	Not described	[115]
		–	–	−9.55	SwissDock server	6Y84	His41, Leu141, Asn142, Glu166, Thr190, Gln192	[145]
		–	–	−8.4	Autodock Vina	6 W63	Arg188, Thr190	[117]
Quercetagetin	*Eriocaulon buerferianum, Citrus unshiu*	1.24 μM	Colorimetric substrate enzyme inhibition assay	–	–	–	Leu141, Glu166	[105]
		–	–	−9.41	Glide XP protocol	6LU7	His41, Leu141, Glu166, Thr190	[113]

(*continued on next page*)

Table 3 (*continued*)

Compounds	Plant source[1]	IC_{50}	Calculation method	Binding energy (kcal/mol)	Software	PDB ID[2]	H-bonds	Reference (s)
Gallic acid	*Pimenta doica*	108 μg/mL	CPE inhibition assay in Vero E6 cells	−4.52	MOE 2019.012	6LU7	Phe140, Gly143, Glu166, Thr190	[116]
Epigallocatechin-3-O-gallate	Green tea, muscadine grape, cacao	7.51 μM	Fluorescent substrate enzyme assay	−8.7	Autodock Vina	6LU7	Not described	[119]
		7.58 μg/mL	FRET-based assay	–	–	–	Glu166	[120]
		–	–	−7.8	Autodock Vina	6LU7	Asn142, Met165, Thr190	[146]
		–	–	−7.6	Autodock Vina	6LU7	Thr26, His41, Gly143, Ser144, Cys145, Glu166, Gln189	[147]
Gallocatechin-3-O-gallate Epicatechin-3-O-gallate Catechin-3-O-gallate	Green tea, muscadine grape, cacao	6.38 μM 5.21 μM 2.98 μM	Fluorescent substrate enzyme assay	−8.7 −8.7 −8.3	Autodock Vina	6LU7	Not described	[119]
	–	–	–	−8.8	Autodock Vina	6LU7	Leu141, His163, Arg188, Gln189, Thr190	[148]
Theaflavin	black tea	8.44 μg/mL	FRET-based assay	–	–	–	Tyr54, Thr190	[120]
Naringenin	Not mentioned	92.0 μM	FRET based assay	−7.83	Glide	6 W63	Thr26, Met49, Glu166, Gln189, Thr190	[121]
Apigenin-7-O-glucoside		74.0 μM		−7.56			Thr26, Met49, Glu166, Gln189, Thr190	
Sennoside B		104 μM		−9.01			Thr190, Glu166, Asn142, Cys44	
2,3′,4,5′,6-pentahydroxybenzophenone		102 μM		−8.34			His164, Glu166, Arg188, Tyr54	
Curcumin	*Curcuma longa*	75.0 μg/mL[6]	FRET-based assay	–	–	–	Asn142, His164, Met165, Arg188	[122]
		–	–	−7.1	Autodock Vina	6LU7	Gly143, Ser144	[130]
		–	–	−8.09	Glide	6LU7	Not described	[124]
		–	–	-7.028[3]	CoVDock	6LU7	Thr26, Gly143	[113]
Chlorogenic acid	*Pimenta doicam Moringa oleifera*	360 μg/mL	CPE inhibition assay in Vero E6 cells	−7.18	MOE 2019.012	6LU7	Not described	[116]
		39.5 μM	FRET-based assay	–	–	–	Not described	[103]
		–	–	−7.2	Autodock VIna	6LU7	Cys145, His163, Arg188, Thr190, Gln192	[107]
Baicalin	*Scutellaria baicalensis*	6.41 μM	FRET-based assay	–	–	–	Not described	[103]
		83.4 μM	Colorimetric substrate enzyme inhibition assay	–	–	–	Not described	[105]

Table 3 (*continued*)

Compounds	Plant source[1]	IC_{50}	Calculation method	Binding energy (kcal/mol)	Software	PDB ID[2]	H-bonds	Reference (s)
		–	–	−8.1	Autodock Vina	6LU7	Ser144, Glu166, Pro168	[123]
		–	–	−8.82	Glide XP protocol	6LU7	Not described	[113]
		–	–	−8.85	Autodock-Lamarckian Genetic Algorithm	6Y84	Not described	[134]
Baicalein	*Scutellaria baicalensis*	0.94 μM	FRET-based assay	–	–	–	Leu141, Gly143, Ser144, His163, Glu166	[103]
		0.39 μM	Colorimetric substrate enzyme inhibition assay	–	–	–	Not described	[105]
Scutellarein	*Scutellaria genus, Erigerontis herba*	3.02 μM	FRET-based assay	–	–	–	Not described	[103]
		5.80 μM	Colorimetric substrate enzyme inhibition assay	–	–	–	Not described	[105]
Forsythoside A	Shuanghuanglian preparation	3.18 μM	FRET-based	–	–	–	Not described	[103]
Forsythoside B		2.88 μM	assay	–	–	–	Not described	
Forsythoside E		6.68 μM		–	–	–	Not described	
Forsythoside H		10.2 μM		–	–	–	Not described	
Forsythoside I		5.47 μM		–	–	–	Not described	
Isoforsythiaside		5.85 μM		–	–	–	Not described	
Betulinic acid	*Olea europaea*	14.6 μM	Fluorescent	−8.1	Autodock	6LU7	His41, Phe140	[128]
Betulin		89.7 μM	substrate	−4.1	Vina		His41, Phe140	
Ursolic acid		12.6 μM	assay	−8.2			His41, Ser144	
		–	–	−8.88	Autodock 4.2	6 M71	Not described	[129]
Maslinic acid	*Olea europaea*	3.22 μM	Flurescent substrate assay	−9.3	Autodock Vina	6LU7	His41, Ser144	[128]
Glycyrrhizin	Not mentioned	0.44 mg/mL	Antiviral activity assay on Vero E6 cells				Not described	[132]
		–	–	−7.9	Autodock Vina	6LU7	Not described	[123]
		–	–	−8.7	Autodock Vina	7BQY	Asn238, Asp289	[133]
		–	–	−9.57	Autodock-Lamarckian Genetic Algorithm	6Y84	Not described	[134]
Vanicoside A	*Reynoutria japonica, Reynoutria sachalinensis*	23.1 μM	Fluoresence substrate enzyme assay	115.78	GOLD 5.7.2	6LU7	Thr 26, Cys 145, Glu 166, Gln 189, Thr 190	[135]
Vanicoside B	*Reynoutria japonica, Reynoutria sachalinensis*	43.6 μM	Fluoresence substrate enzyme assay	129.7	GOLD 5.7.2	6LU7	Cys 44, Tyr 54, Leu 141, Asn 142, Cys 145, His 164, Gln 189	[135]
Acteoside	*Olea europaea, Verbascum phlomoides*	43.0 μM	FRET based assay	−10.13	Glide	6 W63	Cys44, Met49, Asn142, His164, Glu166, Thr190	[121]
		–	–	−11.98 (-6.91[4])	Glide XP protocol	6LU7	Thr26, Phe140, Glu166, Gln189	[113]
		–	–	−8.33	MOE 2019.0102	7BUY	Gly143, Cys145, His164, Glu166	[136]

(*continued on next page*)

Table 3 (*continued*)

Compounds	Plant source[1]	IC_{50}	Calculation method	Binding energy (kcal/mol)	Software	PDB ID[2]	H-bonds	Reference (s)
Procyanidin B2	Green tea, muscadine grape, cacao	75.3 μM	Fluorescent substrate enzyme assay	−9.2	Autodock Vina	6LU7	Not described	[119]
		–	–	−8.56	Glide XP protocol	6LU7	Not described	[113]
Procyanidin B2 3,3′-di-O-gallate	*Reynoutria japonica, Reynoutria sachalinensis*	100 μM[7]	Fluorescence substrate enzyme assay	99.57	GOLD 5.7.2	6LU7	His 41, Cys 44, Met 49, Cys 145, His 163, His 164, Gln 189	[135]
Procyanidin C1		100 μM[8]		103.31			Met 49, Gly 143, Cys 145, His 163, Glu 166	
Emodin		100 μM[9]		92.97			His 41, Tyr 54, Cys 145, Met 165, Glu 166	
24-methylcholesta-7-en-3β-on	*Zingiber officinale, Polyporus sulfureus*	200 μg/mL[10]	FRET-based assay	−68.8	Glide XP protocol	6M2N	Cys44	[137]
Punicalagin	Pomegranate	6.19 μg/mL	Fluorescent substrate protease assay	–	–	–	Not described	[138]
Allyl isothiocyanate	*Brassica nigra, Diplotaxis erucoides*	41.4 μg/mL	FRET-based assay	–	–	–	Not described	[122]

[1] : Plant source mentioned in the respective literature, if any; [2]: PDB ID for the protease structure used in the molecular docking simulation; [3]: Inhibition constant K_i [4]: MOE: Molecular Operating Environment; [5]: Covalent docking score; [6]: This concentration results in 28.1% residual activity; [7]: This concentration results in 63.3 % residual activity; [8]: This concentration results in 77.7% residual activity; [9]: This concentration results in 48.5% residual activity; [10]: This concentration results in 25% residual activity.

PF-07321332 has proven to be effective against emerged SARS-CoV-2 variants, including Lambda (C.37), B.1.1.318, B.1.2, Beta (B.1.351), Omicron (B.1.1.529), Zeta (P.2) and Delta (B.1.617.2), highlighting its universal potency for battling SARS-CoV-2 throughout various stages of the pandemic [63,64]. PF-07304814 (Lufotrelvir), which is the prodrug of PF-00835231, is another covalent inhibitor which has been proposed for intravenous administration and has completed its Phase 1 clinical trial in humans, after showing reduction of viral titer in SARS-CoV-2 infected mice [65,66]. PF-00835231 has exhibited *in vitro* inhibitory effect against SARS-CoV-2 Alpha (B1.1.7), Beta (B.1.351), Gamma (P.1), Delta (B.1.617.2) and Omicron (B.1.1.529) variants as well [67].

Another drug being evaluated in phase I clinical trials is PBI-0451, a covalent, reversible and orally administered M^{pro} inhibitor developed by Pardes Biosciences, Inc.. There is a lack of published *in vitro* or *in vivo* data, but the company reports efficiency of the drug against SARS-CoV-2 and its variants, while FDA recently cleared the Investigational New Drug (IND) application submitted for the compound [68,69]. The case is similar for oral protease inhibitor EDP-235, developed by the company Enanta Pharmaceuticals, which has also been reported to have promising antiviral and pharmacokinetic properties. EDP-235 is in Phase 1 of clinical trials [70]. Data emerging from *in vitro* biochemical and antiviral assays in human airway epithelial cells include an IC_{50} value of 5.8 nm and an EC_{90} value of 33 nM respectively [71].

S-217622 is a non-peptidic, non-covalent M^{pro} inhibitor effective at nanomolar levels (IC_{50} = 13 nM, as calculated from an enzymatic inhibition assay). Its efficiency in restricting viral replication in infected mice, as well as good pharmacokinetic properties and oral bioavailability have led to its further investigation in clinical trials. Currently, it is in the phase 2b/3, while its efficiency has been confirmed in the phase 2a [72,73]. Other protease inhibitors in phase 2 of clinical trials include atazanavir, which has already exhibited an EC_{50} of 0.49 μM in an antiviral assay in Calu-3 cells, as well as a 30% increase of survival in infected mice [74,75], ebselen (SPI-1005) [76] and lopinavir/ritonavir [77]. The latter, however, has been reported to have no significant efficacy against SARS-CoV-2 in both *in vitro* or clinical studies [78,79]. It is worth mentioning that atazanavir in particular is potent against SARS-CoV-2B.1 strains as well as the Gamma variant, as determined from *in vitro* studies in Calu-3 cells and *in vivo* in mice [74], while lopinavir has shown very similar binding affinity to the M^{pro} of the Omicron variant as opposed to that of the wildtype *in silico* [80].

Danoprevir is a repurposed non-covalent hepatitis C virus protease inhibitor that has been positively evaluated for its antiviral effect when administered orally, in combination with ritonavir, to COVID-19 patients and has completed phase 4 of clinical studies [81,82]. Its anti-SARS-CoV-2 activity has been confirmed *in vitro*, with an EC_{50} of 87 μM calculated from an antiviral assay in Vero E6 cells [83]. In addition, previously described inhibitors 13b and GC376 are in preclinical stage, with 13b having exhibited encouraging pharmacokinetic properties in mice [15] and GC376 having resulted in limitation of viral load and mitigation of symptoms in infected K18-hACE2 transgenic mice, such as tissue lesions and inflammation [84]. 13b has also been evaluated via molecular docking for its efficacy against the Omicron variant and has exhibited slightly higher binding affinity compared to the wildtype [80]. The available data regarding the aforementioned inhibitors is summed up in Table 2 while their structures, if available, are presented in Fig. 9.

There are several drugs with promising activity against SARS-CoV-2 for which the evidence to support whether their antiviral activity is attributed to inhibition of M^{pro} is not conclusive. This may be due to the potential drug implication with more than one mechanisms related to the viral life cycle. Being part of the category of HIV protease inhibitors (which also includes previously mentioned drugs atazanavir and lopinavir/ritonavir), darunavir is

a compound that is presently in phase 3 of clinical trials, where it is being evaluated in combination with cobicistat [85]. Both compounds have indicated considerable binding affinity to M^{pro} in *in silico* simulations [86]. However, when tested in a cellular assay, an IC_{50} of 36.1 μM was calculated for darunavir (as opposed to 10.9 μM for lopinavir/ritonavir and 60.7 μM for atazanavir in the same assay), but no inhibitory effect was observed at 100 μM in an enzyme inhibition assay [87]. As for cobicistat, *in vitro* results from an enzyme inhibition assay report an IC_{50} of 6.7 μM [88], while another study refutes these results, reporting no inhibition of M^{pro} [89]. Therefore, the antiviral activity of the two drugs cannot be certainly attributed to inhibition of the main protease.

Celecoxib is a drug currently in phase 2 of clinical trials [90] that is mainly reported as a cyclooxygenase 2 inhibitor [91]. There are indications of inhibitory activity against M^{pro}, resulting in 11.90% inhibition at 50 μM [92]. Dexamethasone is a drug with significant anti-inflammatory properties, that is now in phase 4 clinical trials against COVID-19 [93]. It is mainly reported to have high binding affinity to the glucocorticoid receptor and various cytokines, such as interleukin-6, but it has also emerged as a potential M^{pro} inhibitor from *in silico* studies [94,95]. Likewise, doxycycline is a compound highlighted for its anti-inflammatory properties that is in phase 4 of clinical trials against COVID-19 [96]. It shows anti-SARS-CoV-2 activity *in vitro* [97], but there have only been *in silico* studies supporting the hypothesis that it can inhibit M^{pro} [98]. All-trans retinoic acid is a compound that is being evaluated in Phase 2 clinical trials as a chemopreventive agent, with no reference being made to its potential M^{pro} inhibitory activity *in vivo* [99]. However, such activity is demonstrated in an IC_{50} value of 24.7 μM calculated through an *in vitro* enzyme inhibition assay, while the compound also shows antiviral activity in Calu-3 cells against SARS-CoV-2 and its alpha, beta, gamma and delta mutants, with respective IC_{50} values as low as 0.66, 0.97, 0.87 and 0.79 μM, as determined from an RT-PCR assay [100]. It is interesting to point out that over the course of the COVID-19 pandemic, various mutations were observed in the genes encoding major viral proteins. Among them, the spike protein is the most vulnerable. Interestingly, only few mutations have been reported for M^{pro} of the SARS-CoV-2 variants. For example, in the case of the omicron variant, only one mutation was observed for M^{pro}, as opposed to 36 for the spike protein [80]. Another study investigating frequent SARS-CoV-2 M^{pro} mutants reports six dominant mutations observed in the Lambda, B.1.1.318, B.1.2, Beta, Omicron and Zeta variants [63]. However, as mentioned above, several protease inhibitors remain effective against the main proteases of SARS-CoV-2 variants as well, reinforcing the reliability of M^{pro} as an antiviral target. Moreover, research has proceeded to the study of mutations and their impact on the structure and function of the protease, providing useful insights for the development of mutation-resistant inhibitors. A pathway towards such development may be the identification of residues playing an important role in the formation of the active site and the dimeric form of M^{pro} as mutation coldspots [101,102].

6. Natural compounds as inhibitors of M^{pro}

Apart from drug discovery and repurposing, research has been orientated towards phytochemicals in search for ways to restrain the effect that COVID-19 has on public health. Such strategy may reinforce the action of antiviral drugs and vaccines, which are much more time-consuming to be developed. Natural compounds found in extracts of plants, may be employed, as a tool for boosting immunity and aid protection against infection. Moreover, knowledge on the beneficial action of bioactive phytochemicals, may enhance preparedness for future viral outbreaks. Such phytochemicals may be used for the development of functional food supplements or other functional aids. An overview of reported natural compounds that have demonstrated inhibitory activity against M^{pro} based on *in silico* and *in vitro* methods is presented in Table 3.

Myricetin is a naturally occurring flavonoid that has been identified as an M^{pro} inhibitor, and one of the few natural compounds that has been co-crystallized in complex with the protease. The respective structure has been deposited in the PDB under the ID 7B3E. Among the numerous natural myricetin sources, some reported in literature include plants *Polygoni avicularis, Moringa oleifera* and *Syzygium aromaticum*. A FRET-based enzyme assay demonstrated IC_{50} value of 0.63 for myricetin, while further evaluation of its antiviral effect in Vero E6 cells led to the calculation of EC_{50} value of 8.00 μM. It is interesting that **dihydromyricetin**, the respective flavanone of myricetin, also abundant in natural sources, was tested in the same assays and exhibited higher M^{pro} inhibitory effect but slightly lower antiviral efficacy overall, with IC_{50} and EC_{50} values of 1.14 and 13.56 μM, respectively [103].The binding mode of myricetin, as determined through the crystal structure of its complex with M^{pro}, reveals the crucial role of its pyrogallol group. The group has the role of an electrophile and forms a covalent bond with the nucleophilic sulfur atom of the catalytic cysteine, while its hydroxyl moieties form hydrogen bonds with residues Thr26, Gly143, Ser144 and Cys145 [104]. The interactions that the pyrogallol group forms with the active site residues make it a promising potential warhead for the development of optimized inhibitors. For example, a methyl derivative of myricetin, substituted at its 7-OH, displayed improved properties with an IC_{50} of 0.30 μM and an EC_{50} of 12.59 μM. Bulkier substitutions in the same positions inhibited the protease, but in higher concentrations. Interestingly, comparison of the binding modes of baicalein and myricetin, both of which have a similar backbone that includes a pyrogallol moiety, highlights major differences, such as the fact that baicalein binds non-covalently to the active site, as opposed to myricetin. In both cases, however, pyrogallol participates in interactions that considerably contribute to the stabilization of the molecule in the active site [103].

Myricetin has been widely investigated in literature, leading to the reporting of various IC_{50} values. Kuzikov *et al.* [40] calculated an IC_{50} as low as 0.22 μM, through a FRET-based cleavage assay, while Liu *et al.* [105] mention an IC_{50} of 2.86 μM, through a colorimetric substrate enzyme inhibition assay. A different study reports an IC_{50} of 3.68 μM and conducted molecular docking simulations to investigate the binding of myricetin to M^{pro} (PDB ID: 6LZE) [106]. The calculated a binding energy was equal to −8.47 kcal/mol using the extra precision protocol of Glide software [106]. The simulation also predicted the formation of hydrogen bonds with residues Phe140, Glu166 and Asp187 and interaction with His41. Molecular docking simulation with a different software (Autodock Vina) and on a different protease structure (PDB ID: 6LU7) resulted in binding energy of −7.7 kcal/mol [107].

Myricetin glycosides also seem potent. In the case of myricitrin, a 3-rhamnopyranoside of myricetin, the inhibitory effect was found weaker compared to myricetin, as the compound results in 30.8% inhibition at a concentration of 50 μM [105], while another study reports a binding energy of −7.2 kcal/mol to the active site of M^{pro} [108]. Another derivative, myricetin-3-*O*-rutinoside, detected in *Limoniastrum Guyonianum*, has not been tested *in vitro*, but displayed good binding affinity to the protease in a molecular docking simulation, with a high binding energy of −9.0 kcal/mol.

Another representative of the group of flavonoids with promising indications of antiviral activity is **kaempferol**. A CPE inhibition assay in Vero E6 cells led to the calculation of an IC_{50} value of 34.5 μM, while molecular docking studies have revealed multiple possible hydrogen bonds that can be formed between the com-

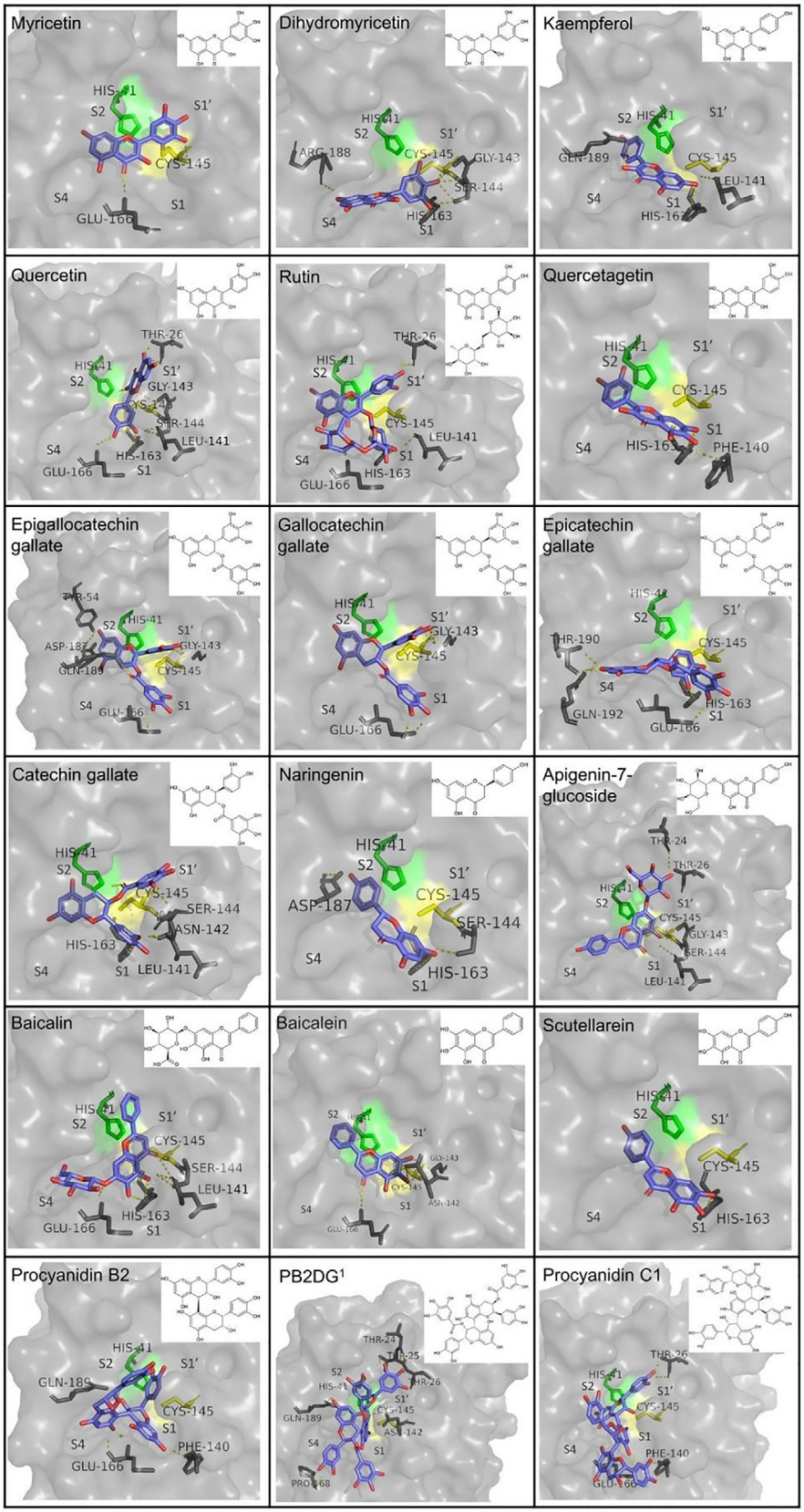

Fig. 10. Binding mode and structure of flavonoids, flavanones and derivatives with *in vitro* demonstrated inhibitory activity in the active site of SARS-CoV-2 M^{pro}. Catalytic residues are colored (His41: Green, Cys145: yellow), residues participating in hydrogen bonds are shown in sticks and hydrogen bonds are depicted as yellow dashes.1: Procyanidin B2 3,3′-di-O-gallate. The receptor-ligand complex was produced by docking simulations using the software YARASA Structure, replicating the binding mode represented in the relevant publication (Available in Table 3). (For interpretation of the references to colour in this figure legend, the reader is referred to the web version of this article.)

pound and important active site residues, such as Phe140, Leu141, His163 and Glu166 [109,110].

Quercetin is another flavonoid with confirmed *in vitro* anti-SARS-CoV-2 M^{pro} activity. A FRET-based assay has shown effective inhibition, with the activity of the enzyme dropping below 10% at a quercetin concentration of 125 μM. Its inhibitory effect is described by an estimated intrinsic inhibition constant K_i = 7.4 μM [111]. *In silico* molecular docking and modelling of its binding to the active site reveal binding energies ranging from −8.5 to −7.2 kcal/mol and key hydrogen bond interactions which differ from study to study and include residues Leu141, Asn142, Ser 144, His163, Glu166 and Gln189 [58,107,112,113]. Numerous quercetin derivatives have also been investigated. More specifically, quercetin-3-*O*-glucoside (also known as isoquercitrin) and quercetin rhamnoside (quercitrin) exhibited a better binding energy than remdesivir in the same molecular docking study (-8.2 and −8.6 kcal/mol respectively, as opposed to −7.9 kcal/mol for remdesivir). Their hydrogen bond interactions include residues similar to these of quercetin [114]. **Rutin** is also a derivative of quercetin (quercetin-3-*O*-rutinoside) with high anti-SARS-CoV-2 potency proven *in vitro*. Its inhibitory potential has been evaluated in a CPE reduction assay in Vero E6 cells, from which an IC_{50} value of 31 μg/mL was calculated. Cytotoxicity was low, as depicted in the CC_{50} value and equal to 8017 μg/mL. Molecular docking simulations have also been performed for rutin and reported binding energies ranging from −11.33 to −8.21 kcal/mol, with the simulation performed using different M^{pro} PDB entries (6LU7, 6Y84 and 6 W63). Docking also indicated the formation of different hydrogen bonds in each simulation, which mainly include residues His41, Phe140, Cys145, His163 and Glu166. Moreover, the suitability of rutin for further development as a potential antiviral compound is reinforced by its favorable pharmacokinetic profile and stability in complex with M^{pro}, as resulted from molecular dynamics simulation [108,113,115]–[118]. Finally, **quercetagetin**, a flavonol structurally related to quercetin, has been found to have good inhibitory effect against the protease, with an IC_{50} of 1.24 μM [105]. The binding mode and structure of reported flavonoids, flavanones and their derivatives is presented in Fig. 10.

Gallic acid is a small, hydroxybenzoic acid which despite having a low docking score (-4.52 kcal/mol, as opposed to −9.22 kcal/mol for positive control N3), showed to hinder the cytopathic effect in infected Vero E6 cells with an EC_{50} of 108 μg/mL [116]. Various esters of gallic acid with flavan-3-ols have also provided promising results in *in silico* and *in vitro* studies. More specifically, **epigallocatechin-3-O-gallate**, **gallocatechin-3-O-gallate** and **epicatechin-3-O-gallate** exhibited the same binding energy of −8.7 kcal/mol and comparable IC_{50} values in a fluorescent substrate assay, equal to 7.51, 6.38 and 5.21 μM respectively, while **catechin-3-O-gallate** showed a slightly lower binding affinity, with a binding energy of −8.3 kcal/mol, but lower IC_{50} of 2.98 μM [119]. In a similar *in vitro* assay performed by Jang *et al.* [120], epigallocatechin gallate showed an IC_{50} of 7.58 μg/mL, as well as no cytotoxicity in HEK293T cells up to a concentration of 40 μg/mL. Its auto-oxidation products were also reported to be active, whereas it showed an additive effect with **theaflavin**, with a coefficient of drug interaction (CDI) of 0.93. Both compounds are found in tea, green and black tea respectively, and theaflavin alone had an inhibitory effect against the protease with an IC_{50} of 8.44 μg/mL.

In the category of flavonoids and derivatives, **naringenin** has been reported to inhibit the enzyme by 50% at a concentration of 92 μM, while showing indications of good bioavailability and drug-likeness properties. Molecular docking simulations with the Glide software resulted in a binding energy of −7.83 kcal/mol, as well as hydrogen bond interaction with residues Tyr54 and Thr190 [121]. The same study calculated a slightly higher binding energy (-7.56 kcal/mol) but lower IC_{50} value (74 μM) for **apigenin-7-O-glucoside**, reporting also more interacting residues which form hydrogen bonds, namely Thr26, Met49, Glu166, Gln189, Thr190. **Sennoside B and 2,3′,4,5′,6-pentahydroxybenzophenone** are included in the aforementioned study, yielding lower binding energies (-9.01 and −8.34 kcal/mol respectively) but slightly higher IC_{50} values (104 and 102 μM, respectively), while establishing Glu166 as a common hydrogen bond forming residue.

Another flavanol included in various studies is **curcumin**, a major constituent of *Curcuma longa*. It has shown *in vitro* inhibitory effect by reducing the activity of the protease to 28.1% at a concentration of 75 μg/mL [122], while more information regarding its binding has been available through molecular docking simulations. Simulation with Autodock Vina resulted in a binding energy of −7.1 kcal/mol and hydrogen bonds with residues Gly143 and Ser144 [123], while the use of Glide gave a binding energy of −8.09 kcal/mol and hydrogen bonds with residues Gly143, Leu141, Glu166, Pro168, Gln189 and Thr190 as an output [124]. The α,β-unsaturated ketone group present in the molecule provides probable cause to investigate the possibility of covalent binding since it can act as a Michael acceptor. More specifically, covalent docking with CoVDock performed by Teli *et al.* [125] resulted in a binding energy of −7.03 kcal/mol, highlighting Gly143 as a hydrogen bond contact, as in the previously mentioned works, along with Thr26.

The major compounds identified in a Chinese herbal extract mixture known as Shuanghuanglian preparation, **chlorogenic acid**, **baicalin** and **baicalein**, also showed inhibitory effect demonstrated by IC_{50} values as low as 39.48, 6.41 and 0.94 μM, respectively [116]. When tested in Vero E6 cells, baicalin and baicalein exhibited EC_{50} values of 27.87 μM and 2.94 μM, respectively. Chlorogenic acid has been tested in other works as well [107,126], and its inhibitory effect is projected on its IC_{50} value, that equals 360 μg/mL, even though molecular docking simulations have resulted in a binding energy considerably lower (-7.18 kcal/mol) as opposed to the positive control (inhibitor N3, −9.22 kcal/mol) [116]. Baicalein has been co-crystallized in complex with M^{pro} (PDB ID: 6M2N) and the co-crystallized structure revealed hydrogen bond interactions with residues Leu141, Gly143, Ser144, His163 and Glu166. Baicalin and baicalein are also major compounds of *Scutellaria baicalensis* and have been reported to have IC_{50} values of 83.4 and 0.39 μM in a different study [105]. The same study further evaluated the antiviral activity of baicalein in Vero cells and calculated an EC_{50} value of 2.92 μM. Other compounds found in the Shuanghuanglian preparation have shown inhibitory activity against M^{pro}, including **Scutellarein** (IC_{50} = 3.02 ± 0.11 μM), **Forsythoside A** (IC_{50} = 3.18 ± 0.12 μM), **Forsythoside B** (IC_{50} = 2.88 ± 0.13 μM), **Forsythoside E** (IC_{50} = 6.68 ± 0.22 μM), **Forsythoside H** (IC_{50} = 10.17 ± 0.39 μM), **Forsythoside I** (IC_{50} = 5.47 ± 0.1 μM) and **Isoforsythiaside** (5.85 ± 0.06 μM) [103]. Scutellarein, in particular, yielded an IC_{50} of 5.80 μM in a colorimetric substrate enzyme assay [105] while its glucoside has been reported to have better binding affinity to the protease than native inhibitor N3 (-9.3 kcal/mol as opposed to −8.93 kcal/mol) in *in silico* molecular docking simulations [127].

Triterpenes are another category of compounds that have provided indications of anti-M^{pro} effects. More specifically, **betulinic acid**, **betulin**, **ursolic acid** and **maslinic acid**, all found in *Olea europaea* leaves extract among other plants, were evaluated *in vitro* through a fluorescent substrate cleavage assay, and showed encouraging results, portrayed by the calculated IC_{50} values of 14.55, 89.67, 12.57 and 3.22 μM. The fact that betulinic acid had considerably higher activity compared to betulin indicates the importance of the carboxyl group at C-17 for the interactions of the molecule with the protease [128]. Ursolic acid in particular has also been included in several virtual screening studies, often

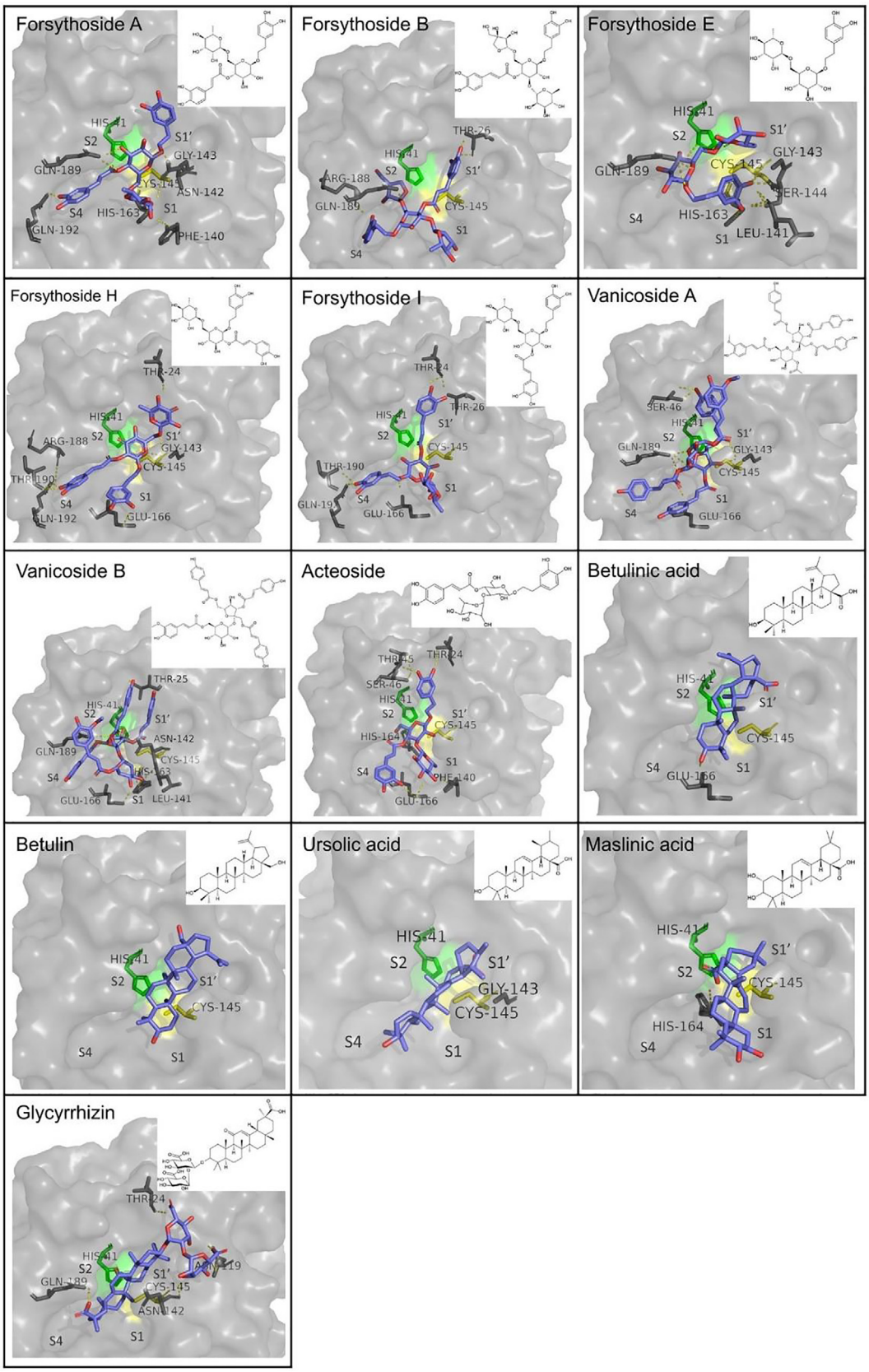

Fig. 11. Binding mode and structure of phenylethanoid glycosides (Forsythoside A-Acteoside) and pentacyclic triterpenoids (Betulinic acid-Glycyrrhizin) with *in vitro* demonstrated inhibitory activity in the active site of SARS-CoV-2 M^{pro}. Catalytic residues are colored (His41: green, Cys145: yellow), residues participating in hydrogen bonds are depicted as yellow dashes. The receptor-ligand complex was produced by docking simulations using the software YARASA Structure, replicating the binding mode represented in the relevant publication (Available in Table 3). (For interpretation of the references to colour in this figure legend, the reader is referred to the web version of this article.)

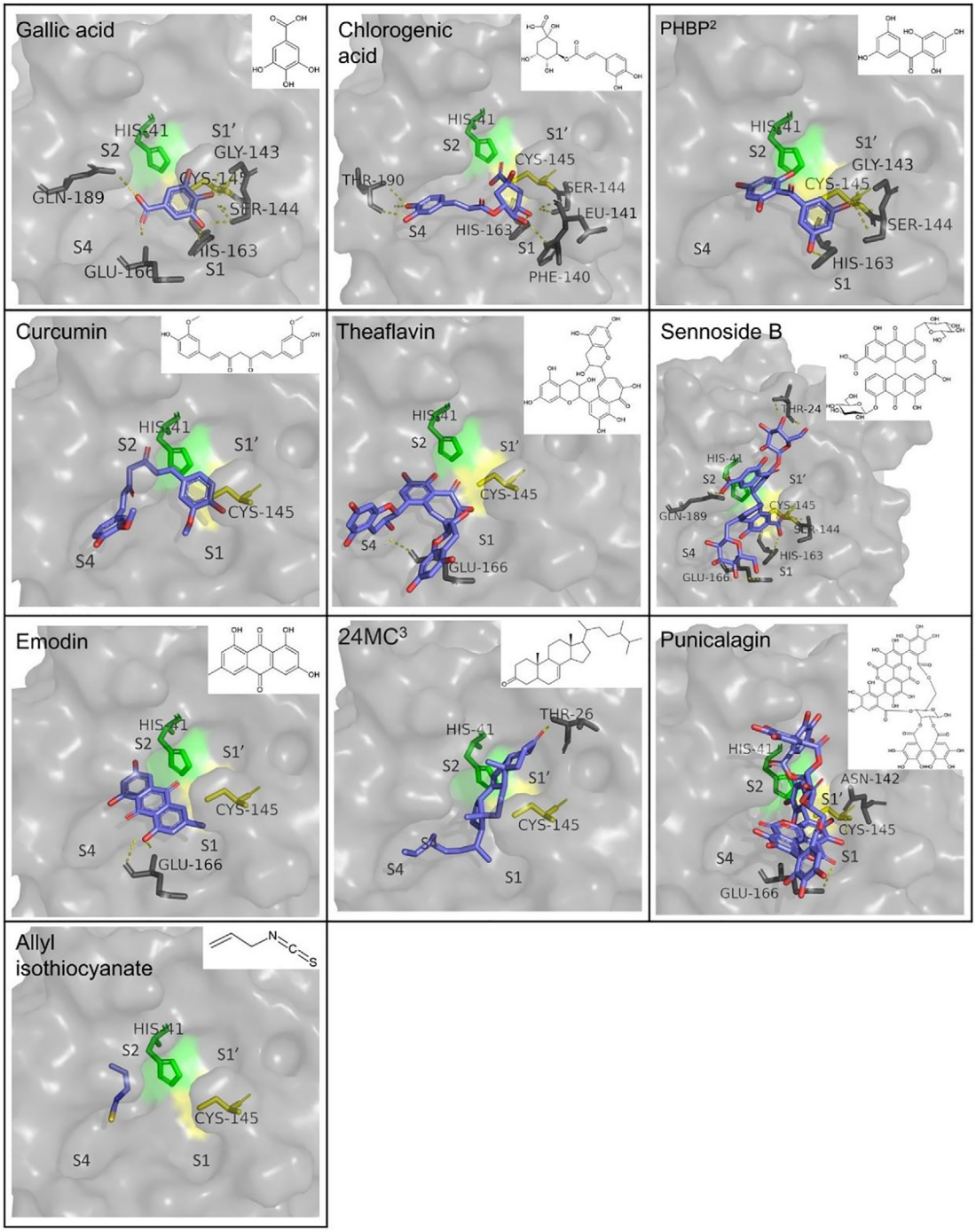

Fig. 12. Binding mode and structure other natural compounds with *in vitro* demonstrated inhibitory activity in the active site of SARS-CoV-2 Mpro. Catalytic residues are colored (His41: green, Cys145: yellow), residues participating in hydrogen bonds are depicted as yellow dashes. 2: 2,3′,4,5′,6-pentahydroxybenzophenone; 3: 24-methylcholesta-7-en-3β-on. The receptor-ligand complex was produced by docking simulations using the software YARASA Structure, replicating the binding mode represented in the relevant publication (Available in Table −3). (For interpretation of the references to colour in this figure legend, the reader is referred to the web version of this article.)

as a constituent of *Ocimum sanctum*, with binding energies ranging from −8.88 to −8.52 kcal/mol, as provided by Autodock Vina and Autodock 4.2. Binding of the molecule is attributed to the conventional active site of the protease in two studies, designating hydrogen bonds with residues Thr24, Leu141 and Ser144 [129,130]. Another study mentiones formation of hydrogen bonds with residues Arg131, Lys137, Asp197, Thr198, Thr199, Tyr237, Asn238, Tyr239, Leu272, Gln273, Gly275, Met276, Leu286 and Leu287, suggesting binding of ursolic to another site [131].

Glycyrrhizin is a triterpenoid saponin with an EC_{50} value of 0.44 mg/mL, as calculated from an antiviral assay performed in Vero E6 cells by van de Sand *et al.* [132]. A fluorescent substrate assay showed 70.3 % reduction of enzymatic activity at a inhibitor concentration of 30 μM and complete inhibition at 2000 μM. Glycyrrhizin has also been investigated in various docking studies, resulting in binding energies between −9.57 and −7.9 kcal/mol, while it has also shown *in silico* indication of inhibitory effect against other viral proteins including the spike protein, the heli-

Table 4
Natural compounds highlighted in molecular docking studies for their potential inhibitory effect against SARS-CoV-2 M^{pro}.

Compounds	Source[1]	Software	PDB[2]	Binding energy (kcal/mol)	H-bonds	Reference
Flemichin A	–	Autodock Vina 4.2	6LU7	−8.9	Arg188	[149]
Delta-Oleanolic acid	–			−8.9	Thr26, Glu166	
Emodin 1-O-beta-D-glucoside	–			−8.7	Leu141, Asn142, Cys145, His163, Glu166, Pro168, Gln189 Thr190	
Procyanidin A2	Grape, strawberry, persimmon, cranberry, blueberry, cacao, green tea	Autodock Vina	6LU7	−9.2	Gly143	[119]
Epigallocatechin				−7.7	Glu166	
Gallocatechin				−7.6	Glu166	
Epicatechin				−7.5	Glu166, Gln189, Thr190	
Catechin				−7.5	Leu141, Glu166	
Epiafzelechin				−7.5	Leu141, Glu166, Gln189	
Afzelechin				−7	Leu141, Glu166	
Mangiferin	*Mangifera indica*	Autodock Vina	6LU7	−8.4	His41, Leu141, Asn142, Gly143, Ser144, Cys145, Arg188, Thr190, Gln192	[107]
Kaempferol	*Mangifera indica, Moringa oleifera*			−7.8	Leu141, Ser144, Gln189	
Lupeol	*Mangifera indica*			−7.6	–	
Nimbolide	*Azadirachta indica*			−7.6	different site	
Ellagic acid	*Mangifera indica, Moringa oleifera*			−7.3	His41, Arg188, Thr190	
Gedunin	*Azadirachta indica*			−7.3	Asn142	
Catechin	*Mangifera indica, Moringa oleifera*			−7.2	Glu166, Asp187, Thr190, Gln192	
Nimbandiol	*Azadirachta indica*			−7.1	Thr26, Gly143	
Epicatechin	*Mangifera indica, Moringa oleifera*			−7	Ser144, His163,Gln189	
Nimbinene	*Azadirachta indica*			−6.5	Asn142, Gly143	
Hesperidin	*Zingiber officinale*			−8.3	Asn142, Met165	[126]
Methyl 3,4,5-trihydroxybenzoate	*Rhus* spp (sumac)	Molegro Virtual	6LU7	−22.6	Phe140, Leu141, Ser144, Cys145, His164	[150]
(Z)-1-(2,4-Dihydroxyphenyl)-3-(3,4-dihydroxyphenyl)-2-hydroxyprop-2-en-1-one		Docker software 6.0		−21.83	Leu141, Ser144, Cys145, His164, Asp187, Gln189	
3,7-Dihydroxy-2-(4-hydroxyphenyl) chroman-4-one				−17.21	Tyr54, Leu141, Ser144, His163, Glu166, Asp187, Gln189	
2-(3,4-Dihydroxyphenyl)-3,5-dihydroxy-7-methoxy-4H-chroman-4-one				−15.57	Tyr54, Gly143, Ser144, Cys145, Glu166, Gln189	
(Z)-2-(3,4-Dihydroxybenzylidene)-6-hydroxybenzofuran-3(2H)-one				−14.31	Leu141, Ser144, Cys145, His164, Asp187, Gln189	
3,5,7-Trihydroxy-2-(4-hydroxyphenyl) chroman-4-one				−13.34	Tyr54, Leu141, Gly143, Ser144, Cys145, Glu166, Asp187, Gln189	
Proanthocyanidin B2	*Uncaria tomentosa* (Cat's claw)	Autodock Vina 1.1.2	6LU7	−9.2	Phe140, Ser144, Cys145, His163, Gln189, Thr190, Gln192	[151]
Cadambine				−8.6	Gly143	
Speciophylline				−8.1	–	
Geraniin	*Phyllanthus amarus*	Autodock Vina	6LU7	−9.3	Leu141, Gly143, Ser144, Cys145, Thr190	[114]
Corilagin				−8.7	Gly 143, Ser 144, Met 165, Glu 166	
Furosin				−8.7	Thr24, Thr26, Asn142, Gly143	
Quercitrin				−8.6	Asn 142	
Astragalin				−8.4	His41, Arg188, Thr190	
Quercetin-3-O-glucoside				−8.2	Leu141, His163, Met165	
Neoandrographolide	*Andrographis paniculata*			−7.8	–	
Squalene	*Olea europaea*	Autodock Vina	6 W63	−6.2	Not described	[152]
Theaflavin-3-3′-digallate	Black tea	AutoDock 4.2.6.	6LU7	−12.41	Thr26, His41, Tyr54, Cys145, His164	[153]
Hypericin	*Hypericum perforatum*			−11.17	Asn142, Cys145, His164, Glu166	
Robustaflavone	*Rhus succedanea*			−10.92	Thr26, His163	
(-)-Solenolide A	*Haliotis laevigata*			−10.82	–	
Hesperedin	*Citrus* spp., *Mentha* spp., *Linaria vulgaris*	Autodock Vina	6LU7	−8.3	Phe140, Ser144, Cys145, Glu166	[146]
Rhoifolin	Rhus succedanea, *Citrus* spp., *Lablab purpureus, Lycopersicon esculentum, Cynara scolymus, Musa* spp., *Vitis vinifera*			−8.2	–	
Pectolinarin	*Cirsium* spp., *Linaria vulgaris*			−8.2	Ser144, Cys145, His163, Glu166	
Nabiximols	*Cannabis* spp.			−8	Asn142, Met165, Thr190	
Quercetin-3-vicianoside		Autodock Vina	6LU7	−8.3	Thr26, Leu141, Gly143, Ser144, His163, Glu166	[154]
Absinthin	*Artemisia Absinthium*			−8.2	His 163	
Delphinidin 3-O-glucoside	*Phaseolus Vulgaris*			−8	Thr26, His41, Phe140, Met165	
Petunidin 3-O-glucoside	*Phaseolus Vulgaris*			−8	Thr26, His41, Phe140, Glu166	
Quercetin 3-glucuronide-7-glucoside	*Phaseolus Vulgaris*			−7.9	His41, Phe140, Gly143, Glu166	
Chrysoeriol 8-C-glucoside	*Phaseolus Vulgaris*			−7.9	Phe140, Glu166, Thr190	
Piperolactam A	*Piper Longum*			−7.7	Leu141, Gly143, Ser144, Cys145,	

Table 4 (*continued*)

Compounds	Source[1]	Software	PDB[2]	Binding energy (kcal/mol)	H-bonds	Reference
					His163, Gln189	
Oleanolic acid	*Ocimum Gratissimum*			−7.7	Leu141, Ser144, Cys145	
Schaftoside	*Phaseolus Vulgaris*			−7.7	Asn142, Gly143, Glu166, Thr190	
Riboflavin	*Curcuma Longa*			−7.6	Leu141, Ser144, Cys145, His163	
Echinacoside	*Echinacea-angustifolia*	GLIDE (XP protocol)	5R82	−14.17	Thr25, Cys44, Asn142, Gly143, Gln189, Thr190	[155]
Quercetagetin 7-glucoside				−15.2	Cys44, Leu141, Cys145, Glu166, Gln189	
Levan N				−12.92	His41, Cys44, Asn142, Gly143, Gln189	
Inulin from chicory				−11.72	Leu141, Gly143, Glu166, Gln189	
1,3-Dicaffeoylquinic acid				−10.01	Thr25, Thr26, Gly143, Arg188	
Hydroxycinnamic acid	*Avicennia officinalis*	Autodock Vina	6LU7	−7.5	His164, Thr190, Gln192	[156]
Phenethyl alcohol				−7.3	Met49, Val186, Arg187, Arg188, Thr190, Gln192	
Dihydroartemisinin				−7	Cys145, His164	
caffeic acid phenethyl ester	Honeybee propolis	GLIDE (XP protocol)	6LU7	−4.79	Asn142, Glu166	[157]
Withanone	Ashwagnadha			−4.42	Cys 145	
Thalimonine	*Thalictrum simplex*	AutoDock 4.2.6.	6LU7	−8.79	Gly143, Ser144, Cys145, Thr190, Gln192	[158]
Sophaline D	*Sophora alopecuriodes*			−8.39	His41, Tyr54, Asn142, Cys 145	
Isorhamnetin	Horchata herbal infusion	GOLD software	6Y2G	−7.3	His163, Glu166, Asp187	[159]
l-Leucine, N-isobutoxycarbonyl-N-methyl-, heptyl ester				−8.27	–	
Benzoic acid, 2-(ethylthio)-, ethyl ester				−7.63	Gly143	
Mearnsitrin	*Manilkara hexandra*	Not specified	6LU7	−7.59	Not described	[108]
Quercetin 3-O-β-D-glucoside				−7.68	Not described	
Bonducellpin D	*Caesalpinia minax*	AutoDock4.2	6Y2F	−9.28	Glu166, Thr190	[160]
5,7-DimethoxyflavaN-4′-O-β-dglucopyranoside	–			−9.23	Glu166, Thr190, Gln192	
Caesalmin B	–			−8.82	Glu166, Thr190	
11-Oxa-dispiro[4.0.4.1]undecan-1-ol	*Leucas zeylanica*	Glide	6LU7	−5.76	Glu 166	[161]
Azetidin-2-one 3,3-dimethyl-4-(1-aminoethyl)				−5.39	Tyr54, Gln189	
Lorazepam, 2TMS derivative				−5.25	Gly 143	
Jaceidin	*Crepis sancta*	Autodock Vina	6LU7	−7.3	Leu141, Gly143, Ser144, Cys145, Arg188	[162]
(6S,9R)-Roseoside				−7.2	Thr26, Leu141, Gly143, Ser144, Cys145, His163, Glu166	
Panduletin				−7.1	Leu141, Gly143, Ser144, Cys145, His163	
Pachypodol				−7.1	Gly143, Ser144, Cys145	
Chrysoplenetin				−7.1	Leu141, Gly143, Ser144, Cys145	
Isorhamnetin-3-O-β-D	*Calendula officinalis*	Autodock Vina	6LU7	−8.7	Not described	[163]
Calendoflaside				−8.5		
Narcissin				−8.4		
Calendulaglycoside B				−8.2		
Calenduloside				−7.9		
Legalon	*Silybum marianum*	Autodock 4.2	6 M71	−8.47	Not described	[129]
Robinetinidol	*Acacia mearnsii*			−8.44		
Mesquitol	*Prosopis juliflora*			−7.55		
Hesperidin	–	SwissDock server	6Y84	−9.02	Thr24, Thr25, His41, Thr45, Ser46, Cys145	[145]
Berberine	*Tinospora cordifolia*	Autodock Vina	6LU7	−7.3	Thr25, Ser46, His163	[164]
b-Sitosteryl ferulate	–	Autodock Vina	6LU7	−7.8	Not described	[165]
Cordifolioside	*Tinospora cordifolia*	Autodock Vina	6LU7	−7	His41, Tyr54, Phe140, Leu141, Ser144, Cys145, His163, Met165, Glu166, Leu167, Pro168, Asp187	[166]
Fagaronine	*Fagaraz anthoxyloides*	Autodock 4.2.	6LU7	−6.21	Glu14, Gly71, Lys97, Ser121	[167]
Isoboldine	*Corydaliscava, Glaucium flavum, Peumus boldo*			−5.99	Gly11, Lys12, Pro96, Lys97, Asp155	
Sageone	*Salvia officinalis*			−5.97	Arg298	
Lycorine	*Clivia miniata*			−5.86	Leu141, Ser144, Cys145, His164	
Wogonin	*Scutellaria baicalensis*			−5.62	Thr199, Tyr239, Leu271	
Epicatechingallate	Green tea	Autodock Vina	6LU7	−9.0	Phe140, Gly143, Ser144, Cys145, His163	[147]
Gallocatechin-3-gallate				−8.2	Thr26, His41, Gly143, Ser144, Cys145, Glu166	
Epigallocatechin				−7.2	Ser144, His163, Thr190, Gln192	
Gallocatechin				−7.2	Ser144, His163, Arg188, Thr190	
Catechin				−7.1	Phe140, Glu166, Arg188, Gln192	

(*continued on next page*)

Table 4 (*continued*)

Compounds	Source[1]	Software	PDB[2]	Binding energy (kcal/mol)	H-bonds	Reference
Epicatechin				−7.1	Leu141, Ser144, His163, Gln192	
Catechin gallate				−7	Ser144, His163, Gln192	
Deacetylnomilin	–	AutoDock 4.2	7BQY	−8.35	Thr26, Gly143, Glu166	[168]
Ichangin	–			−8.4	His41, Glu166, Gln189	
Nomilin	–			−8.51	Asn142, Ser144, Glu166	
β-Amyrin	–			−8.79	Gln192	
Hyperoside	Neem	Autodock Vina	6LU7	−8.6	Leu141, Ser 144, His163, Arg188, Thr190, Gln192	[130]
α-Hederin	*Nigella sativa*			−8.5	His 163, Glu166, Gln189	
Nimbaflavone	Neem			−8	His163	
Epigallocatechin	*Camellia sinensis*			−7.3	Leu141, Ser144, Cys145, His163	
Catechin				−7.1	Thr26, Gln189	
Piperine	*Piper nigrum*			−6.7	Thr25, Ser144, Cys145	
Echinocystic acid diacetate	*Luffa cylindrica*			−6.8	Glu166	
Hypericin	–	Autodock Vina	6LU7	−10.7	Leu141, Asn142, Glu166	[123]
Pseudohypericin	–			−10.7		
Cyanidin-3-Glucoside	–			−8.4	Thr26, Leu141, Gly143, Glu166, Asp187, Gln189	
Glabridin	–			−8.1	–	
Amentoflavone	*Torreya nucifera*	Autodock Vina	6LU7	−9.2	Thr26, Glu166	[169]
Bilobetin				−9.1	–	
Ginkgetin				−9	Thr26, Asn142	
3′-(3-methylbut-2-enyl)-3′,4′,7-trihydroxyflavane	*Broussonetia papyrifera*	Autodock Vina	6LU7	−8.2	Leu141, Asn142, Gly143, Cys145, Glu166	[170]
Broussochalcone A				−8.1	Thr26, Gly143, Ser144, Cys145, Glu16	
Kazinol F				−8.1	Leu141, Gly143, Met165	
Kazinol J				−8	Ser144, His163, Thr190	
Papyriflavonol A				−7.9	Leu141, Cys145, Arg188	
Broussoflavan A				−7.8	Gly143, Glu166	
Heptafuhalol A	*Sargassum spinuligerum*	Autodock Vina	6LU7	−15.4	Thr24, His41, Ser46, Asn142, Gly143, Glu166, Pro168	[171]
Phlorethopentafuhalol B				−14.6	Thr26, Leu27, Phe140, His163, Glu166, Gln189, Thr190	
Pseudopentafuhalol C				−14.5	Thr26, Phe140, Asn142, Gly143, His163, Glu166, Gln189, Thr190	
Phlorethopentafuhalol A				−14	Phe140, Asn142, His163, Glu166, Gln189, Thr190	
Hydroxypentafuhalol A				−14.6	Thr25, Thr26, His41, Cys145, Glu166	
Pentaphlorethol B				−13.9	Thr26, Asn142, Gly143, Cys145, His163, Glu166, Gln189, Thr190	
8,8′-Bieckol				−13.7	Thr26, Ser46, Asn142, Glu166, Gln189, Thr190	
Apigenin-7-O-neohesperidoside				−12.4	Phe140, Leu141, His163, Glu166, Thr190	
Luteolin-7-rutinoside				−12.1	Phe140, Glu166, Thr190	
6,6′-Bieckol				−12.2	Thr26, His41, Asn142, Gly143, Arg188, Gln189	
Dieckol				−12	–	
Pseudotheonamide D				−12.2	Asn142, Ser144, Cys145, Glu166, Asp187	
Aeruginosin 98B				−12.1	Gly143, Cys145, Glu166, Gln189, Thr190	
Resinoside B				−12.2	Thr26, Phe140, Leu141, Asn142, His163, Glu166, Thr190	
Pentaphlorethol A				−12.8	Thr25, Thr26, Asn119, Gly143, Cys145, His163, Glu166	
Tunichrome An2				−11.5	Thr26, Glu166, Gln189, Thr190	
Pseudotheonamide C				−10.5	Thr26, Asn142, Gly143, Ser144, Cys145, Pro168	
Berbamine	*Berberis asiatica*	Autodock Vina	6 W63	−9.7	Met165	[117]
Oxyacanthine				−8.5	Asn142, Thr190	
1-(3-(2,5,9-trimethyl-7-oxo-3-phenyl-7H-furo[3,2–g]chromen-6-yl) propanoyl)piperidine-4-carboxamide (ZINC02123811)	–	Autodock Vina	6LU7	−9.6	Phe140, Gly143, Ser144, Cys145, Glu166	[172]
Palmatine	–	Autodock Vina	6 W63	−8.9	His41, Met49	[173]
Sauchinone	*Saururus chinensis*			−8.7	Thr26, His41, Gln189, Thr190	
Diosmetin	*Citrus limon*	Not mentioned	5R84	−7.35	Met49, Asn142, Ser144, His163, Glu166	[144]
Apigenin				−7.29	Arg298	
Luteolin				−7.26	Arg298	
Eriodictoyl				−6.92	Arg298	
Spinacetin			5R80	−6.6	Arg298	

Table 4 (*continued*)

Compounds	Source[1]	Software	PDB[2]	Binding energy (kcal/mol)	H-bonds	Reference
Taraxerol	*Clerodendrum* spp	Autodock	6LU7	−8.4	–	[174]
Friedelin		Vina		−7.9	–	
Stigmasterol				−7.7	–	
Demethoxyguiaflavine	*Strychnos nux-vomica*	Autodock	6Y2G	−10.1	Arg188, Thr190	[175]
Strychnoflavine		Vina		−9.9	Arg188, Thr190	
Nb-Methyllongicaudatine				−9.6	Thr26, Asn142, Glu166	
Bis-nor-dihydrotoxiferine				−9.4	Asn142	
Strychnochrysine				−9.1	Arg188	
Guianensine				−8.8	Ser46, Arg188	
Vomicine				−8.7	Gly143, Ser144	
10-Hydroxyl-icajine				−8.6	His41, Leu141, Gly143, Cys145	
N-methyl-*sec*-pseudo-beta-colubrine				−8.3	His41, Phe140, Gly143, His163, Glu166	
Stryvomicine				−8.3	Leu141, Gly143, Ser144	
Fostularin 3	Family *Aplysinidae*	MOE	6MO3	−7.58	Ser46, Met49, Asp187, Gln192, Ala194, Thr169, Gln189	[109]
Gartanin	–	Glide	6LU7	−7.74	His41, Asn142, Gly143, Gln189	[124]
Robinetin	–			−7.51	Thr26, His41, Met165, Asp187	
Vitexin	*Moringa olifera*	Autodock Vina	6 W63	−8.4	Tyr54, Asn142, Gly143, Ser144, His163, Glu166, ASp187	[176]
Kaempferol-3-O-rutinoside				−8.2	His41, Glu166, Leu167, Arg188, Thr190	
Neoandrographolide	*Andrographis paniculata*	Autodock Vina	6LU7	−7.1	Phe140, Leu141, Ser144, His163, Glu166	[177]
Psi-taraxasterol	–	Autodock Vina	6LU7	−8.5	Met49, Cys145, Met165	[148]
Kazinol T	*Broussonetia kazinoki*	Piper algorithm	6Y7M	−14.36	His41, Gly143, Thr190	[178]
Butyrolactone I 3-sulfate	*Aspergillus terreus*			−13.85	His41, Gly143, Cys145, Glu166	
Ebenfuran III	Onobrychis ebenoides			−13.56	Asn142, Met165	
Paulowniones A	*Paulownia tomentosa*			−13.47	Ser144, Gln189	
3,5,7-Trihydroxy-8-(3-Methoxy-3-Methylbutyl)-2-(4-Methoxyphenyl) Chromen-4-One	–			−12.73	Not described	
Schizolaenone B	–			−12.72	Not described	
Praeruptorin B	–			−12.7	Not described	
NPC67197	–			−12.59	Not described	
Variecolorin G	–			−12.58	Not described	
2-Hydroxygarvin A	–			−12.23	Not described	
Toddacoumaquinone	–			−12.05	Not described	
(4-Hydroxy-3-Methoxycarbonyl-2,5-Dimethylphenyl) 3-Formyl-2,4-Dihydroxy-6-Methylbenzoate	–			−12.02	Not described	
Withanolide R	*Withania somnifera*	Autodock 4.2.	6LU7	−9.63	Not described	[179]
27-Deoxy-14-hydroxywithaferin A				−10.8	Not described	
Nimolicinol				−10.09	Not described	
17-Hydroxywithaferin				−10.08	Not described	
Urso-deoxycholic acid	*Ipomoea obscura*	Glide 5.5	6LU7	−7.11	Ser46, Phe140	[180]
Demeclocycline				−6.81	Gly143, Glu166	
Tetracycline				−5.95	Glu166	
Chlorotetracycline				−4.72	Thr26, Leu141, Gly143, Ser144	
Ethyl *iso*-allocholate				−4.42	Thr26, Gln189	
Agathisflavone	*Anacardium occidentale*	Autodock	5R81	−8.2	Arg40, Pro52, Asp187	[181]
Rubusic acid	*Pedalium murex*	Vina		−8.1	Not described	
Solanocapsine	*Solanum nigrum*			−7.9	Not described	
Chlorogenin	*Solanum torvum*			−7.7	Not described	
Lupeol	*Carica papaya* and *Azadirachta indica*			−7.7	Not described	
Cyanin	*Zingiber officinale*			−7.7	Thr26, Ser46, Glu166	
3-O-*trans*-caffeoyltormentic acid	*Terminalia chebula*			−7.7	Not described	
Luteolin 7-O-(6′′-malonylglucoside)	*Vitex negundo*			−7.7	Not described	
Agnuside	*Vitex negundo*			−7.6	Not described	
Luteolin 7-O-beta-D-glucoside	*Vitex negundo*			−7.6	Not described	
Afzelin	*Euphorbia Hirta*	Autodock	6LU7	−9.3	Tyr54, Thr190, Leu141, Ser14, Glu166	[110]
Phloroglucinol	*Hypericum perforatum L.*	Vina		−9.3	Arg188 Gln189	
Myricetin-3-O-rutinoside	*Limoniastrum Guyonianum*			−9	Leu141 Gly143	
Tricin 7-neohesperidoside	*Chamaerops humilis L*			−8.5	Glu 166 Thr26 Ser144 Cys145	
Silybin	*Silybum marianum*			−8.3	Glu166, Ser144, Cys145	
Silychristin	*Silybum marianum L.*			−8.3	Arg188, Asn142	
Germacranolide	*Costus speciosus*	Autodock 4.2.	6LU7	−7.4	His163	[182]
Andrograpanin	Andrographis paniculata			−7.37	Not described	
Hetisinone	*Aconitum heterophyllum*			−7.37	Not described	
Costunolide	*Costus speciosus*			−7.3	Not described	
14-deoxy-14,15-didehydroandrographolide	*Andrographis paniculata*			−7.26	Not described	

(*continued on next page*)

Table 4 (*continued*)

Compounds	Source[1]	Software	PDB[2]	Binding energy (kcal/mol)	H-bonds	Reference
Palmatine	*Tinosporia cordifolia*			−7.12	Not described	
Hetisine	*Aconitum heterophyllum*			−7.1	Not described	
14-deoxy-11,12-didehydroandrographolide	Andrographis paniculata			−7.06	Not described	
Isoarboreol	*Gmelina arborea*			−6.97	Not described	
Serratin	*Clerodendrum serratum*			−6.95	Not described	
Piperamide	*Piper nigrum*			−6.84	Not described	
Bamipine	*Piper nigrum*			−6.77	Not described	
Abscisic acid	*Pterocarpus marsupium*			−6.68	Not described	
Gmelinol	*Gmelina arborea*			−6.47	Not described	
Laurotetanin	*Litsea glutinosa*			−6.38	Not described	
Phyllantidine	*Phyllanthus emblica*			−6.36	Not described	
Cepharadione	*Piper longum*			−6.06	Not described	
Pogopyrone	*Pogostemon cablin*			−6.03	Not described	
Boldine	*Litsea glutinosa*			−5.86	Not described	
Vomifoliol	*Sidaacuta*			−5.59	Not described	
N-isobutyl-(2E,4Z,8Z,10E)-dodecatetraenamide	*Anacyclus pyrethrum*			−5.5	Not described	
Delphinidin 3,5-diglucoside	Pomegranate	Glide	6LU7	−12.2	Leu141, Asn142, Cys145, His164, Glu166, Thr‘190	[127]
3,5-Di-O-galloylshikimic acid	–			−10.3	Asn142, Gly143, His163, Glu166, Gln189, Thr190	
Avicularin	*Polygonum aviculare,Rhododendron aureum, Taxillus kaempferi*			−9.6	Cys145, His164, Glu166, Thr190	
Scutellarein 7-glucoside	*Verbena officinalis L; Buddleja madagascariensis Lam, Plantago asiatica L, Polygonum odoratum*			−9.3	Cys145, His163, Glu166, Gln192	
3,8′-biapigenin	*Hypericum perforatum*	Autodock	6 W63	−10.4		[183]
Methyl amentoflavone	*Selaginella sinensis, Ginkgo biloba, Cupressaceae* spp.	Vina		−10.1	Thr26, Ser46, Asn142, His163, Glu166	
Podocarpusflavone A	*Podocarpus macrophyllus, Garcinia* spp.			−10	His41, Met49, Glu166, Leu167	
Kaempferol-3-robinobioside	*Piper nigrum, Annona coriacea*			−9.8	Thr26, Tyr54, Leu141, Asn142, Cys145, His163, Glu166	
Isoginkgetin	*Ginkgo biloba*			−9.8	His41, Met49, Glu166, Leu167	
Theasinensin B	*Camelia sinensis*			−9.8	Not described	
3,5 digalloylepicatechin	*Camelia sinensis*			−9.8	Not described	
Neotheoflavin 3-gallate	*Camelia sinensis*			−9.7	Not described	
Quercetin 3-O-xylosyl glucuronide	apache fruit, blackberry, and raspberry			−9.5	Not described	
Vitamin D2	–			−9.5	Not described	
Albanin F	*Morus alba*			−9.4	Leu141, Cys145, Glu166, Asp187	
Bianthraquinone	*Polygonaceae, Rhamnaceae, Rubiaceae, Fabaceae, Xanthorrhoeaceae*			−9.4	Not described	
Isoquercitrin	*Mangifera indica, Rheum rhabarbarum, Annona reticulata, camelia sinensis*			−9.3	Not described	
Withastramonolide	*Withania somnifera*			−8.9	Not described	
Luteolin 7-O-b-glucopyranoside	*Amphilophium paniculatum*	MOE 2019.0102	7BUY	−9.54	Asn142, Gly143, Cys145, Glu166	[136]
Acacetin 7-O-b-rutinoside				−8.54	Gly143, Cys145	
Isoacteoside				−8.46	Thr26, His41, Met49, Gly143, His164, Met165, Glu166, Gln189	
Luteolin				−8.34	Cys44	
(+)-Lyoniresinol 3a-O-b-glucopyranoside				−7.95	Met49, Leu141, Cys145	
Amphipaniculoside A				−7.56	Asn142, Gly143, Glu166	
()-Lyoniresinol 3a-O-b-glucopyranoside				−7.45	Thr26, Met49, Asn142, Cys145, Met165	
2‴,3‴-Diacetyl martynoside				−7.02	Met49, Asn142, Met165	
Isomartynoside				−6.68	Asn142, Met165, Glu166, Leu167	
Cinnamtannin B2	*Cinnamomum zeylenicum*	Autodock	6LU7	−10	Glu166, Gln189	[184]
Cyanin	*Allium sativum*	Vina		−9.4	Asn142, Glu166, Thr190	
Withanoside V	*Withania somnifera*	Autodock	6LU7	−10.32	Asn84, Arg40	[131]
Somniferine	*Withania somnifera*	Vina		−9.62	Leu141, His 164, Thr 24, Glu 166, Asn 142, Phe 140, His 163	
Tinocordiside	*Tinospora cordifolia*			−8.1	Leu141, Gly143	
Vicenin	*Ocimum sanctum*			−8.97	Glu166, Pro168, Gln189, Thr190	
Isorientin 4′-O-glucoside 2″-O-p-hydroxy-benzoagte	*Ocimum sanctum*			−8.55	Arg40, Tyr54, Arg105, Arg188	
Capsazepine	*Capsicum annuum* L.	Autodock	6LU7	−8.8/-7.0	His41, Cys145, Gln189	[112]
Aronadendin	*Alium cepa L.*	4.2/		−8.7/-7.9	Glu166	
Leucopelargonidin	*Alium cepa L.*	Autodock		−7.8/	Glu166, Gln189	

Table 4 (*continued*)

Compounds	Source[1]	Software	PDB[2]	Binding energy (kcal/mol)	H-bonds	Reference
		Vina		−6.7		
Astragalin	*Opuntia ficus-indica*	Autodock	6Y84	−7.9	Phe140, GLu166	[185]
Isorhamnetin		Vina		−7.3	Thr26, Asn142, Gln189	
Isorhamnetin 3-O-glucoside				−7.5	Thr24, Thr26, His41, Leu141, Asn142, Gly143, Gln189	
3-O-caffeoyl quinic acid				−7.1	Thr26, Leu141, Ser144, Cys145, His163	
Quercetin 5,4′-dimethyl ether				−7.3	His41, Asn142	
E, E, Z-1,3,12-nonadecatrienome-5,14-diol	*Halymenia durvillei*	GOLD software version 1.10.5/	6LU7	27.4/-5.0	Not described	[186]
1–2 tetradecandiol		Autodock		21.7/ −3.8		
Cholest-5-En-3-Ol (3.Beta.)-				25.7/ −3.6		
Withanoside V	*Withania somnifera*	Glide	6LU7	−8.96	Thr24, Thr25, Thr26, His163Glu166	[187]
Solanine	*Solanum genus*	Glide XP	6LU7	−10.3	Leu141, His164, Glu166	[113]
Procyanidin A3	–	protocol		−12.86	Thr26, Leu141, Glu166, Thr190	
Procyanidin A4	–			−10.01	Glu166, Pro168, Gln189, Thr190	
Procyanidin B4	litchi pericarp, grape seeds			−9.94	Leu141, Asn142, Gly143, Glu166	
Hypericin	*Hypericum perforatum*			−9.56	Leu141, His164, Glu166, Gln189	
Procyanidin	–			−9.21	Leu141, Asn142, Glu166, Thr190	
Astragalin	*Allium ursinum, Allium sativum, Cassia alata, Cuscuta chinensis, Phytolacca americana*			−9.12	Leu141, Thr190	
Salicin	–			−8.45	Not described	
Emodin-8-glucoside	–			−8.21	Not described	
Hinokiflavone	–			−8.13	–	
Procyanidin C2	–			−8.11	Not described	
Indican	–			−8.08	–	
Chebulic acid	–			−8.08	Not described	
Amentoflavone	–			−7.98	–	
(-)-Catechin gallate	–			−7.96	Not described	
Fisetin	–			−7.94		
18,β-Glycyrrhetinic acid	–	Autodock-Lamarckian Genetic Algorothm	6Y84	−9.19	Not described	[134]
Rhodiolin	–			−9.05	–	
Silymarin	–			−8.71	Not described	
Lucyoside H	*Luffa cylindrica*	PyRx 0.9.4	6LU7	−7.54		[188]
Lucyoside F				−7.47	Not described	
3-O-β-D-Glucopyranosyl-oleanolic acid				−7.29	–	
3-O-β-D-Glucopyranosyl-spinasterol				−7.13	–	
Anisotine	*Justicia adhatoda*	Autodock	6LU7	−8.4	Gly143	[189]
Amarogentin	*Sertia chirata*	Vina		−8.0	His41, Glu166	
Adhatodine	*Justicia adhatoda*			−7.9	Thr26	
Beta-carotene	*Ocimum sanctum*			−7.8	–	
Mangiferin	*Sertia chirata*			−7.8	Leu141, Gly143, Ser144, His164, Glu166, Thr190	
Eugenol	*Ocimum sanctum*			−7.6	Glu166	
Vasicoline	*Justicia adhatoda*			−7.4	–	
Vasicolinone	*Justicia adhatoda*			−7.3	Gly143, Ser144, Cys145	
Caryophyllene	*Ocimum sanctum*			−7.1	Pro168, Gln189	
Crocin	*Crocus Sativus L.*	Autodock Vina	6LU7	−8.2	Phe3, Arg4, Lys5, Arg131, Asn133, Thr135, Lys137, Thr199	[190]
Digitoxigenine	*Nerium Oleander*			−7.2	Gln110, Asp135	
β-Eudesmol	*Lauris Nobilis L*			−7.1	Thr111	
Bergenin	*Dictyophora indusiata*	Autodock 4.2	6LU7	−7.86	Gly143, Ser144, His163, Glu166, Gln189	[191]
Quercitrin	*Geassstrum triplex*			−10.2	Tyr54, His163, Thr190, Gln192	
Dihydroartemisinin	*Cyathus stercoreus*			−7.2	Gly143, Ser144, Cys145	
Dihydro-onnamide A	Marine sponges (*Theonella* and	MOE	6Y2G	−10.2	–	[192]
Onnamide C	*Trachycladus* genera)	2019.012		−9.60	Pro168	
Pseudo-onnamide A		suite		−9.81	Thr26, Gly170	
Theopederin G	*Theonella* marine sponges			−8.45	Gly143, His164	
Pederin	*Paederus littoralis*			−7.95	Asn142, Cys145, His164	
Pyranonigrin A		Autodock Vina		−7.3	Leu141, Asn142, Gly143, Ser144, Cys145, His163, Glu166, Gln189	[193]
Citriquinochroman	*Penicillium citrinum*	Autodock Vina		−14.7	Thr26, Asn142, Gly143, Cys145, Glu166, Asp187, Arg188, Gln189, Thr190, Gln192	[194]
Holyrine B	Marine-derived actinomycetes			−14.5	Leu141, Asn142, Gly143, Ser144, Cys145, His163, His164, Glu166, Pro168, Asp187, Arg188, Gln189,	

(*continued on next page*)

Table 4 (*continued*)

Compounds	Source[1]	Software	PDB[2]	Binding energy (kcal/mol)	H-bonds	Reference
					Thr190, Gln192	
Proximicin C	Marine actinomycete Verrucosispora MG-37			−14.1	Gly143, Ser144, Cys145, Glu166, Pro168, Asp187, Arg188, Gln189, THr190	
Pityriacitrin B	Human pathogenic yeast *Malassezia furfur*			−13.4	Phe140, Leu141, Gly143, Ser144, Cys145, His163, His164, Met165, Glu166, Gln189	
Anthrabenzoxocinone	A soil-derived *Streptomyces* sp.			−13.2	Thr26, His41, Cys44, Asn142, Gly143, Cys145, His164, Met165, Glu166, Val186, Asp187, Arg188, Gln189, Thr190, Gln192	
Penimethavone A	Gorgonian marine soft coral-derived *Penicillium chrysogenum*			−12.1	Leu141, Gly143, Ser144, Cys145, His164, Met165, Glu166, His172, Val186, Asp187, Arg188, Gln189, Gln192	
Spinasterone	*Zingiber officinale*	Glide XP protocol	6M2N	−87.41	–	[137]
Spinasterol				−78.11	Thr190	
24-methylcholesta-7-en-3β-on				−68.8	Cys44	
Cryptomisirine	*Cryptolepis sanguinolenta*	Autodock Vina	6LU7	−10.6	Met165	[195]
Cryptospirolepine				−10	Gly143, Asn142	
Cryptoquindoline				−9.5	Glu166	
Biscryptolepine				−8.8	Gln189	
Arzanol	–	Autodock Vina	6LU7	−6.3	Gln189	[196]
Ferulic acid	–			−4.7	Glu14, Met17, Gly71	
Genistein	–			−6.6	Thr26, Asn142, Gly143, Glu166	
Resveratrol	–			−5.8	Pro52, Asn180, Arg188	
Rosmanol	–			−6.7	Asn142, Gln189	
Thymohydroquinone	–			−5.0	Ala70, Asn95	

[1] : Natural source of the compound mentioned in the respective reference (plant or a microorganism) [2]: The PDB ID for the protease structure that was used as receptor for the molecular docking simulation.

case and RdRp. It is interesting that Muhseen *et al.* [133] report Asn238 and Asp289 as residues participating in hydrogen bonds with the compound, suggesting its binding affinity to a different site of the protease than the active site [123,133,134].

Vanicoside A and B are two phenylpropanoid glycosides detected in plants *Reynoutria japonica* and *Reynoutria sachalinensis* that have been found to inhibit M^{pro} *in vitro* with IC_{50} values of 23.10 and 43.59 μM, respectively. *In silico* analysis of their binding to the protease using the software GOLD reveals a higher docking score than inhibitor N3 (115.78 and 129.7 as opposed to 86.56) and hydrogen bonds with residues Thr26, Cys145, Glu166, Gln189, Thr190 and Cys44, Tyr54, Leu141, Asn142, Cys145, His164, Gln189 for each of the compounds respectively [135]. Another compound is **acteoside**, for which an IC_{50} of 43 μM and a binding energy of −10.13 kcal/mol calculated through the Glide software have been reported. The molecular docking simulation pointed out the formation of hydrogen bonds with residues Cys44, Met49, Asn142, His164, Glu166 and Thr190. The binding mode of acteoside in the active site of M^{pro} is more likely to be non-covalent, despite the presence of an α,β-unsaturated ester moiety, which could theoretically act as a covalent warhead [121]. Another work describes the results of both covalent and non-covalent docking simulations for acteoside and reports docking scores of −11.98 and −6.91 kcal/mol, respectively [125]. A third study including the compound conducted non-covalent docking and calculated a higher binding energy (-8.33 kcal/mol) with quite different interactions, showing formation of hydrogen bonds with major residues Gly143, Cys145, His164 and Glu166 [136].

Another category of compounds with confirmed anti-SARS-CoV-2 M^{pro} activity by *in vitro* assays is procyanidins. More specifically, **procyanidin B2** appeared to block S1, S1′ and S2 subsites of the protease and form hydrogen bonds with residues Gly143, Cys145 and Glu166 in a molecular docking simulation performed using Autodock Vina. The binding energy was calculated to be as low as −9.2 kcal/mol. Its inhibitory effect was confirmed *in vitro*, with an IC_{50} of 75.31 μM calculated through a fluorescent substrate assay [119]. A derivative of the compound, Procyanidin B2 3,3′-di-*O*-gallate, has been tested in a different study, with a similar type of assay, and resulted in approximately 37% inhibition at a concentration of 100 μM. Procyanidin C1 reduced enzymatic activity to 77.7% at the same concentration [135]. Other procyanidins, namely procyanidin A3, A4, B4 and C2, have displayed very promising binding energies in an *in silico* study (-12.86, −10.01, −9.94 and −8.11 kcal/mol). It is worth mentioning that all four compounds have a more favorable binding energy than inhibitor N3, which was used as positive control and had a binding energy of −7.93 kcal/mol. It is worth to notice that three of of four procyanidins showed higher binding affinity than the *in vitro* documented active procyanidin B2, for which a binding energy of −8.56 kcal/mol was calculated in the same study [125].

24-methylcholesta-7-en-3β-on is a phytosterol, detected among many plant sources including *Zingiber officinale*, while also being the most abundant sterol in *Polyporus sulfureus*. When its inhibitory effect was evaluated with a FRET-based assay, the compound caused 75% enzyme inhibition at 200 μg/mL, while the positive control GC376 resulted in 77% inhibition at 100 μM. Moreover, molecular dynamics simulation indicated good stability of its complex with M^{pro}, as well as hydrogen bonding with residue Cys44 [137].

Punicalagin is a large, complex natural compound found in abudance in pomegranate. It reduced the activity of M^{pro} by half at a concentration of 6.19 μg/mL in a fluorescent substrate assay, while it displayed synergy with zinc sulfate, reducing the activity of the protease 24% more than punicalagin alone, when the two compounds were at concentrations of 10 μg/mL and 3 mg/mL, respectively [138].

The binding mode and structure of reported triterpenoids and phenylethanoid glycosides is presented in Fig. 11, while other compounds are presented in Fig. 12. In addition, there have been

numerous studies providing indications of the potency of various phytochemicals against the M^{pro}, which employ molecular docking simulations and other *in silico* tools, however the enzyme inhibition is not confirmed yet by *in vitro* assays. The compounds that stood out from these studies are summarized in Table 4.

7. Plant extracts with inhibitory activity against SARS-CoV-2 M^{pro}

Apart from pure natural compounds, extracts containing various constituents have been evaluated for their overall inhibitory effect against M^{pro}. The inhibition in such cases is often attributed to the synergistic effect of the major bioactive compounds in the extract. A study performed by Guijarro-Real *et al.* [122] tested various plant extracts for their ability to inhibit M^{pro} in a FRET-based assay and underlined mustard seeds, wall rocket and turmeric extracts as plant extracts with high inhibitory potential. More specifically, the IC_{50} values calculated were 15.74 μg/mL for the turmeric extract, 128.1 μg/mL for the mustard seeds extract and 257.4 μg/mL for the wall rocket extract. Commercial curcumin, present in turmeric extracts, showed inhibitory activity against M^{pro}, as mentioned previously. However, the inhibitory effect of the compound combined with the fact that reported concentrations of curcumin in turmeric powder do not exceed 3%, suggest that the activity of the extract is not due to curcumin alone, but also due to other components of the extract. Moreover, allyl isothiocyanate, a hydrolysis derivative of sinigrin, which naturally occurs in wall rocket and mustard extracts, demonstrated strong inhibition of M^{pro}, with an IC_{50} of 41.43 μg/mL, providing an encouraging lead for further investigation. Celery leaves, parsley, oregano, aloe vera leave and wasabi powder extracts also exhibited moderate inhibitory activity, resulting in reduction of the activity of the enzyme to 35.8–54.8% at a concentration of 500 μg/mL.

The traditional Chinese patent medicine, Shuanghuanglian preparation, which is being used for treatment of acute respiratory tract infections has been also investigated in *in vitro* assays. A FRET assay was used to determine the inhibitory effect of the medicine in the form of oral liquid, as produced from three different companies, and resulted in the calculation of IC_{50} values of 0.090 ± 0.004, 0.064 ± 0.011 and 0.076 ± 0.007 μL/mL respectively. When tested in Vero E6 cells, the three oral liquids resulted in an EC_{50} of 1.20 ± 0.18, 1.07 ± 0.04 and 0.93 ± 0.19 μL/mL respectively. The high content of the oral liquids in baicalin (12.72 to 17.52 mg/mL) as opposed to baicalein (0.06–0.22 mg/mL) leads to the conclusion that baicalin is mainly responsible for the inhibitory effect of the preparation against SARS-CoV-2 M^{pro} [103].

Plants *Reynoutria japonica* and *Reynoutria sachalinensis* have been used in Chinese traditional medicine to combat upper respiratory tract infections, too. Both their acetone and butanol extracts have been evaluated for their SARS-CoV-2 M^{pro} inhibitory activity, yielding encouraging results. Overall, *R. sachalinensis* showed better inhibitory effect, with IC_{50} values of 9.42 and 4.03 μg/mL for the acetone and butanol extracts respectively, compared to 16.90 and 7.88 μg/mL for *R. japonica*. Evidently, the butanol extracts performed better compared to the acetone ones. The higher inhibitory activity was attributed to the presence of more procyanidins and phenylpropanoid disaccharide esters [135].

Low IC_{50} values were also provided by the extract of *Cuphea ignea*. A crystal violet assay was used to evaluate both the ethanolic extract of the plant and a self-nanoemulsifying formulation containing oleic acid, Tween 20 and propylene glycol with improved solubility. The respective IC_{50} values were almost identical, 2.47 and 2.46 μg/mL [139]. Comparable IC_{50} values were also calculated for the flavonoid-rich fraction of the aqueous extract of *Salvadora persica* (IC_{50} = 8.59 μg/mL), the aqueous extracts of green (IC_{50} = 8.9 μg/mL) and black tea (IC_{50} = 10.0 μg/mL) and *Terminalia chebula* (IC_{50} = 8.8 μg/mL), as well as the ethanol extract of *Scutellaria baicalensis* (IC_{50} = 8.52 μg/mL), calculated through a fluorescent, colorimetric and casein substrate inhibition assays [105,140,141]. Lastly, the aqueous extract of licorice is reported to have an antiviral effect at a concentration of 2 mg/mL in Vero E6 cells infected with a viral load of 100 times the 50% tissue culture infective dose/mL [132]. The information on the inhibitory effect of the plants extracts is presented in Table 5.

Table 5
Plant extracts with tested inhibitory activity against SARS-CoV-2 M^{pro} by *in vitro* assays.

Plant	Type of extract	Major constituent(s)	IC_{50} (μg/mL)	Method	Reference
Curcuma longa	methanolic extract	Curcumin	15.74	FRET assay	[122]
Brassica nigra	methanolic extract	Sinigrin, allyl isothiocyanate	128.1		
Diplotaxis erucoides	methanolic extract	Sinigrin, allyl isothiocyanate	257.4		
Lonicera japonica, Scutellaria baicalensis, Forsythia suspense	commercial shuanghuanglian oral liquids	Chlorogenic acid, phillyrin, baicalin, baicalein,	0.064–0.090	FRET assay	[103]
Reynoutria japonica	butanol extract	Proanthocyanidins, flavan-3-ols, phenylpropanoid disaccharide esters	7.88	Fluorescent substrate assay	[135]
Reynoutria sachalinensis	butanol extract	Proanthocyanidins, flavan-3-ols, phenylpropanoid disaccharide esters	4.03		
Cuphea ignea	ethanolic leaf extract	p-Coumaric acid, Myricetin-3-O-rhamnoside, Gallic acid, Rutin, Syringic acid	2.47	Crystal violet assay	[139]
Salvadora persica L.	FRF (flavonoid rich fraction) from the aqueous extract of the plant leaves and stems	Kaempferol and isorhamnetin glycosides	8.59	Fluorescent substrate assay	[140]
Scutellaria baicalensis	70% ethanol extract	Baicalein, baicalin, wogonin, wogonoside	8.52	Colorimetric substrate enzyme inhibition assay	[105]
Camelia sinensis (green tea)	aqueous leaf extract	Thearubigin, quercetin-3-O-rutinoside, hesperidin	8.9	Casein substrate enzymatic assay	[141]
Camelia sinensis (black tea)	aqueous extract	Thearubigin, quercetin-3-O-rutinoside, hesperidin	10.0		
Terminalia chebula	aqueous extract	Not described	8.8		
Licorice	acqueous root extract	Glycyrrhizin			[132]

8. Conclusions

Overall, research has resulted in very promising leads regarding both the design of targeted drugs and the utilization of isolated natural compounds or crude plant extracts. The former are able to very efficiently inhibit M^{pro}, even at micromolar concentration levels, while the latter, despite displaying an inhibitory effect at overall higher concentrations compared to the designed drugs, can open up various possibilities for valorization of biomass and developing alternative solutions for boosting immunity. In both cases, it is very encouraging that there are numerous effective candidates with high potential against M^{pro}, while some also show indication of action against other viral proteins. Taking into consideration the high conservation observed in the sequences encoding M^{pro} among coronaviruses, many of these compounds have originated from research targeting the main proteases of SARS-CoV-1, MERS or other viruses. In a similar manner, the large number of data emerging from current research is not only useful for combating the ongoing pandemic, but also for laying foundations for ways to fight future viral outbreaks. In this context, it is important to point out that *in silico* methods play a major role in identifying potent hits, facilitating the study of structure–activity relationships and the prediction of suitable structural groups, the rapid screening of large number of candidates, as well as the investigation of the impact of potential mutations on the efficacy of these candidates. However, it is necessary that both the antiviral and the pharmacokinetic properties of these compounds are further investigated *in vitro* and *in vivo,* so as to determine whether they can be used as pharmaceutical products or functional foods, respectively.

CRediT authorship contribution statement

Io Antonopoulou: Conceptualization, Investigation, Methodology, Resources, Supervision, Validation, Visualization, Writing – original draft, Writing – review & editing. **Eleftheria Sapountzaki:** Conceptualization, Investigation, Methodology, Visualization, Writing – original draft, Writing – review & editing. **Ulrika Rova:** Conceptualization, Methodology, Resources, Validation, Writing – review & editing. **Paul Christakopoulos:** Conceptualization, Methodology, Resources, Validation, Writing – review & editing.

Declaration of Competing Interest

The authors declare that they have no known competing financial interests or personal relationships that could have appeared to influence the work reported in this paper.

References

[1] Hu Y, Ma C, Szeto T, Hurst B, Tarbet B, Wang J. Boceprevir, Calpain Inhibitors II and XII, and GC-376 Have Broad-Spectrum Antiviral Activity against Coronaviruses. ACS Infect Dis 2021;7(3):586–97. https://doi.org/10.1021/acsinfecdis.0c00761.

[2] Wu C et al. Analysis of therapeutic targets for SARS-CoV-2 and discovery of potential drugs by computational methods. Acta Pharm Sin B 2020;10(5):766–88. https://doi.org/10.1016/j.apsb.2020.02.008.

[3] S. V. Stoddard *et al.*, "Optimization rules for SARS-CoV-2 Mpro antivirals: Ensemble docking and exploration of the coronavirus protease active site," *Viruses*, vol. 12, no. 9, 2020, doi: 10.3390/v12090942.

[4] Rubin D, Chan-Tack K, Farley J, Sherwat A. FDA Approval of Remdesivir — A Step in the Right Direction. N Engl J Med Dec. 2020;383(27):2598–600. https://doi.org/10.1056/NEJMp2032369.

[5] U.S. Food and Drug administration, "Know Your Treatment Options for COVID-19," 2021. https://www.fda.gov/consumers/consumer-updates/know-your-treatment-options-covid-19.

[6] Koudelka T et al. N-Terminomics for the Identification of In Vitro Substrates and Cleavage Site Specificity of the SARS-CoV-2 Main Protease. Proteomics 2021;21. https://doi.org/10.1002/pmic.202000246.

[7] Z. Jin, X. Du, Y. Xu, Y. Deng, M. Liu, and Y. Zhao, "Structure of M pro from SARS-CoV-2 and discovery of its inhibitors," *Nature*, vol. 582, no. June, 2020, doi: 10.1038/s41586-020-2223-y.

[8] Hegyi A, Ziebuhr J. Conservation of substrate specificities among coronavirus main proteases. J Gen Virol 2002;83(3):595–9. https://doi.org/10.1099/0022-1317-83-3-595.

[9] Dai W et al. Structure-based design of antiviral drug candidates targeting the SARS-CoV-2 main protease. Science (80-) 2020;368(6497):1331–5. https://doi.org/10.1126/science.abb4489.

[10] Kneller DW et al. Malleability of the SARS-CoV-2 3CL M pro Active-Site Cavity Facilitates Binding of Clinical Antivirals. Struct Des 2020;28(12):1313–1320. e3. https://doi.org/10.1016/j.str.2020.10.007.

[11] Macdonald EA, Frey G, Namchuk MN, Harrison SC, Hinshaw SM, Windsor IW. Recognition of Divergent Viral Substrates by the SARS-CoV - 2 Main Protease. Infect Dis (Auckl) 2021;7:2591–5. https://doi.org/10.1021/acsinfecdis.1c00237.

[12] Mengist HM, Fan X, Jin T. Designing of improved drugs for COVID-19: Crystal structure of SARS-CoV-2 main protease Mpro. Signal Transduct Target Ther 2020;5(1):2–3. https://doi.org/10.1038/s41392-020-0178-y.

[13] Świderek K, Moliner V. Revealing the molecular mechanisms of proteolysis of SARS-CoV-2 Mproby QM/MM computational methods. Chem Sci 2020;11(39):10626–30. https://doi.org/10.1039/d0sc02823a.

[14] Yoshino R, Yasuo N, Sekijima M. Identification of key interactions between SARS-CoV-2 main protease and inhibitor drug candidates. Sci Rep 2020;10(1):12493. https://doi.org/10.1038/s41598-020-69337-9.

[15] Zhang L et al. Crystal structure of SARS-CoV-2 main protease provides a basis for design of improved a-ketoamide inhibitors. Science (80-) 2020;368(6489):409–12. https://doi.org/10.1126/science.abb3405.

[16] Kneller DW et al. Structural plasticity of SARS-CoV-2 3CL Mpro active site cavity revealed by room temperature X-ray crystallography. Nat Commun 2020;11(1):7–12. https://doi.org/10.1038/s41467-020-16954-7.

[17] M. D. Sacco *et al.*, "Structure and inhibition of the SARS-CoV-2 main protease reveals strategy for developing dual inhibitors against Mpro and cathepsin L," *bioRxiv*, no. December, 2020, doi: 10.1101/2020.07.27.223727.

[18]] J. Qiao *et al.*, "SARS-CoV-2 Mpro inhibitors with antiviral activity in a transgenic mouse model," vol. 1378, no. March, pp. 1374–1378, 2021

[19] J. W. D. Griffin, "Since January 2020 Elsevier has created a COVID-19 resource centre with free information in English and Mandarin on the novel coronavirus COVID- 19 . The COVID-19 resource centre is hosted on Elsevier Connect , the company ' s public news and information ," no. January, 2020.

[20] Cannalire R, Cerchia C, Beccari AR, Di Leva FS, Summa V. Targeting SARS-CoV-2 Proteases and Polymerase for COVID-19 Treatment: State of the Art and Future Opportunities. J Med Chem Nov. 2020. https://doi.org/10.1021/acs.jmedchem.0c01140.

[21] Hoffman RL et al. Discovery of Ketone-Based Covalent Inhibitors of Coronavirus 3CL Proteases for the Potential Therapeutic Treatment of COVID-19. Cite This J Med Chem 2020;63:12725–47. https://doi.org/10.1021/acs.jmedchem.0c01063.

[22] Sharun K, Tiwari R, Dhama K. Protease inhibitor GC376 for COVID-19: Lessons learned from feline infectious peritonitis. Ann Med Surg Dec. 2020;61:122–5. https://doi.org/10.1016/j.amsu.2020.12.030.

[23] Fu L et al. Both Boceprevir and GC376 efficaciously inhibit SARS-CoV-2 by targeting its main protease. Nat Commun 2020;11(1):1–8. https://doi.org/10.1038/s41467-020-18233-x.

[24] Vuong W et al. Feline coronavirus drug inhibits the main protease of SARS-CoV-2 and blocks virus replication. Nat Commun 2020;11(1):1–8. https://doi.org/10.1038/s41467-020-18096-2.

[25] C. S. Dampalla, J. Zheng, K. Dinali, L. R. Wong, and D. K. Meyerholz, "Postinfection treatment with a protease inhibitor increases survival of mice with a fatal SARS-CoV-2 infection," vol. 118, no. 29, 2021, doi: 10.1073/pnas.2101555118/-/DCSupplemental.Published.

[26] Yang KS et al. A Quick Route to Multiple Highly Potent SARS-CoV-2 Main Protease Inhibitors**. ChemMedChem 2021;16(6):942–8. https://doi.org/10.1002/cmdc.202000924.

[27] Xia Z et al. Rational Design of Hybrid SARS-CoV-2 Main Protease Inhibitors Guided by the Superimposed Cocrystal Structures with the Peptidomimetic Inhibitors GC-376, Telaprevir, and Boceprevir. ACS Pharmacol Transl Sci Aug. 2021;4(4):1408–21. https://doi.org/10.1021/acsptsci.1c00099.

[28] S. W. Mason, M. E. Mcgrath, S. Noell, R. S. Obach, and N. O. Matthew, "Title : Discovery of a Novel Inhibitor of Coronavirus 3CL Protease for the Potential Treatment of COVID-19," 2021, doi: https://doi.org/10.1101/2020.09.12.293498.

[29] De Vries M et al. A Comparative Analysis of SARS-CoV-2 Antivirals Characterizes 3CL pro Inhibitor PF-00835231 as a Potential New Treatment for. Virology 2021.

[30] O. D. R. *et al.*, "An oral SARS-CoV-2 Mpro inhibitor clinical candidate for the treatment of COVID-19," *Science (80-.).*, vol. 374, no. 6575, pp. 1586–1593, Dec. 2021, doi: 10.1126/science.abl4784.

[31] Vandyck K, Deval J. Considerations for the discovery and development of 3-chymotrypsin-like cysteine protease inhibitors targeting SARS-CoV-2 infection. Curr Opin Virol 2021;49:36–40. https://doi.org/10.1016/j.coviro.2021.04.006.

[32] Konno S et al. 3CL Protease Inhibitors with an Electrophilic Arylketone Moiety as Anti-SARS-CoV-2 Agents. J Med Chem Jul. 2021. https://doi.org/10.1021/acs.jmedchem.1c00665.

[33] S. ichiro Hattori, et al. A small molecule compound with an indole moiety inhibits the main protease of SARS-CoV-2 and blocks virus replication. Nat Commun 2021;12(1):1–12. https://doi.org/10.1038/s41467-021-20900-6.
[34] Iketani S et al. Lead compounds for the development of SARS-CoV-2 3CL protease inhibitors. Nat Commun 2021;12(1):2016. https://doi.org/10.1038/s41467-021-22362-2.
[35] Ghahremanpour MM et al. Identification of 14 Known Drugs as Inhibitors of the Main Protease of SARS-CoV-2. ACS Med Chem Lett Dec. 2020;11(12):2526–33. https://doi.org/10.1021/acsmedchemlett.0c00521.
[36] Oerlemans R et al. Repurposing the HCV NS3–4A protease drug boceprevir as COVID-19 therapeutics. RSC Med Chem 2021;12:370–9. https://doi.org/10.1039/d0md00367k.
[37] Bai Y et al. Structural basis for the inhibition of the SARS-CoV-2 main protease by the anti-HCV drug narlaprevir. Signal Transduct Target Ther 2021;6(1):2020–2. https://doi.org/10.1038/s41392-021-00468-9.
[38] Ma C et al. Boceprevir, GC-376, and calpain inhibitors II, XII inhibit SARS-CoV-2 viral replication by targeting the viral main protease. Cell Res 2020;30(8):678–92. https://doi.org/10.1038/s41422-020-0356-z.
[39] Redhead MA et al. Bispecific repurposed medicines targeting the viral and immunological arms of COVID - 19. Sci Rep 2021:1–14. https://doi.org/10.1038/s41598-021-92416-4.
[40] Kuzikov M et al. Identification of Inhibitors of SARS-CoV-2 3CL-Pro Enzymatic Activity Using a Small Molecule in Vitro Repurposing Screen. ACS Pharmacol Transl Sci 2021. https://doi.org/10.1021/acsptsci.0c00216.
[41] S. Günther *et al.*, "X-ray screening identifies active site and allosteric inhibitors of SARS-CoV-2 main protease," *Science (80-.).*, vol. 372, no. 6542, pp. 642 LP – 646, May 2021, doi: 10.1126/science.abf7945.
[42] E. C. Vatansever *et al.*, "Bepridil is potent against SARS-CoV-2 In Vitro," *bioRxiv*, p. 2020.05.23.112235, Jan. 2020, doi: 10.1101/2020.05.23.112235.
[43] Zhang L et al. Comparative Antiviral Efficacy of Viral Protease Inhibitors against the Novel SARS-CoV-2 In Vitro. Virol Sin 2020;35(6):776–84. https://doi.org/10.1007/s12250-020-00288-1.
[44] Lockbaum GJ et al. Pan-3C Protease Inhibitor Rupintrivir Binds SARS-CoV - 2 Main Protease in a Unique Binding Mode. Biochemistry 2021;60:2925–31. https://doi.org/10.1021/acs.biochem.1c00414.
[45] Wang Z et al. Identification of proteasome and caspase inhibitors targeting SARS-CoV-2 Mpro. Signal Transduct Target Ther 2021;6(1):214. https://doi.org/10.1038/s41392-021-00639-8.
[46] H. Sies and M. J. Parnham, "Potential therapeutic use of ebselen for COVID-19 and other respiratory viral infections," no. January, 2020.
[47] Amporndanai K et al. Inhibition mechanism of SARS-CoV-2 main protease by ebselen and its derivatives. Nat Commun 2021;12(1):1–7. https://doi.org/10.1038/s41467-021-23313-7.
[48] Jin Z et al. Structural basis for the inhibition of SARS-CoV-2 main protease by antineoplastic drug carmofur. Nat Struct Mol Biol 2020;27(6):529–32. https://doi.org/10.1038/s41594-020-0440-6.
[49] Ghosh AK et al. Indole Chloropyridinyl Ester-Derived SARS-CoV - 2 3CLpro Inhibitors: Enzyme Inhibition, Antiviral E ffi cacy, Structure – Activity Relationship, and X - ray Structural Studies. J Med Chem 2021;64:14702–14. https://doi.org/10.1021/acs.jmedchem.1c01214.
[50] Douangamath A et al. Crystallographic and electrophilic fragment screening of the SARS-CoV-2 main protease. Nat Commun 2020;11(1):1–11. https://doi.org/10.1038/s41467-020-18709-w.
[51] M. M. Ghahremanpour *et al.*, "Identi fi cation of 14 Known Drugs as Inhibitors of the Main Protease of SARS-CoV 2," 2020, doi: 10.1021/acsmedchemlett.0c00521.
[52] Zhang CH et al. Potent Noncovalent Inhibitors of the Main Protease of SARS-CoV-2 from Molecular Sculpting of the Drug Perampanel Guided by Free Energy Perturbation Calculations. ACS Cent Sci 2021. https://doi.org/10.1021/acscentsci.1c00039.
[53] Deshmukh MG et al. Structure-guided design of a perampanel-derived pharmacophore targeting the SARS-CoV-2 main protease. Structure 2021;29(8):823–833.e5. https://doi.org/10.1016/j.str.2021.06.002.
[54] G. J. Lockbaum *et al.*, "Crystal Structure of SARS-CoV-2 Main Protease in Complex with the Non-Covalent Inhibitor ML188," *Viruses*, vol. 13, no. 2, 2021, doi: 10.3390/v13020174.
[55] Han SH et al. Structure-Based Optimization of ML300-Derived, Noncovalent Inhibitors Targeting the Severe Acute Respiratory Syndrome Coronavirus 3CL Protease (SARS-CoV-2 3CLpro). J Med Chem Aug. 2021. https://doi.org/10.1021/acs.jmedchem.1c00598.
[56] Kitamura N et al. Expedited Approach toward the Rational Design of Noncovalent SARS-CoV-2 Main Protease Inhibitors. J Med Chem Apr. 2021. https://doi.org/10.1021/acs.jmedchem.1c00509.
[57] Cantrelle F-X et al. NMR spectroscopy of the main protease of SARS-CoV-2 and fragment-based screening identify three protein hotspots and an antiviral fragment. Angew Chemie Int Ed 2021. https://doi.org/10.1002/anie.202109965.
[58] L. Panchariya *et al.*, "Zinc^{2+} ion inhibits SARS-CoV-2 main protease and viral replication in vitro," *bioRxiv*, p. 2021.06.15.448551, Jan. 2021, doi: 10.1101/2021.06.15.448551.
[59] Vandyck K et al. ALG-097111, a potent and selective SARS-CoV-2 3-chymotrypsin-like cysteine protease inhibitor exhibits in vivo efficacy in a Syrian Hamster model. Biochem Biophys Res Commun 2021;555:134–9. https://doi.org/10.1016/j.bbrc.2021.03.096.
[60] Pfizer, "Pfizer's Novel COVID-19 Oral Antiviral Treatment Candidate Reduced Risk of Hospitalization or Death by 89% in Interim Analysis of Phase 2/3 EPIC-HR Study," 2021. https://www.pfizer.com/news/press-release/press-release-detail/pfizers-novel-COVID-19-oral-antiviral-treatment-candidate.
[61] Pfizer, "EPIC-HR: Study of Oral PF-07321332/Ritonavir Compared With Placebo in Nonhospitalized High Risk Adults With COVID-19," 2022. https://clinicaltrials.gov/ct2/show/NCT04960202?term=pf-07321332&cond=COVID-19&draw=2&rank=1.
[62] FDA, "Coronavirus (COVID-19) Update: FDA Authorizes First Oral Antiviral for Treatment of COVID-19," 2021. https://www.fda.gov/news-events/press-announcements/coronavirus-covid-19-update-fda-authorizes-first-oral-antiviral-treatment-covid-19.
[63] S. Ullrich, K. B. Ekanayake, G. Otting, and C. Nitsche, "Main protease mutants of SARS-CoV-2 variants remain susceptible to PF-07321332," *bioRxiv*, p. 2021.11.28.470226, 2021, [Online]. Available: https://www.biorxiv.org/content/10.1101/2021.11.28.470226v1%0Ahttps://www.biorxiv.org/content/10.1101/2021.11.28.470226v1.abstract.
[64] Abdelnabi R et al. The oral protease inhibitor (PF-07321332) protects Syrian hamsters against infection with SARS-CoV-2 variants of concern. Nat Commun 2022;13(1):719. https://doi.org/10.1038/s41467-022-28354-0.
[65] Pfizer, "First-In-Human Study To Evaluate Safety, Tolerability, And Pharmacokinetics Following Single Ascending And Multiple Ascending Doses of PF-07304814 In Hospitalized Participants With COVID-19.," 2021. https://clinicaltrials.gov/ct2/show/NCT04535167?term=PF-07304814&cond=COVID-19&draw=2&rank=1.
[66] Boras B et al. Preclinical characterization of an intravenous coronavirus 3CL protease inhibitor for the potential treatment of COVID19. Nat Commun 2021;12(1):6055. https://doi.org/10.1038/s41467-021-26239-2.
[67] Takashita E et al. Efficacy of Antibodies and Antiviral Drugs against Covid-19 Omicron Variant. N Engl J Med Jan. 2022. https://doi.org/10.1056/NEJMc2119407.
[68] Pardes Biosciences, "Pipeline." https://www.pardesbio.com/pipeline/#our-lead-program.
[69] Pardes Biosciences, "No TitlePardes Biosciences Announces FDA Clearance of IND Application for PBI-0451, an Oral Antiviral Drug Candidate for the Treatment and Prevention of SARS-CoV-2 Infections," 2022. https://ir.pardesbio.com/news-releases/news-release-details/pardes-biosciences-announces-fda-clearance-ind-application-pbi.
[70] Enanta Pharmaceuticals, "SARS-COV-2 (COVID-19)." https://www.enanta.com/research/COVID-19/default.aspx.
[71] Enanta Pharmaceuticals, "ENANTA PHARMACEUTICALS PRESENTS NEW DATA FOR EDP-235, ITS LEAD ORAL PROTEASE INHIBITOR DESIGNED FOR THE TREATMENT OF COVID-19, AT THE ISIRV–WHO VIRTUAL CONFERENCE 2021," 2021. https://www.enanta.com/investors/news-releases/press-release/2021/Enanta-Pharmaceuticals-Presents-New-Data-for-EDP-235-its-Lead-Oral-Protease-Inhibitor-Designed-for-the-Treatment-of-COVID-19-at-the-ISIRVWHO-Virtual-Conference-2021/default.aspx.
[72] Y. Unoh *et al.*, "Discovery of S-217622, a Non-Covalent Oral SARS-CoV-2 3CL Protease Inhibitor Clinical Candidate for Treating COVID-19," *bioRxiv*, p. 2022.01.26.477782, Jan. 2022, doi: 10.1101/2022.01.26.477782.
[73] Shionogi, "Notice Regarding the Progress of S-217622 to Fight COVID-19." https://www.shionogi.com/global/en/news/2022/01/e-220120.html.
[74] O. A. Chaves *et al.*, "Atazanavir Is a Competitive Inhibitor of SARS-CoV-2 Mpro, Impairing Variants Replication In Vitro and In Vivo," *Pharmaceuticals* , vol. 15, no. 1. 2022, doi: 10.3390/ph15010021.
[75] . "Antiviral Agents Against COVID-19 Infection (REVOLUTIOn)" 2021. , https://clinicaltrials.gov/ct2/show/NCT04468087?term=Atazanavir&cond=SARS-CoV+Infection&draw=2&rank=3.
[76] Patients", Sound Pharmaceuticals Incorporated, "SPI-1005 Treatment in Moderate COVID-19 2022.
[77] V. U. M. Center, "Trial of Early Therapies During Non-hospitalized Outpatient Window for COVID-19 (TREATNOW)," 2021. https://clinicaltrials.gov/ct2/show/NCT04372628?term=Lopinavir&rslt=Without&cond=SARS-CoV-2&draw=2&rank=4.
[78] M. Jang *et al.*, "Lopinavir-ritonavir is not an effective inhibitor of the main protease activity of SARS-CoV-2 in vitro," *bioRxiv*, p. 2020.09.16.299800, Jan. 2020, doi: 10.1101/2020.09.16.299800.
[79] Cao B et al. A Trial of Lopinavir-Ritonavir in Adults Hospitalized with Severe Covid-19. N Engl J Med Mar. 2020;382(19):1787–99. https://doi.org/10.1056/NEJMoa2001282.
[80] S. A. Parvez, M. K. Saha, and Y. Araf, "Insights from a computational analysis of the SARS-CoV-2 Omicron variant : Host-pathogen interaction , pathogenicity , and possible therapeutics.".
[81] The Ninth Hospital of Nanchang, "Evaluation of Ganovo (Danoprevir) Combined With Ritonavir in the Treatment of SARS-CoV-2 Infection." https://clinicaltrials.gov/ct2/show/NCT04291729?term=danoprevir&rslt=Without&cond=SARS-CoV-2&draw=2&rank=2.
[82] H. Chen *et al.*, "First clinical study using HCV protease inhibitor danoprevir to treat COVID-19 patients.," *Medicine (Baltimore).*, vol. 99, no. 48, p. e23357, Nov. 2020, doi: 10.1097/MD.0000000000023357.
[83] G. K. A. *et al.*, "Hepatitis C Virus Protease Inhibitors Show Differential Efficacy and Interactions with Remdesivir for Treatment of SARS-CoV-2 In Vitro," *Antimicrob. Agents Chemother.*, vol. 65, no. 9, pp. e02680-20, Feb. 2022, doi: 10.1128/AAC.02680-20.
[84] Cáceres CJ et al. Efficacy of GC-376 against SARS-CoV-2 virus infection in the K18 hACE2 transgenic mouse model. Sci Rep 2021;11(1):9609. https://doi.org/10.1038/s41598-021-89013-w.

[85] Shanghai Public Health Clinical Center, "Efficacy and Safety of Darunavir and Cobicistat for Treatment of COVID-19 (DC-COVID-19)," 2020. https://clinicaltrials.gov/ct2/show/NCT04252274?term=cobicistat&rslt=Without&cond=SARS-CoV-2&draw=2&rank=2.
[86] Pant S, Singh M, Ravichandiran V, Murty USN, Srivastava HK. Peptide-like and small-molecule inhibitors against Covid-19. J Biomol Struct Dyn May 2021;39(8):2904–13. https://doi.org/10.1080/07391102.2020.1757510.
[87] Mahdi M, Mótyán JA, Szojka ZI, Golda M, Miczi M, Tőzsér J. Analysis of the efficacy of HIV protease inhibitors against SARS-CoV-2's main protease. Virol J Nov. 2020;17(1):190. https://doi.org/10.1186/s12985-020-01457-0.
[88] Gupta A et al. Structure-Based Virtual Screening and Biochemical Validation to Discover a Potential Inhibitor of the SARS-CoV-2 Main Protease. ACS Omega Dec. 2020;5(51):33151–61. https://doi.org/10.1021/acsomega.0c04808.
[89] Ma C, Tan H, Choza J, Wang Y, Wang J. Validation and invalidation of SARS-CoV-2 main protease inhibitors using the Flip-GFP and Protease-Glo luciferase assays. Acta Pharm Sin B 2021. https://doi.org/10.1016/j.apsb.2021.10.026.
[90] Leidos Life Sciences, "Leidos-Enabled Adaptive Protocol (LEAP-CT) for Evaluation of Post-exposure Prophylaxis for Newly-infected COVID-19 Patients (Addendum 2)," 2022. https://clinicaltrials.gov/ct2/show/NCT05077969?term=celecoxib&cond=COVID-19&draw=2&rank=2.
[91] Baghaki S, Yalcin CE, Baghaki HS, Aydin SY, Daghan B, Yavuz E. COX2 inhibition in the treatment of COVID-19: Review of literature to propose repositioning of celecoxib for randomized controlled studies. Int J Infect Dis 2020;101:29–32. https://doi.org/10.1016/j.ijid.2020.09.1466.
[92] A. Gimeno *et al.*, "Prediction of Novel Inhibitors of the Main Protease (M-pro) of SARS-CoV-2 through Consensus Docking and Drug Reposition," *International Journal of Molecular Sciences* , vol. 21, no. 11. 2020, doi: 10.3390/ijms21113793.
[93] University of Oklahoma, "Dexamethasone for COVID-19." https://clinicaltrials.gov/ct2/show/NCT04707534?term=dexamethasone&cond=COVID-19&draw=2&rank=1.
[94] Fadaka AO, Sibuyi NRS, Madiehe AM, Meyer M. Computational insight of dexamethasone against potential targets of SARS-CoV-2. J Biomol Struct Dyn Jan. 2022;40(2):875–85. https://doi.org/10.1080/07391102.2020.1819880.
[95] P. Morgan, S. J. Arnold, N.-W. Hsiao, and C.-W. Shu, "A Closer Look at Dexamethasone and the SARS-CoV-2-Induced Cytokine Storm: In Silico Insights of the First Life-Saving COVID-19 Drug," *Antibiotics* , vol. 10, no. 12. 2021, doi: 10.3390/antibiotics10121507.
[96] S. Eugene, "Safety and Efficacy of Doxycycline and Rivaroxaban in COVID-19 (DOXYCOV)," *Yaounde Central Hospital*, 2021. https://clinicaltrials.gov/ct2/show/NCT04715295?term=main+protease+inhibitor+doxycycline&cond=COVID-19&draw=2&rank=1
[97] M. Gendrot *et al.*, "In Vitro Antiviral Activity of Doxycycline against SARS-CoV-2," *Molecules* , vol. 25, no. 21. 2020, doi: 10.3390/molecules25215064.
[98] Bharadwaj S, Lee KE, Dwivedi VD, Kang SG. Computational insights into tetracyclines as inhibitors against SARS-CoV-2 Mpro via combinatorial molecular simulation calculations. Life Sci 2020;257:. https://doi.org/10.1016/j.lfs.2020.118080118080.
[99] Mahmoud Ramadan mohamed Elkazzaz. Combination of Chemopreventive Agents (All- Trans Retinoic Acid and Tamoxifen) as Potential Treatment for the Lung Complication of COVID-19. Kafrelsheikh University; 2020.
[100] T. Morita *et al.*, "All-Trans Retinoic Acid Exhibits Antiviral Effect against SARS-CoV-2 by Inhibiting 3CLpro Activity," *Viruses* , vol. 13, no. 8. 2021, doi: 10.3390/v13081669.
[101] Krishnamoorthy N, Fakhro K. Identification of mutation resistance coldspots for targeting the SARS-CoV2 main protease. IUBMB Life Apr. 2021;73(4):670–5. https://doi.org/10.1002/iub.2465.
[102] Cross TJ et al. Sequence Characterization and Molecular Modeling of Clinically Relevant Variants of the SARS-CoV-2 Main Protease. Biochemistry Oct. 2020;59(39):3741–56. https://doi.org/10.1021/acs.biochem.0c00462.
[103] H. Su *et al.*, "Anti-SARS-CoV-2 activities in vitro of Shuanghuanglian preparations and bioactive ingredients," no. July, 2020, doi: 10.1038/s41401-020-0483-6.
[104] Su H et al. Identification of pyrogallol as a warhead in design of covalent inhibitors for the SARS-CoV-2 3CL protease. Nat Commun 2021:1–12. https://doi.org/10.1038/s41467-021-23751-3.
[105] Liu H et al. Scutellaria baicalensis extract and baicalein inhibit replication of SARS-CoV-2 and its 3C-like protease in vitro. J Enzyme Inhib Med Chem Jan. 2021;36(1):497–503. https://doi.org/10.1080/14756366.2021.1873977.
[106] T. Xiao *et al.*, "Myricetin Inhibits SARS-CoV-2 Viral Replication by Targeting Mpro and Ameliorates Pulmonary Inflammation ," *Frontiers in Pharmacology* , vol. 12. p. 1012, 2021, [Online]. Available: https://www.frontiersin.org/article/10.3389/fphar.2021.669642.
[107] Umar HI, Josiah SS, Saliu TP, Jimoh TO, Ajayi A, Danjuma JB. In-silico analysis of the inhibition of the SARS-CoV-2 main protease by some active compounds from selected African plants. J Taibah Univ Med Sci 2021;16(2):162–76. https://doi.org/10.1016/j.jtumed.2020.12.005.
[108] Abd El-Mordy FM et al. Inhibition of SARS-CoV-2 main protease by phenolic compounds from Manilkara hexandra (Roxb.) Dubard assisted by metabolite profiling and in silico virtual screening. RSC Adv 2020;10(53):32148–55. https://doi.org/10.1039/D0RA05679K.
[109] Khan A et al. In silico and in vitro evaluation of kaempferol as a potential inhibitor of the SARS-CoV-2 main protease (3CLpro). Phyther Res Jun. 2021;35(6):2841–5. https://doi.org/10.1002/ptr.6998.
[110] M. Ouassaf, S. Belaidi, S. Chtita, T. Lanez, F. Abul Qais, and H. Md Amiruddin, "Combined molecular docking and dynamics simulations studies of natural compounds as potent inhibitors against SARS-CoV-2 main protease," *J. Biomol. Struct. Dyn.*, pp. 1–10, Jul. 2021, doi: 10.1080/07391102.2021.1957712.
[111] Abian O et al. Structural stability of SARS-CoV-2 3CLpro and identification of quercetin as an inhibitor by experimental screening. Int J Biol Macromol Dec. 2020;164:1693–703. https://doi.org/10.1016/j.ijbiomac.2020.07.235.
[112] D. Sen, P. Debnath, B. Debnath, S. Bhaumik, and S. Debnath, "Identification of potential inhibitors of SARS-CoV-2 main protease and spike receptor from 10 important spices through structure-based virtual screening and molecular dynamic study," *J. Biomol. Struct. Dyn.*, pp. 1–22, Sep. 2020, doi: 10.1080/07391102.2020.1819883.
[113] Teli DM, Shah MB, Chhabria MT. In silico Screening of Natural Compounds as Potential Inhibitors of SARS-CoV-2 Main Protease and Spike RBD: Targets for COVID-19. Front Mol Biosci 2021;7(January):1–25. https://doi.org/10.3389/fmolb.2020.599079.
[114] Hiremath S et al. "In silico docking analysis revealed the potential of phytochemicals present in Phyllanthus amarus and Andrographis paniculata, used in Ayurveda medicine in inhibiting SARS-CoV-2", *3*. Biotech 2021;11(2):44. https://doi.org/10.1007/s13205-020-02578-7.
[115] Das P, Majumder R, Mandal M, Basak P. In-Silico approach for identification of effective and stable inhibitors for COVID-19 main protease (Mpro) from flavonoid based phytochemical constituents of Calendula officinalis. J Biomol Struct Dyn 2020:1–16. https://doi.org/10.1080/07391102.2020.1796799.
[116] H. A. El Gizawy *et al.*, "Pimenta dioica (L.) Merr. Bioactive Constituents Exert Anti-SARS-CoV-2 and Anti-Inflammatory Activities: Molecular Docking and Dynamics, In Vitro, and In Vivo Studies," *Molecules* , vol. 26, no. 19. 2021, doi: 10.3390/molecules26195844.
[117] Joshi T, Bhat S, Pundir H, Chandra S. Identification of Berbamine, Oxyacanthine and Rutin from Berberis asiatica as anti-SARS-CoV-2 compounds: An in silico study. J Mol Graph Model 2021;109:. https://doi.org/10.1016/j.jmgm.2021.108028108028.
[118] Shivanika C, Deepak Kumar S, Venkataraghavan R, Pawan T, Sumitha A, Brindha Devi BD. Molecular docking, validation, dynamics simulations, and pharmacokinetic prediction of natural compounds against the SARS-CoV-2 main-protease. J Biomol Struct Dyn 2020:1–27. https://doi.org/10.1080/07391102.2020.1815584.
[119] Y. Zhu and D.-Y. Xie, "Docking Characterization and in vitro Inhibitory Activity of Flavan-3-ols and Dimeric Proanthocyanidins Against the Main Protease Activity of SARS-Cov-2 ," *Frontiers in Plant Science* , vol. 11. p. 1884, 2020, [Online]. Available: https://www.frontiersin.org/article/10.3389/fpls.2020.601316.
[120] Jang M et al. Tea Polyphenols EGCG and Theaflavin Inhibit the Activity of SARS-CoV-2 3CL-Protease *In Vitro*. Evidence-Based Complement Altern Med 2020;2020:5630838. https://doi.org/10.1155/2020/5630838.
[121] H. M. Abdallah *et al.*, "Repurposing of Some Natural Product Isolates as SARS-COV-2 Main Protease Inhibitors via In Vitro Cell Free and Cell-Based Antiviral Assessments and Molecular Modeling Approaches," *Pharmaceuticals* , vol. 14, no. 3. 2021, doi: 10.3390/ph14030213.
[122] C. Guijarro-Real, M. Plazas, A. Rodríguez-Burruezo, J. Prohens, and A. Fita, "Potential In Vitro Inhibition of Selected Plant Extracts against SARS-CoV-2 Chymotripsin-Like Protease (3CLPro) Activity," *Foods* , vol. 10, no. 7. 2021, doi: 10.3390/foods10071503.
[123] Islam R et al. A molecular modeling approach to identify effective antiviral phytochemicals against the main protease of SARS-CoV-2. J Biomol Struct Dyn Jun. 2021;39(9):3213–24. https://doi.org/10.1080/07391102.2020.1761883.
[124] Mahmud S et al. Virtual screening and molecular dynamics simulation study of plant-derived compounds to identify potential inhibitors of main protease from SARS-CoV-2. Brief Bioinform Mar. 2021;22(2):1402–14. https://doi.org/10.1093/bib/bbaa428.
[125] D. M. Teli, M. B. Shah, and M. T. Chhabria, "In silico Screening of Natural Compounds as Potential Inhibitors of SARS-CoV-2 Main Protease and Spike RBD: Targets for COVID-19 ," *Frontiers in Molecular Biosciences* , vol. 7. p. 429, 2021, [Online]. Available: https://www.frontiersin.org/article/10.3389/fmolb.2020.599079.
[126] R. Jahan *et al.*, "Zingiber officinale: Ayurvedic Uses of the Plant and In Silico Binding Studies of Selected Phytochemicals With Mpro of SARS-CoV-2," *Nat. Prod. Commun.*, vol. 16, no. 10, p. 1934578X211031766, Oct. 2021, doi: 10.1177/1934578X211031766.
[127] Sharma P, Shanavas A. Natural derivatives with dual binding potential against SARS-CoV-2 main protease and human ACE2 possess low oral bioavailability: a brief computational analysis. J Biomol Struct Dyn Oct. 2021;39(15):5819–30. https://doi.org/10.1080/07391102.2020.1794970.
[128] H. A. Alhadrami, A. M. Sayed, A. M. Sharif, E. I. Azhar, and M. E. Rateb, "Olive-Derived Triterpenes Suppress SARS COV-2 Main Protease: A Promising Scaffold for Future Therapeutics," *Molecules* , vol. 26, no. 9. 2021, doi: 10.3390/molecules26092654.
[129] Dey D, Dey N, Ghosh S, Chandrasekaran N, Mukherjee A, Thomas J. Potential combination therapy using twenty phytochemicals from twenty plants to prevent SARS- CoV-2 infection: An in silico Approach. VirusDisease 2021;32(1):108–16. https://doi.org/10.1007/s13337-021-00658-7.
[130] Halder P et al. Evaluation of potency of the selected bioactive molecules from Indian medicinal plants with MPro of SARS-CoV-2 through in silico analysis. J Ayurveda Integr Med 2021. https://doi.org/10.1016/j.jaim.2021.05.003.

[131] P. Shree *et al.*, "Targeting COVID-19 (SARS-CoV-2) main protease through active phytochemicals of ayurvedic medicinal plants – Withania somnifera (Ashwagandha), Tinospora cordifolia (Giloy) and Ocimum sanctum (Tulsi) – a molecular docking study," *J. Biomol. Struct. Dyn.*, pp. 1–14, Aug. 2020, doi: 10.1080/07391102.2020.1810778.
[132] L. van de Sand *et al.*, "Glycyrrhizin Effectively Inhibits SARS-CoV-2 Replication by Inhibiting the Viral Main Protease," *Viruses* , vol. 13, no. 4. 2021, doi: 10.3390/v13040609.
[133] Z. T. Muhseen, A. R. Hameed, H. M. H. Al-Hasani, S. Ahmad, and G. Li, "Computational Determination of Potential Multiprotein Targeting Natural Compounds for Rational Drug Design Against SARS-COV-2," *Molecules* , vol. 26, no. 3. 2021, doi: 10.3390/molecules26030674.
[134] M. F. Rehman *et al.*, "Effectiveness of Natural Antioxidants against SARS-CoV-2? Insights from the In-Silico World," *Antibiotics* , vol. 10, no. 8. 2021, doi: 10.3390/antibiotics10081011.
[135] I. Nawrot-Hadzik *et al.*, "Reynoutria Rhizomes as a Natural Source of SARS-CoV-2 Mpro Inhibitors–Molecular Docking and In Vitro Study," *Pharmaceuticals* , vol. 14, no. 8. 2021, doi: 10.3390/ph14080742.
[136] Samy MN et al. Phytochemical investigation of Amphilophium paniculatum; an underexplored Bignoniaceae species as a source of SARS-CoV-2 Mpro inhibitory metabolites: Isolation, identification, and molecular docking study. South African J Bot 2021;141:421–30. https://doi.org/10.1016/j.sajb.2021.05.023.
[137] M. S. Zubair, S. Maulana, A. Widodo, R. Pitopang, M. Arba, and M. Hariono, "GC-MS, LC-MS/MS, Docking and Molecular Dynamics Approaches to Identify Potential SARS-CoV-2 3-Chymotrypsin-Like Protease Inhibitors from Zingiber officinale Roscoe," *Molecules* , vol. 26, no. 17. 2021, doi: 10.3390/molecules26175230.
[138] Saadh MJ et al. Punicalagin and zinc (II) ions inhibit the activity of SARS-CoV-2 3CL-protease in vitro. Eur Rev Med Pharmacol Sci May 2021;25 (10):3908–13. https://doi.org/10.26355/eurrev_202105_25958.
[139] Mahmoud DB et al. Delineating a potent antiviral activity of Cuphea ignea extract loaded nano-formulation against SARS-CoV-2: In silico and in vitro studies. J Drug Deliv Sci Technol Dec. 2021;66:. https://doi.org/10.1016/j.jddst.2021.102845102845.
[140] Owis AI et al. Flavonoids of Salvadora persica L. (meswak) and its liposomal formulation as a potential inhibitor of SARS-CoV-2. RSC Adv 2021;11 (22):13537–44. https://doi.org/10.1039/D1RA00142F.
[141] Upadhyay S, Tripathi PK, Singh M, Raghavendhar S, Bhardwaj M, Patel AK. Evaluation of medicinal herbs as a potential therapeutic option against SARS-CoV-2 targeting its main protease. Phyther Res Dec. 2020;34(12):3411–9. https://doi.org/10.1002/ptr.6802.
[142] Jin Z et al. Structure of Mpro from SARS-CoV-2 and discovery of its inhibitors. Nature 2020;582(7811):289–93. https://doi.org/10.1038/s41586-020-2223-y.
[143] R. Alaaeldin, M. Mustafa, G. E.-D. A. Abuo-Rahma, and M. Fathy, "In vitro inhibition and molecular docking of a new ciprofloxacin-chalcone against SARS-CoV-2 main protease," *Fundam. Clin. Pharmacol.*, p. 10.1111/fcp.12708, Jul. 2021, doi: 10.1111/fcp.12708.
[144] J. Khan *et al.*, "Identification of potential phytochemicals from Citrus Limon against main protease of SARS-CoV-2: molecular docking, molecular dynamic simulations and quantum computations," *J. Biomol. Struct. Dyn.*, pp. 1–12, Jul. 2021, doi: 10.1080/07391102.2021.1947893.
[145] S. Das, S. Sarmah, S. Lyndem, and A. Singha Roy, "An investigation into the identification of potential inhibitors of SARS-CoV-2 main protease using molecular docking study," *J. Biomol. Struct. Dyn.*, vol. 39, no. 9, pp. 3347–3357, Jun. 2021, doi: 10.1080/07391102.2020.1763201.
[146] Tallei TE et al. Potential of Plant Bioactive Compounds as SARS-CoV-2 Main Protease (M^{pro}) and Spike (S) Glycoprotein Inhibitors: A Molecular Docking Study. Scientifica (Cairo) 2020;2020:6307457. https://doi.org/10.1155/2020/6307457.
[147] Ghosh R, Chakraborty A, Biswas A, Chowdhuri S. Evaluation of green tea polyphenols as novel corona virus (SARS CoV-2) main protease (Mpro) inhibitors–an in silico docking and molecular dynamics simulation study. J Biomol Struct Dyn 2020:1–13. https://doi.org/10.1080/07391102.2020.1779818.
[148] S. Mahmud *et al.*, "Plant-Based Phytochemical Screening by Targeting Main Protease of SARS-CoV-2 to Design Effective Potent Inhibitors," *Biology* , vol. 10, no. 7. 2021, doi: 10.3390/biology10070589.
[149] Mahmud S et al. Molecular docking and dynamics study to explore phytochemical ligand molecules against the main protease of SARS-CoV-2 from extensive phytochemical datasets. Expert Rev Clin Pharmacol Oct. 2021;14(10):1305–15. https://doi.org/10.1080/17512433.2021.1959318.
[150] Sherif YE, Gabr SA, Hosny NM, Alghadir AH, Alansari R. Phytochemicals of *Rhus* spp. as Potential Inhibitors of the SARS-CoV-2 Main Protease: Molecular Docking and Drug-Likeness Study. Evidence-Based Complement Altern Med 2021;2021:8814890. https://doi.org/10.1155/2021/8814890.
[151] Yepes-Pérez AF, Herrera-Calderon O, Sánchez-Aparicio J-E, Tiessler-Sala L, Maréchal J-D, Cardona-G W. Investigating Potential Inhibitory Effect of *Uncaria tomentosa* (Cat's Claw) against the Main Protease $3CL^{pro}$ of SARS-CoV-2 by Molecular Modeling. Evidence-Based Complement Altern Med 2020;2020:4932572. https://doi.org/10.1155/2020/4932572.
[152] V. Ragunathan and K. Chithra, "Extraction and characterization of metabolites from Olea europaea pulp and their molecular docking against SARS-CoV-2 main-protease (Mpro)," *Nat. Prod. Res.*, pp. 1–7, Sep. 2021, doi: 10.1080/14786419.2021.1983813.
[153] S. C, D. K. S, V. Ragunathan, P. Tiwari, S. A, and B. D. P, "Molecular docking, validation, dynamics simulations, and pharmacokinetic prediction of natural compounds against the SARS-CoV-2 main-protease," *J. Biomol. Struct. Dyn.*, pp. 1–27, Sep. 2020, doi: 10.1080/07391102.2020.1815584.
[154] Joshi T et al. In silico screening of natural compounds against COVID-19 by targeting Mpro and ACE2 using molecular docking. Eur Rev Med Pharmacol Sci 2020;24(8):4529–36. https://doi.org/10.26355/eurrev_202004_21036.
[155] S. Bharadwaj *et al.*, "Structure-Based Identification of Natural Products as SARS-CoV-2 Mpro Antagonist from Echinacea angustifolia Using Computational Approaches," *Viruses* , vol. 13, no. 2. 2021, doi: 10.3390/v13020305.
[156] S. Mahmud *et al.*, "Efficacy of Phytochemicals Derived from Avicennia officinalis for the Management of COVID-19: A Combined In Silico and Biochemical Study," *Molecules* , vol. 26, no. 8. 2021, doi: 10.3390/molecules26082210.
[157] Kumar V, Dhanjal JK, Kaul SC, Wadhwa R, Sundar D. Withanone and caffeic acid phenethyl ester are predicted to interact with main protease (Mpro) of SARS-CoV-2 and inhibit its activity. J Biomol Struct Dyn Jul. 2021;39 (11):3842–54. https://doi.org/10.1080/07391102.2020.1772108.
[158] Garg S, Roy A. In silico analysis of selected alkaloids against main protease (Mpro) of SARS-CoV-2. Chem Biol Interact 2020;332:. https://doi.org/10.1016/j.cbi.2020.109309109309.
[159] Tejera E et al. Computational modeling predicts potential effects of the herbal infusion 'horchata' against COVID-19. Food Chem 2022;366:. https://doi.org/10.1016/j.foodchem.2021.130589130589.
[160] Gurung AB, Ali MA, Lee J, Farah MA, Al-Anazi KM. Unravelling lead antiviral phytochemicals for the inhibition of SARS-CoV-2 Mpro enzyme through in silico approach. Life Sci 2020;255:. https://doi.org/10.1016/j.lfs.2020.117831117831.
[161] M. Dutta *et al.*, "Phytochemicals from Leucas zeylanica Targeting Main Protease of SARS-CoV-2: Chemical Profiles, Molecular Docking, and Molecular Dynamics Simulations," *Biology* , vol. 10, no. 8. 2021, doi: 10.3390/biology10080789.
[162] Ebada SS et al. Anti-inflammatory, antiallergic and COVID-19 protease inhibitory activities of phytochemicals from the Jordanian hawksbeard: identification, structure–activity relationships, molecular modeling and impact on its folk medicinal uses. RSC Adv 2020;10(62):38128–41. https://doi.org/10.1039/D0RA04876C.
[163] Das P, Majumder R, Mandal M, Basak P. In-Silico approach for identification of effective and stable inhibitors for COVID-19 main protease (Mpro) from flavonoid based phytochemical constituents of Calendula officinalis. J Biomol Struct Dyn Nov. 2021;39(16):6265–80. https://doi.org/10.1080/07391102.2020.1796799.
[164] Chowdhury P. In silico investigation of phytoconstituents from Indian medicinal herb 'Tinospora cordifolia (giloy)' against SARS-CoV-2 (COVID-19) by molecular dynamics approach. J Biomol Struct Dyn Nov. 2021;39 (17):6792–809. https://doi.org/10.1080/07391102.2020.1803968.
[165] Bondhon TA, Al Mahamud R, Jannat K, Hasan A, Jahan R, Rahmatullah M. in silico binding studies with b-sitosterol and some of its fatty acid esters to 3C-like protease of SARS-CoV-2. J Med Plants Stud 2020;8(5):86–90. https://doi.org/10.22271/plants.2020.v8.i5b.1198.
[166] Manne M et al. "Cordifolioside: potent inhibitor against Mpro of SARS-CoV-2 and immunomodulatory through human TGF-β and TNF-α", *3*. Biotech 2021;11(3):136. https://doi.org/10.1007/s13205-021-02685-z.
[167] Chaturvedi M, Nagre K, Yadav JP. In silico approach for identification of natural compounds as potential COVID 19 main protease (Mpro) inhibitors. VirusDisease 2021;32(2):325–9. https://doi.org/10.1007/s13337-021-00701-7.
[168] Giofrè SV et al. Interaction of selected terpenoids with two SARS-CoV-2 key therapeutic targets: An in silico study through molecular docking and dynamics simulations. Comput Biol Med 2021;134:. https://doi.org/10.1016/j.compbiomed.2021.104538104538.
[169] R. Ghosh, A. Chakraborty, A. Biswas, and S. Chowdhuri, "Computer aided identification of potential SARS CoV-2 main protease inhibitors from diterpenoids and biflavonoids of Torreya nucifera leaves," *J. Biomol. Struct. Dyn.*, pp. 1–16, Nov. 2020, doi: 10.1080/07391102.2020.1841680.
[170] Ghosh R, Chakraborty A, Biswas A, Chowdhuri S. Identification of polyphenols from Broussonetia papyrifera as SARS CoV-2 main protease inhibitors using in silico docking and molecular dynamics simulation approaches. J Biomol Struct Dyn Nov. 2021;39(17):6747–60. https://doi.org/10.1080/07391102.2020.1802347.
[171] D. Gentile, V. Patamia, A. Scala, M. T. Sciortino, A. Piperno, and A. Rescifina, "Putative Inhibitors of SARS-CoV-2 Main Protease from A Library of Marine Natural Products: A Virtual Screening and Molecular Modeling Study," *Marine Drugs* , vol. 18, no. 4. 2020, doi: 10.3390/md18040225.
[172] Jairajpuri DS et al. Identification of natural compounds as potent inhibitors of SARS-CoV-2 main protease using combined docking and molecular dynamics simulations. Saudi J Biol Sci 2021;28(4):2423–31. https://doi.org/10.1016/j.sjbs.2021.01.040.
[173] Joshi T, Joshi T, Pundir H, Sharma P, Mathpal S, Chandra S. Predictive modeling by deep learning, virtual screening and molecular dynamics study of natural compounds against SARS-CoV-2 main protease. J Biomol Struct Dyn Nov. 2021;39(17):6728–46. https://doi.org/10.1080/07391102.2020.1802341.
[174] Kar P, Sharma NR, Singh B, Sen A, Roy A. Natural compounds from Clerodendrum spp. as possible therapeutic candidates against SARS-CoV-2:

An in silico investigation. J Biomol Struct Dyn Sep. 2021;39(13):4774–85. https://doi.org/10.1080/07391102.2020.1780947.
[175] B. Kumar, P. Parasuraman, T. P. K. Murthy, M. Murahari, and V. Chandramohan, "In silico screening of therapeutic potentials from Strychnos nux-vomica against the dimeric main protease (Mpro) structure of SARS-CoV-2," *J. Biomol. Struct. Dyn.*, pp. 1–19, Mar. 2021, doi: 10.1080/07391102.2021.1902394.
[176] S. Mathpal, P. Sharma, T. Joshi, T. Joshi, V. Pande, and S. Chandra, "Screening of potential bio-molecules from Moringa olifera against SARS-CoV-2 main protease using computational approaches," *J. Biomol. Struct. Dyn.*, pp. 1–12, Jun. 2021, doi: 10.1080/07391102.2021.1936183.
[177] Murugan NA, Pandian CJ, Jeyakanthan J. Computational investigation on Andrographis paniculata phytochemicals to evaluate their potency against SARS-CoV-2 in comparison to known antiviral compounds in drug trials. J Biomol Struct Dyn Aug. 2021;39(12):4415–26. https://doi.org/10.1080/07391102.2020.1777901.
[178] Muhammad I et al. Screening of potent phytochemical inhibitors against SARS-CoV-2 protease and its two Asian mutants. Comput Biol Med 2021;133:. https://doi.org/10.1016/j.compbiomed.2021.104362104362.
[179] Parida PK, Paul D, Chakravorty D. Nature to nurture-Identifying Phytochemicals from Indian Medicinal Plants as Prophylactic Medicine by Rational Screening to Be Potent Against Multiple Drug Targets of SARS-CoV-2. J Offshore Technol 2020;14(2):10–1. https://doi.org/10.37113/ideaj.vi0.244.
[180] Poochi SP et al. Employing bioactive compounds derived from Ipomoea obscura (L.) to evaluate potential inhibitor for SARS-CoV-2 main protease and ACE2 protein. Food Front Jun. 2020;1(2):168–79. https://doi.org/10.1002/fft2.29.
[181] S. Nallusamy *et al.*, "Exploring Phytochemicals of Traditional Medicinal Plants Exhibiting Inhibitory Activity Against Main Protease, Spike Glycoprotein, RNA-dependent RNA Polymerase and Non-Structural Proteins of SARS-CoV-2 Through Virtual Screening ," *Frontiers in Pharmacology* , vol. 12. p. 1704, 2021, [Online]. Available: https://www.frontiersin.org/article/10.3389/fphar.2021.667704.
[182] Singh P et al. The dual role of phytochemicals on SARS-CoV-2 inhibition by targeting host and viral proteins. J Tradit Complement Med 2021. https://doi.org/10.1016/j.jtcme.2021.09.001.
[183] M. Sharma, J. K. Mahto, P. Dhaka, N. Neetu, S. Tomar, and P. Kumar, "MD simulation and MM/PBSA identifies phytochemicals as bifunctional inhibitors of SARS-CoV-2," *J. Biomol. Struct. Dyn.*, pp. 1–14, Aug. 2021, doi: 10.1080/07391102.2021.1969285.
[184] M. Rajendran *et al.*, "In silico screening and molecular dynamics of phytochemicals from Indian cuisine against SARS-CoV-2 MPro," *J. Biomol. Struct. Dyn.*, pp. 1–15, Nov. 2020, doi: 10.1080/07391102.2020.1845980.
[185] C. Vicidomini, V. Roviello, and G. N. Roviello, "In Silico Investigation on the Interaction of Chiral Phytochemicals from Opuntia ficus-indica with SARS-CoV-2 Mpro," *Symmetry* , vol. 13, no. 6. 2021, doi: 10.3390/sym13061041.
[186] Tassakka ACMAR et al. Potential bioactive compounds as SARS-CoV-2 inhibitors from extracts of the marine red alga Halymenia durvillei (Rhodophyta) – A computational study. Arab J Chem 2021;14(11):. https://doi.org/10.1016/j.arabjc.2021.103393103393.
[187] Tripathi MK, Singh P, Sharma S, Singh TP, Ethayathulla AS, Kaur P. Identification of bioactive molecule from Withania somnifera (Ashwagandha) as SARS-CoV-2 main protease inhibitor. J Biomol Struct Dyn Oct. 2021;39(15):5668–81. https://doi.org/10.1080/07391102.2020.1790425.
[188] Cao TQ, Kim JA, Woo MH, Min BS. SARS-CoV-2 main protease inhibition by compounds isolated from Luffa cylindrica using molecular docking. Bioorg Med Chem Lett 2021;40:. https://doi.org/10.1016/j.bmcl.2021.127972127972.
[189] P. Kar *et al.*, "Anisotine and amarogentin as promising inhibitory candidates against SARS-CoV-2 proteins: a computational investigation," *J. Biomol. Struct. Dyn.*, pp. 1–11, Dec. 2020, doi: 10.1080/07391102.2020.1860133.
[190] Aanouz I, Belhassan A, El-Khatabi K, Lakhlifi T, El-ldrissi M, Bouachrine M. Moroccan Medicinal plants as inhibitors against SARS-CoV-2 main protease: Computational investigations. J Biomol Struct Dyn May 2021;39(8):2971–9. https://doi.org/10.1080/07391102.2020.1758790.
[191] Patel RS, Vanzara AG, Patel NR, Vasava AM, Patil SM, Rajput KS. In-silico Discovery of Fungal Metabolites Bergenin, Quercitrin and Dihydroartemisinin as Potential Inhibitors against Main Protease of SARSCoV- 2. Coronaviruses 2020;2(8):1–23. https://doi.org/10.2174/2666796701999201223163604.
[192] El-Demerdash A, Al-Karmalawy AA, Abdel-Aziz TM, Elhady SS, Darwish KM, Hassan AHE. Investigating the structure–activity relationship of marine natural polyketides as promising SARS-CoV-2 main protease inhibitors. RSC Adv 2021;11(50):31339–63. https://doi.org/10.1039/D1RA05817G.
[193] Rao P et al. Reckoning a fungal metabolite, Pyranonigrin A as a potential Main protease (Mpro) inhibitor of novel SARS-CoV-2 virus identified using docking and molecular dynamics simulation. Biophys Chem 2020;264:. https://doi.org/10.1016/j.bpc.2020.106425106425.
[194] A. M. Sayed *et al.*, "Microbial Natural Products as Potential Inhibitors of SARS-CoV-2 Main Protease (Mpro)," *Microorganisms* , vol. 8, no. 7. 2020, doi: 10.3390/microorganisms8070970.
[195] Borquaye LS et al. Alkaloids from *Cryptolepis sanguinolenta* as Potential Inhibitors of SARS-CoV-2 Viral Proteins: An *In Silico* Study. Biomed Res Int 2020;2020:5324560. https://doi.org/10.1155/2020/5324560.
[196] Salman S et al. Virtual screening of immunomodulatory medicinal compounds as promising anti-SARS-CoV-2 inhibitors. Future Virol 2020;15(5):267–75. https://doi.org/10.2217/fvl-2020-0079.